Design and simulation of shaped can products.

Davies, David Lloyd

Engineering Doctorate Thesis

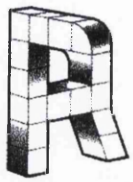

Design and Simulation of Shaped Can Products

Academic Supervisor: Prof. D. R. J. Owen

Industrial Supervisor: Dr. A. J. Morris

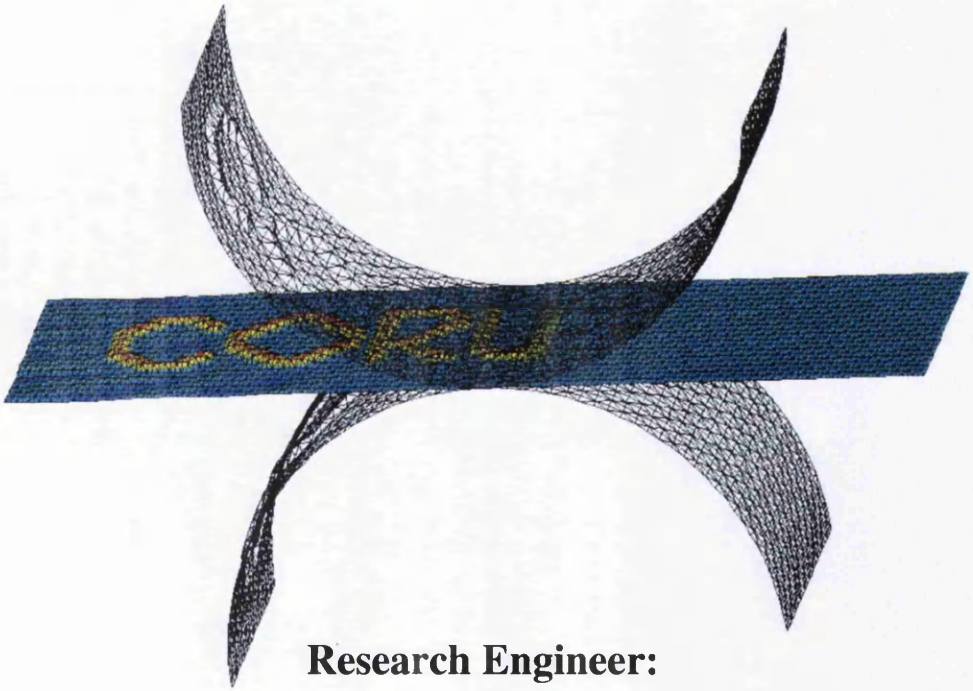

Research Engineer:

D. L. Davies

ProQuest LLC.
789 East Eisenhower Parkway
P.O. Box 1346
Ann Arbor, MI 48106 – 1346

DECLARATION

This work has not previously been accepted in substance for any degree and is not being concurrently submitted in candidature for any degree

Signed .... (candidate)

Date .....25/08/04.....

STATEMENT 1

This thesis is the result of my own investigations, except where otherwise stated. Other sources are acknowledged by footnotes giving explicit references. A bibliography is appended.

Signed .... (candidate)

Date .....25/08/04.....

STATEMENT 2

I hereby give consent for my thesis, if accepted, to be available for photocopying and for inter-library loan, and for the title and summary to be made available to outside organisations

Signed .... (candidate)

Date .....25/08/04.....

SUMMARY

The drawn and wall ironing process (DWI), the primary method in making beverage cans, is a precise procedure where a large number of parameters influence the resultant can shape and performance. With the goal of expanding the capability of production or optimising its efficiency a finite element (FE) model is set-up parametrically such that once validated, new designs can be investigated via this model. The introduction of factorial analysis is utilised in conjunction with FE in order to optimise some variables whilst simultaneously gaining a rounded understanding as to their effect. The thesis describes how the model is set up including the material properties and attention to the contact set-up.

In addition to the DWI modelling, the embossing of cans is simulated. Various embossing models have been created that range from embossing arbitrary designs onto can wall material to embossing squares into flat strip tinplate samples. The validation is made with the flat strip samples that contain features similar to the embossing of squares onto can wall, and so the validation is implied to all of the embossing models.

Some of the key conclusions are: -

- The DWI process can be modelled accurately, predicting features such as final gauge to within 5% and also average cup height
- The factorial analysis package can be applied to the DWI process to ascertain the friction coefficients in all contact areas
- The flat strip embossing model correctly predicts the occurrence of the "spike" and "saddle" features when they exists and their magnitude. The model also correctly predicts when the embossing process will result in material failure.

D L Davies dave.davies@orange.net

CONTENTS

D L Davies dave.davies@orange.net

1. INTRODUCTION

The project aims to simulate the production of a 2-piece can from a circular blank, measure it structural integrity properties, and then onto modelling the shapeforming technology of embossing. The can making process to be simulated is the DWI process (Draw &Wall Ironing), which includes the doming stage at the end of the redraw punch travel. The reason for modelling the can from the circular tinplate blank is to maintain a history of the material properties as it passes through various stages of production, and hence making the modelling of post-forming operations more realistic. In fact the project contains two FE (Finite Element) doming simulations; one that contains the material history pre-doming and the other only the correct starting geometry with the original material properties, the results of which are compared (3.4.2.4).

Overall, the project contains a number of FE models, five of which are detailed in Appendix A, all of which are set-up in and use the ELFEN software (1.1). But also the development and techniques applied to the project are detailed within various chapters, and in most cases have needed extra computer programs (Appendix B).

The DWI process itself is a precise can making procedure that is influenced by many parameters. With the developments made, the entire process can be simulated for a wide range of engineering settings, or even the model adapted slightly to model similar processes such as DRD (draw & re-draw). One particular technique was developed in aiding the DWI, namely factorial analysis, a tool that is very good for capturing trends and effects of parameters in any parametric study. A generic package has been created that can be used for any type of parametric study, and put to use with the DWI model in determining the equivalent friction coefficients.

D L Davies dave.davies@orange.net

The embossing of cans is a secondary forming process designed primarily to enhance the aesthetics of the can; although it can be done to improve the structural integrity of the can, similar to the way can beads improve its panelling performance. The availability and knowledge of what shapes and designs can be embossed with various materials is very limited if not non-existent.

The aim of this work is to be able to simulate the embossing of arbitrary designs primarily applied to can preforms, although not exclusively, to check its feasibility of production and to help design the tooling dies required to emboss such a design. The work includes a model that simulates the embossing of an arbitrary design created by the user on an adjoining self written software package. To make this work useful there must exist confidence that the FE code simulates the embossing process realistically.

An attempt to validate some embossing work was done via an existing embossing tool set. The design of the tool set is a sequence of squares with several parameters defining them, e.g. square size and differing corner radii. The idea of this tool set was to develop understanding into the embossing process by comparisons with the squares with slightly differing parameters. Although the idea seemed good in that it's systematic, and it does highlight some features, there are more fundamental features with the process that completely outweigh the effects of the changing parameters looked at. It's also these fundamental features of the process that made validation of this model inappropriate as will be explained in detail later.

D L Davies dave.davies@orange.net

1.1. ELFEN

All the models in this project use the finite element software ELFEN, created by Rockfield Software Ltd. The software is made up of three main parts; prepost, analysis and post-processing.

The prepost is a user interface where all the geometry can be input, manually with co-ordinates or imported. All the conditions such as constraints, loading, material and mesh are all defined within the prepost. A useful aspect of the geometry definition is the concept of tokens – variables that are named and its value set by the user. These tokens can then be used in the definition of the co-ordinates of points, such that by changing the value of a token automatically changes the co-ordinates correspondingly.

The analysis has the availability of solving the system explicitly or implicitly. The implicit analysis has multiple different solvers that can be used, both direct or iterative.

The post-processing is a user interface where the results can be viewed and analysed. Various plots and contours such as effective plastic strain or displacements of elements can be displayed.

D L Davies dave.davies@orange.net

2. LITERATURE REVIEW

2.1. Drawing & Redrawing

The drawing and redrawing are the pre-stages involved in performing the DWI process. The difficulty in successfully modelling this process lies in the ironing stage - a process that is very sensitive in reality. So in order to model the ironing process with any accuracy and/or assurance the drawing and redrawing stages must be modelled accurately. Simulations of deep drawing a beverage can have been done before, and have achieved acceptable accuracy. The ability to model the drawing stages so easily and accurately relative to the ironing can be explained by the complex interactions at the deformation area in the ironing ring. During ironing there is a mixture of tensile and compressive forces, whilst drawing only involves a relatively simple tensile force created by the punch stroke.

A typical example of modelling the drawing and redrawing stages is the model generated by Tufekci et al. [1] covering drawing, redrawing and ironing of an aluminium sheet. Simulated axisymmetrically, and hence 2-D, "Deform 2D" uses an implicit rigid-plastic formulation. The redraw stage gave the largest CPU times owing to the facts, the stage has three contact surfaces, whereas ironing only has one, and having a longer punch stroke than the draw stage. It was found that large blankholder forces gave rise to fracture at the corner of the cup and for low forces the blankholder itself is lifted up.

After drawing there is a non-uniform wall thickness, the thickest part being at the top, which is equally true for redrawing. By looking at the punch force / stroke distance plot it can be seen at which point on the cup wall that sizing (thickening) occurs. As

D L Davies dave.davies@orange.net

shown in Figure 1, typically the graph will start with a steep gradient, taper off, then drop, and then at the point of thickening the graph will increase again [2].

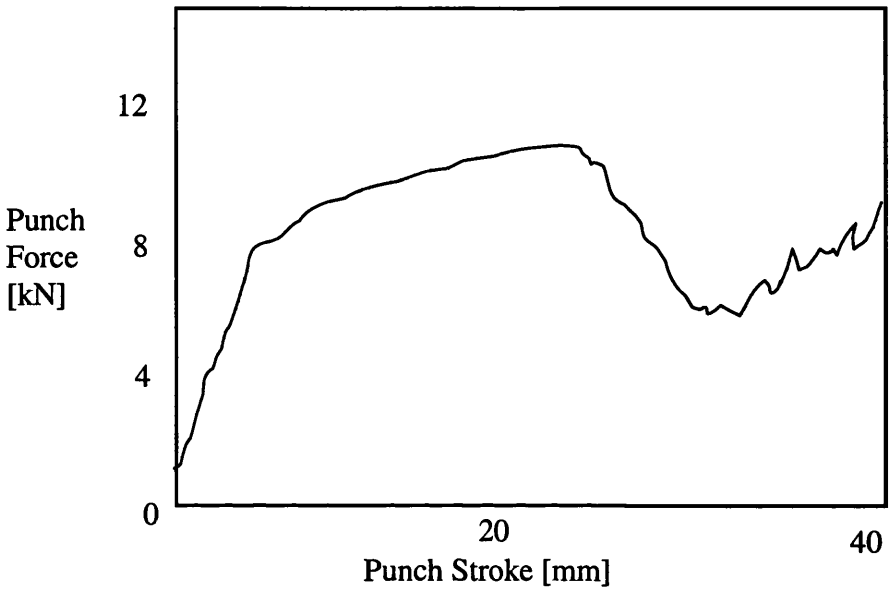

Figure 1: Typical punch load/stroke during redraw

Plots comparing actual measurements against predicted values of the profile of the formed cup validate Tufekci's model. The plots for both the drawing stages concur with physical readings in that the cup height was correct in each case, and the non-uniform wall thickness corresponded.

In another model by Schünemann et al. [2] non-isothermal drawing is considered. As before, modelled using "Deform 2-D", and implicit rigid-plastic code. Before starting analysis selective points were chosen for tracking purposes, temperature and axial stress. In drawing, there was no thermal change in the base - this is because negligible deformation takes place in the base. Noticeable temperature increase (5°C) occurs in the low wall - quite a lot of deformation, and considerable increase (30°C) at the top wall - high frictional interaction. The redrawing follows a similar pattern - no change in the base, 25°C increase in lower wall and 40°C increase in upper wall.

2.2. Ironing

As mentioned earlier, the ironing process involves some complex interactions, and so it would be of interest to know how it affects the properties of the cup. Merchant et al. [3] measured that the strength of an ironed wall is typically 10-15% stronger than the initial sheet.

Tufekci et al. [1] modelled the ironing process by firstly retaining the strain history from the redrawing stage modelled previously. They found that the punch load/stroke distance plot contained large amounts of scatter. Huang et al. [5] agreed with this and found that the load significantly decreased/increased when elements left/entered the deformation zone. Moreover they realised that scatter could be greatly reduced using a very fine mesh.

Schünermann compared simulation with experimental data using punch load/stroke distance plots [2]. During the first ironing ring the punch load increased noticeably more than the other rings [6]. This was explained by the increasing thickness of the wall after redrawing, so not only was there strain-hardening as the cup height increased but also the ironing ratio increased. Only strain hardening occurs at the other ironing rings since the 1st ring makes the wall a uniform thickness and so a constant ironing ratio.

According to manufacturers ironing should be done separately, i.e. the distance between any two consecutive ironing dies should be greater than or equal to the cup height to ensure reduction only takes place at one place at a time. Schünermann highlighted that during tandem ironing the total punch force is equal to the sum of forces reacting on the die [2]. The effects of stress and punch force were looked at and the results say that the effective stress doesn't change whether single or tandem

ironing is taking place, whereas both the axial stress and punch force are lower when single ironing. Sachs & Lubahn state that maximum reductions increased considerably when wall thickness is reduced simultaneously in two dies, and that bigger spacing between dies results in a larger 2nd reduction [7]. Pankinin characterised parameters for ironing and built design rules, which implied that there was no advantage in tandem ironing, and infact that bulging between dies would occur [8].

Shawki made physical tests for brass cartridges, stating that the optimum semi-angle was in the range 8-10°, and that given a reduction ratio the minimum punch load occurs with a die semi-angle 7-10.5° [9].

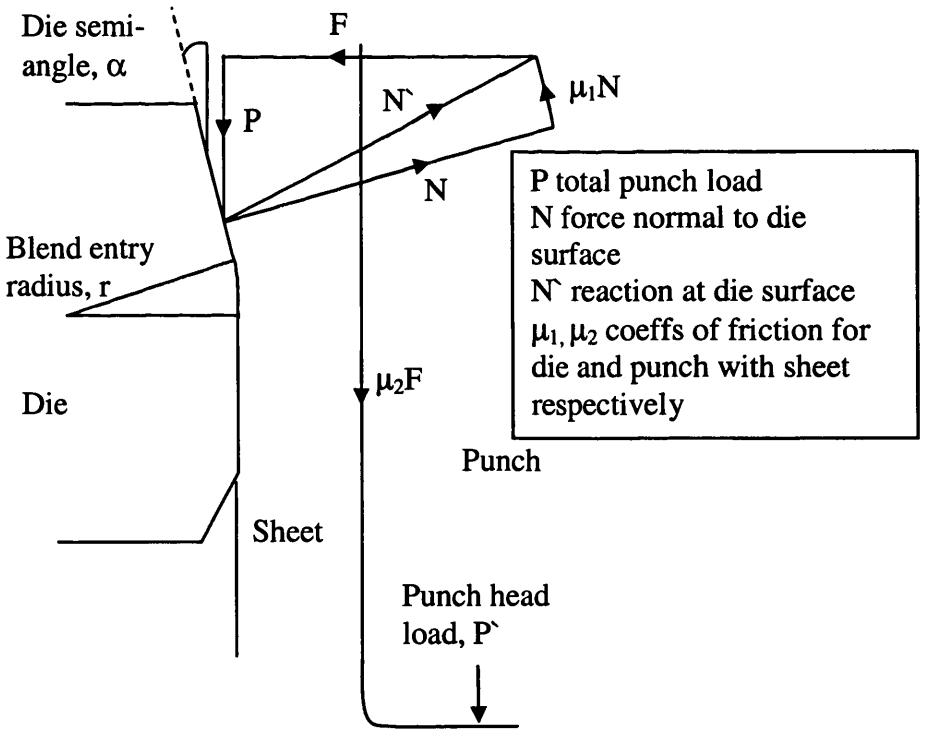

Figure 2: Geometry and forces during ironing

Tufekci et al. added that this optimum die angle was independent of friction (0.05-0.15) [1]. Alternatively Swift says the optimum die semi-angle lies between 10-15° [10].

Shawki also gives the result, for a given percentage reduction the punch load essentially increases linearly with the throat length of the die [9]. An arc to prevent stress concentration (entry radius, r, Figure 2) and to obtain a larger reduction ratio should connect the intersection of semi-angle and the straight [5].

Relations

- $P = c.R1.25$, where c is the punch load at R=1, and R is the reduction ratio. Experiment gives $c \approx 9700kPa \approx 10MPa$ (Shawki for brass [9])
- Ironing load $\propto$ wall reduction (Swift [10])

Tufekci et al. performed a parametric study of thickness reduction, die angle, friction [1]. A very good reference paper with numerous plots, highlighting many trends. For example, increasing the reduction ratio results in increasing both punch load and axial stress.

Non-isothermal models were performed by Schünermann & Tufekci et al [1,2]. Continuing from their drawing models the same points were tracked during the ironing stage. These tracked points confirm the theory that the high flow stresses in the upper part of the cup results in high temperatures. Simulation temperatures up to 130°C are reached - possibly significant for a change in material properties. Tufekci et al. [1] also made a parametric study of punch speed, percentage reduction taking temperature into account. As above, it contains plots with trends, but also temperature distributions. A standard result being increased punch speed, or

reduction ratio results in increased temperatures. It is suggested for future studies that due to high punch speeds and hence heat generation, that temperature should be taken into account. Also mentioned is the use of Coulomb friction being unrealistic due to the influence of the interface temperature in the deformation zone.

2.3. Friction

Bunten & Kopp [11] made an FE study on friction - they mention the different types of friction with definitions for geometric, normal, tangential and micro (Figure 3).

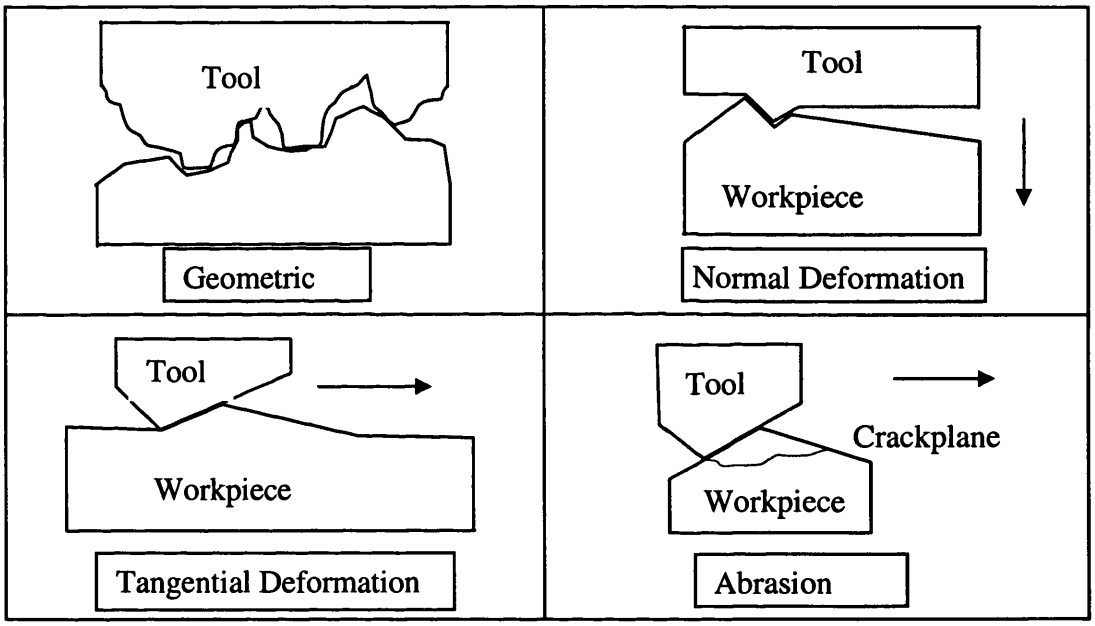

Figure 3: Illustration of the different types of friction that exist

Coulomb's friction is a combination of the above frictions,

$$\mu_{macro} = \mu_{geometric} + \mu_{normal} + \mu_{tangential} + \mu_{micro}$$

The model points out that (Coulomb's) friction coefficients are not needed if the microscopic geometry known. This is not the case during ironing and so all models so far have used Coulomb's friction coefficients when dealing with sliding contact.

D L Davies dave.davies@orange.net

For brass it is suggested that the die/sheet, punch/sheet friction coefficients (Coulomb) should be 0.03-0.06, 0.10-0.13 respectively, depending on lubrication conditions [9]. This is worked out by comparing experimental results with the theory developed by inspecting the physics taking place in the ironing ring.

$$F/P = (\cot\alpha-\mu_1)/(1+\mu_1-\cot\alpha)$$

$$\mu_2 = (P-P`)/F, \qquad \text{(see Figure 2)}$$

Schünermann tried using various educated guesses for punch and die frictions, and each friction pair the punch load/stroke is plotted and compared with experimental data [2]. The pair with the best approximation is then assumed as the friction coefficients. The best pair turns out to be 0.06 and 0.09 for the punch/sheet and die/sheet respectively, where the sheet used is aluminium. Rajagopal & Misra [12] tried to determine the punch and die friction coefficients separately, but their results are only applicable to small reductions.

If the friction coefficient has been ascertained for the 1st reduction ratio in the simulation with the same material, ironing ring, and lubrication condition, the load of the other reduction ratio can be determined precisely by using the same friction coefficient [5].

Relations

Increasing the punch friction has the effect of decreasing axial stress and thus allowing higher percentage reductions, limited by surface scratching if too high [1].

Increasing the die friction causes both the punch load and axial stress to rise, even more so if the percentage reduction high [1].

3. DWI

3.1. Introduction

The DWI process is a precise can making procedure that is influenced by many parameters. The production of cans with very thin gauges already available in the marketplace has a small operating window with regards to the tooling geometry and blank-holder pressures. Optimisation of the process via physical experimentation alone would be a costly and time consuming process. A working and an adaptable simulation model could aid with this.

Moreover, similar existing can making methods could be simulated such as the draw and re-draw (DRD), as well as the possibility of developing shape-forming technology by using the pre-formed simulated can as an input.

3.2. DWI Process

The process that is to be simulated is made up of three main stages; cupping, redraw & ironing, and doming. The cupping is performed in a prior operation, with the remaining DWI process carried out in a body maker toolpack.

For this analysis a blank of diameter 136mm is drawn to a cup of diameter 91mm, approximately 27mm tall, with ≈ 10000N blank-holder force. The cup is then placed into the bodymaker (Figure 4) with a punch ≈ 66mm diameter, is pushed through the

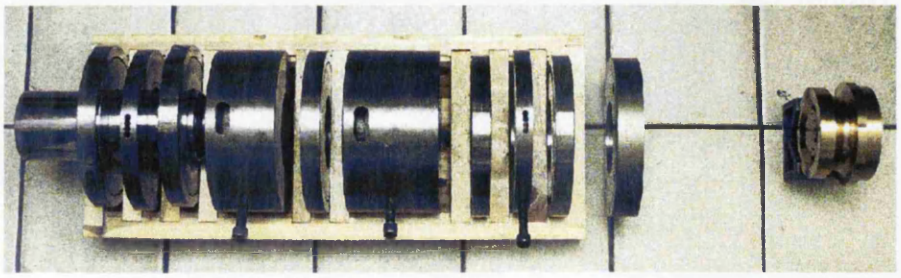

Figure 4: DWI bodymaker toolset and cup progression sizes

D L Davies dave.davies@orange.net

redraw die and four ironing rings, and is then domed making an untrimmed can height ≈120mm. The redraw sleeve force ≈ 4000N and dome ring pressure force ≈15000N.

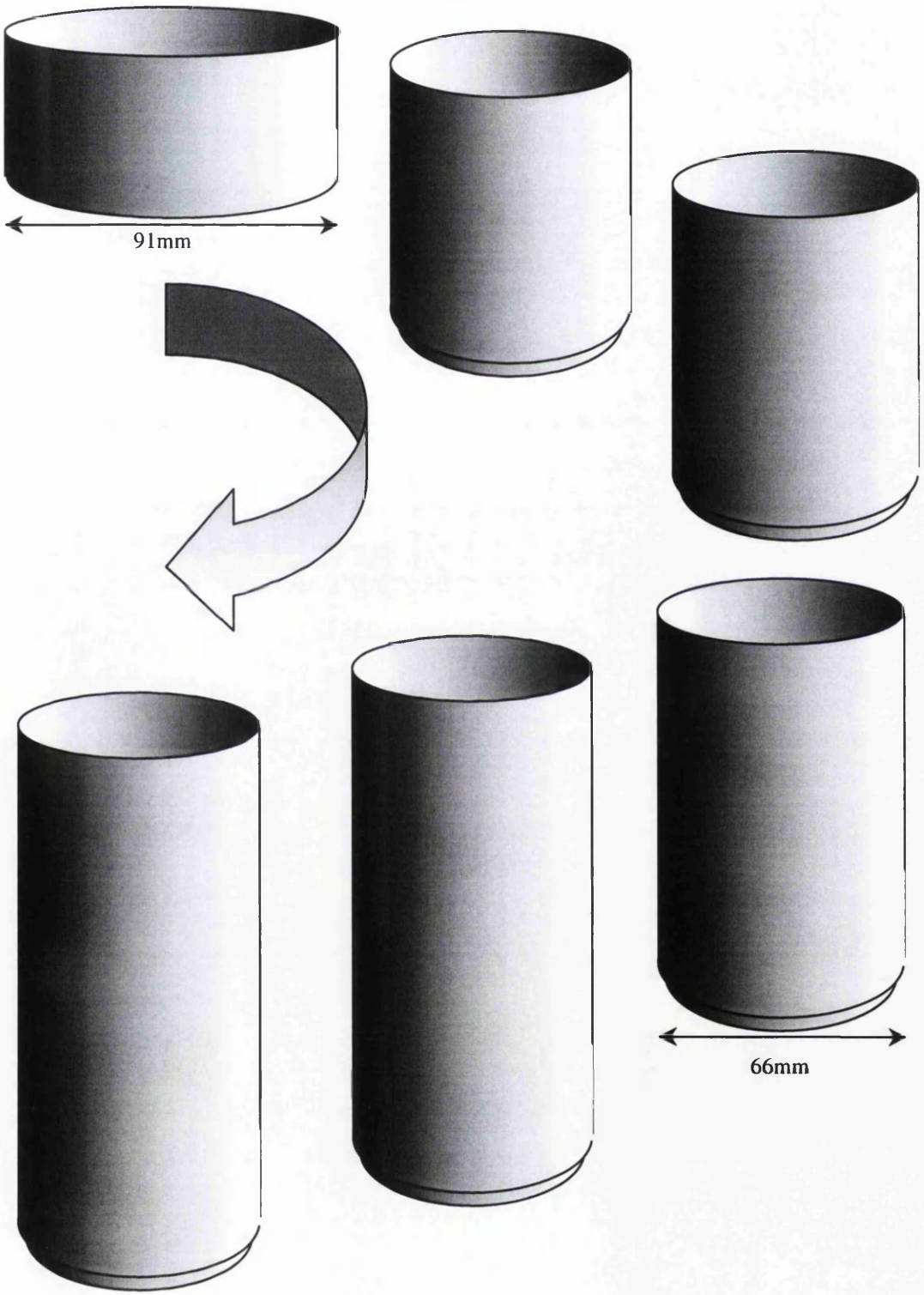

Figure 5: DWI cupping progression from cup to 4th ironing ring

D L Davies dave.davies@orange.net

3.3. DWI Model

A single model is set-up axi-symmetrically in 2D (Figure 6), such that the whole process from cupping to doming is simulated. All the token values, load curves and special features of the model are listed or in Appendix A.i. A feature of the software used is the ability to switch individual element groups on and off. In this way it is then possible to set up all tooling involved with the process in one model, primarily because the cupping tooling is switched off when modelling the redraw section and vice-versa.

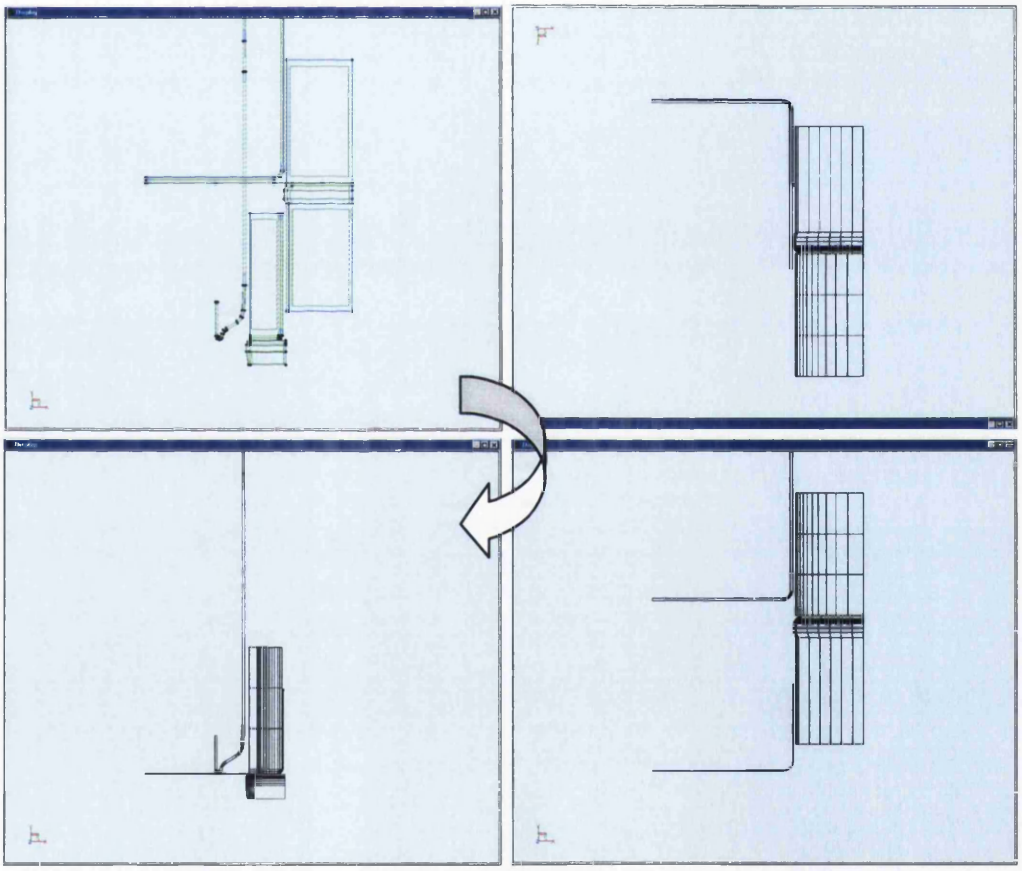

Figure 6: Geometry transition between cupping and redraw

An important feature of the set-up is that all dimensions are entered parametrically, such as draw radius or tool spacing. This provides the means of adapting tooling set-

ups quickly and/or running sensitivity analysis. An example of which is illustrated in Figure 7 showing how the redraw punch is parametrically defined from 4 radii.

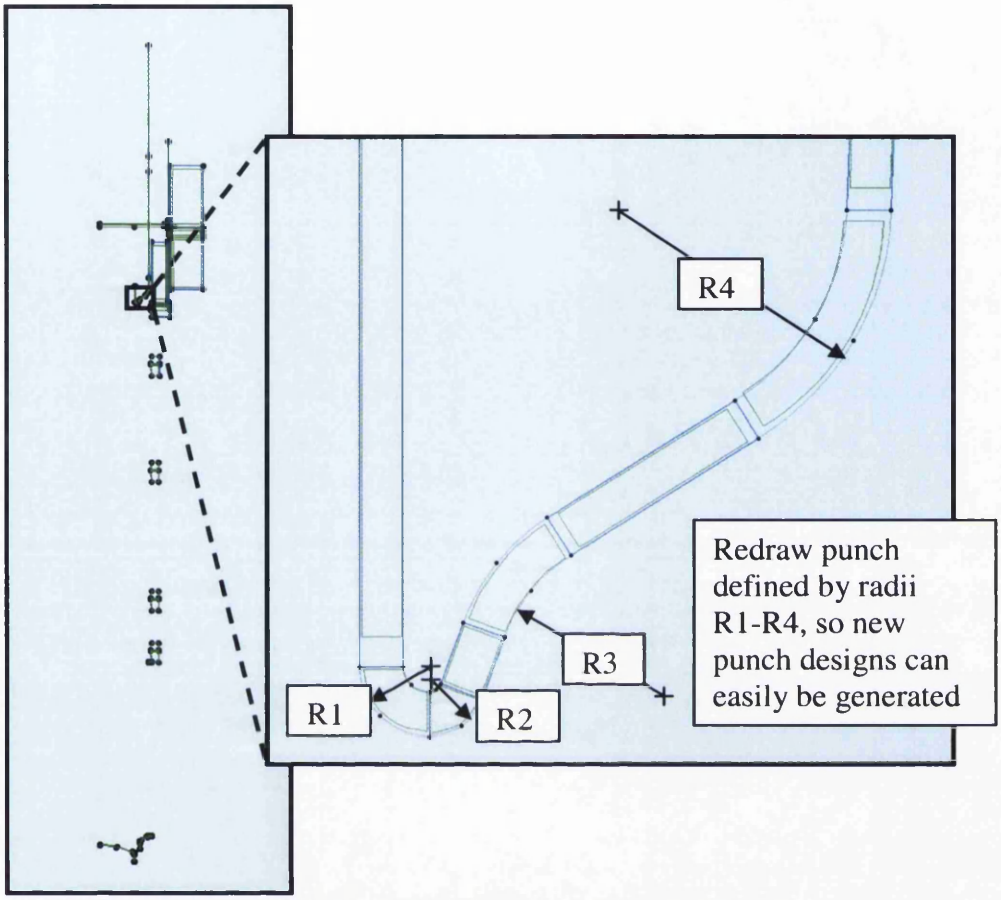

Figure 7: Parametric definition of redraw punch nose

3.3.1. Modelling Obstacles

In the cupping there is some difficulty in simulating the cup thickness throughout the can, based on physical data. The problem is a twin problem in that, ensuring the profile is correct in one area causes the profile to differ from reality elsewhere. Friction coefficients also have significant effect on the thickness distribution, and due to aspects such as lubrication, cannot be known specifically. For this reason early model trials included running various friction levels during the cupping stage to develop further understanding of the forming process.

D L Davies dave.davies@orange.net

3.3.1.1.Base Thinning

According to physical data, base thinning during cupping should be negligible, but in most cases during early model trials the base thins too much. This thinning takes place early on in the cupping simulation; it starts at the onset of the punch hitting the strip until the strip between the die and punch is nearly vertical (Figure 8).

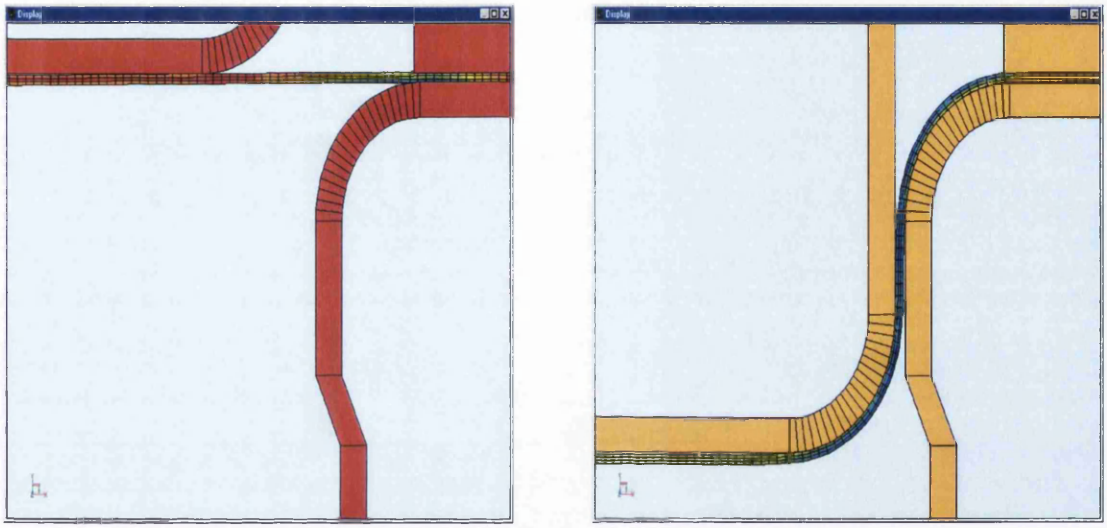

Figure 8: Thinning of cup base (scale – strain through thickness)

After this point there is no further thinning in the simulation. This base-thinning problem is soluble though, but at the expense of another problem.

3.3.1.2.Top Wall Over Thickening

A method to prevent the base-thinning problem is to reduce the blank holder pressure. This means that the strip that passes between blankholder and draw die has a smaller clamping force, and hence a weaker resistance against the strip thickening in this area. It only thickens it by an extra 10 microns, but that is enough at that position to cause problems further down the line, namely the redraw stage.

The problem that occurs in the redraw stage is near the end, due to the over thickening of the can top. The problem lies between the redraw punch and the redraw die,

D L Davies dave.davies@orange.net

because the allowance between the two is less than the thickness of the strip towards the top. This results in wall ironing, which is unwanted (at this stage anyway), but even worse is that it occurs in tandem with the 1st ironing ring. Amongst other things this causes the base and chime to thin rapidly (Figure 9), whereas it is expected that both should thin no more than 10 microns.

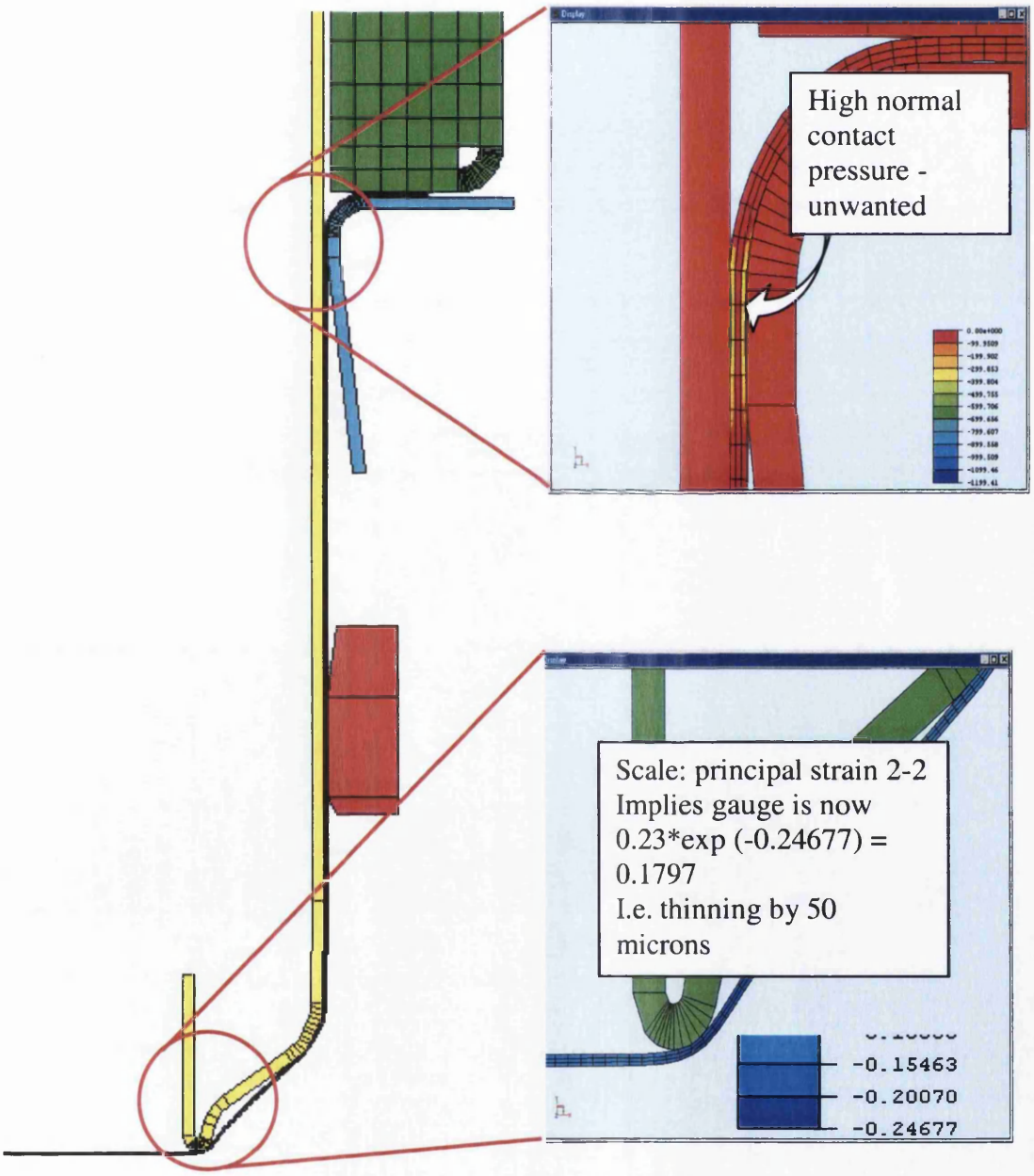

Figure 9: Top wall over thickening

D L Davies dave.davies@orange.net

3.3.1.3.Friction Coefficients

To investigate the effects of the friction coefficients the cupping model was run a number of times changing the friction values at all contact areas (Figure 10), then looking at the thickness variation in the resultant formed can wall.

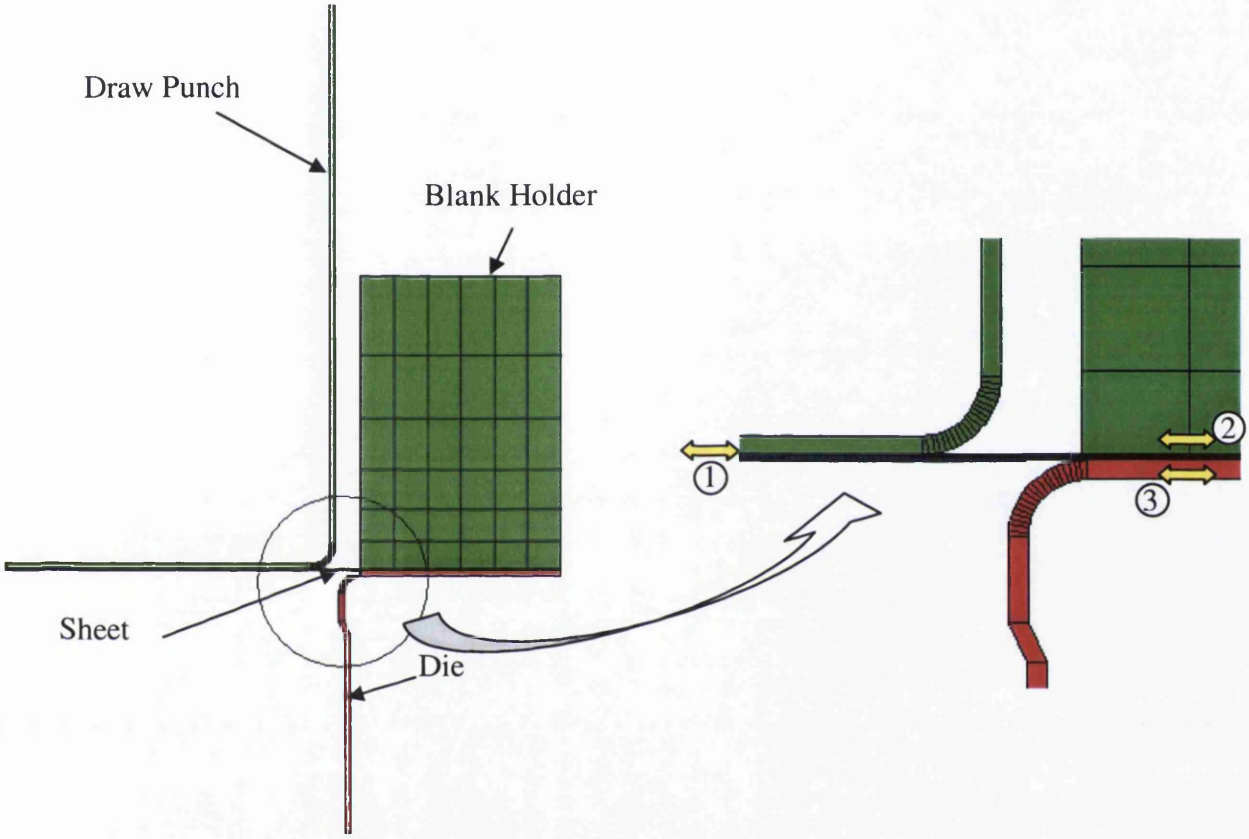

Figure 10: Cupping contact definition

1. Sliding friction between sheet and punch
2. Sliding friction between sheet and blank holder
3. Sliding friction between sheet and die

The thickness measurements taken are of the average wall thickness paired with its distance from the cup base (Figure 11).

D L Davies dave.davies@orange.net

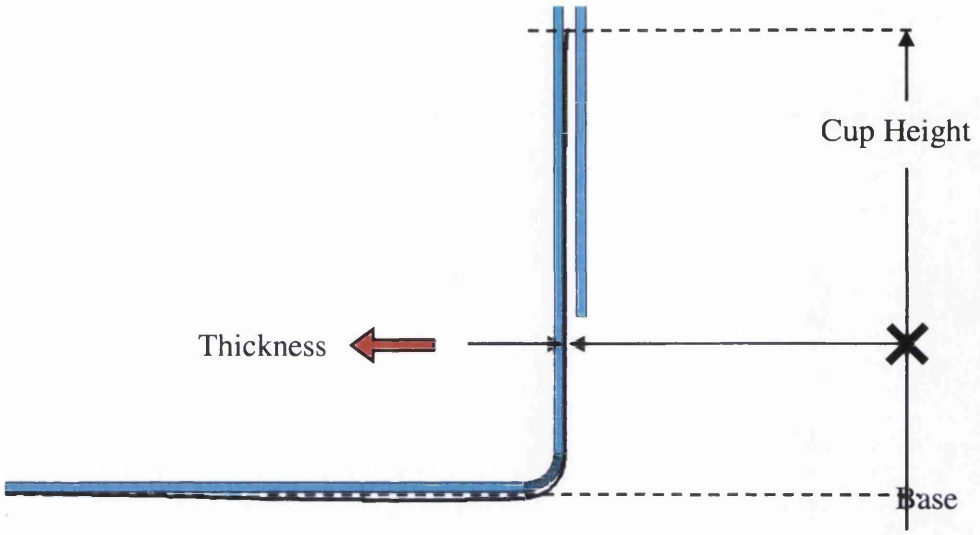

Figure 11: Cup profile measurement

Friction between sheet and punch

(a) Low: -

If the friction is set very low then all the material near the punch is drawn away resulting in severe thinning at the base of the cup, and spreads some of the way up the wall of the cup also. Correspondingly, due to the excess thinning the cup is drawn to a greater height than normal (Figure 12).

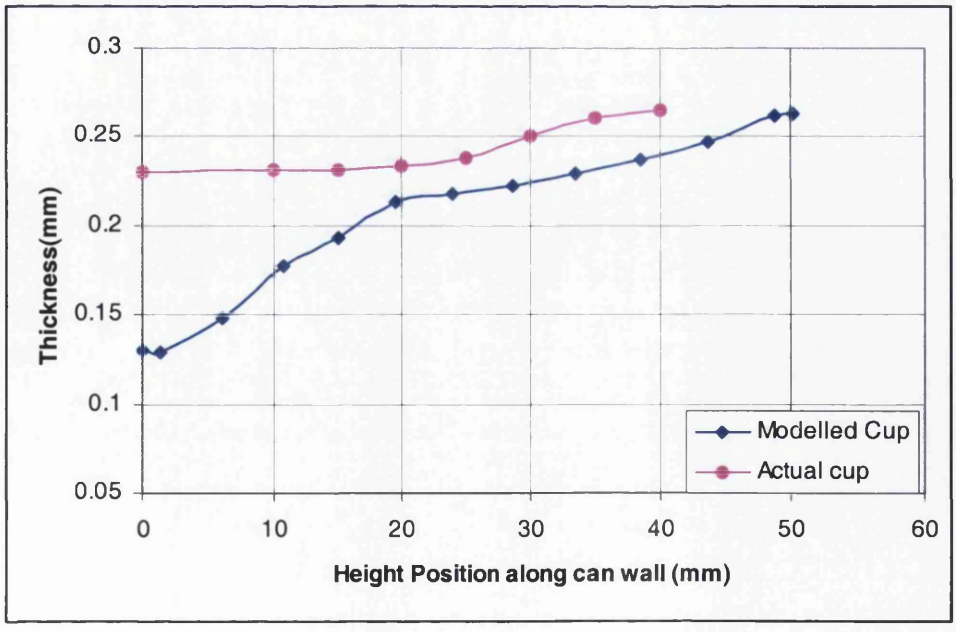

Figure 12: Punch friction low

D L Davies dave.davies@orange.net

(b) High: -

Conversely then, if the friction is high the punch holds on to nearby material, and hence reduces thinning in the base (Figure 13). Also provided that the die & blank holder frictions are comparatively low then the cup height will be lower than usual.

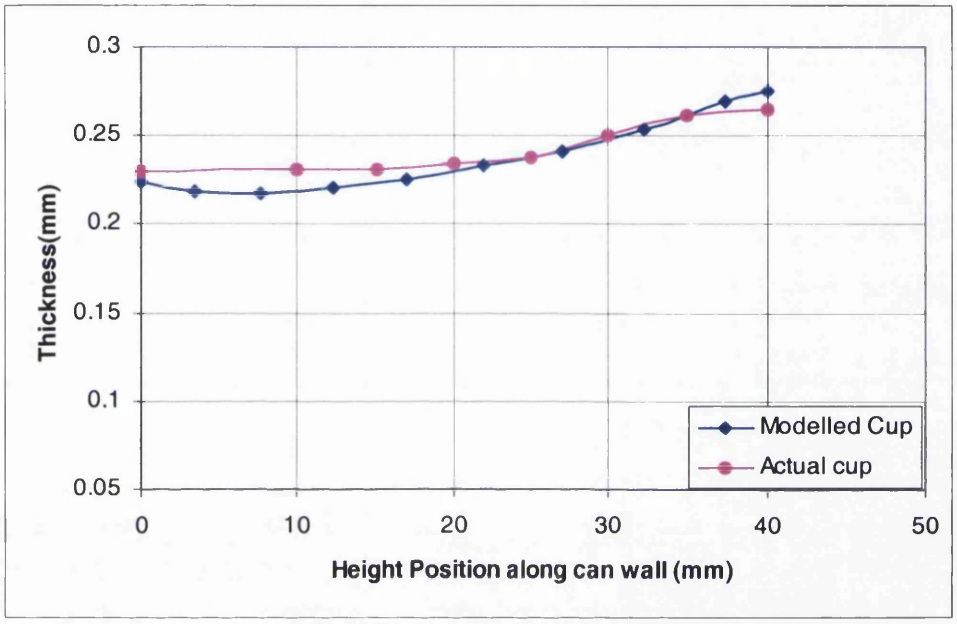

Figure 13: Punch friction high

Friction between sheet and blank holder

(a) Low: -

Low friction at the blank holder means there is less resistance to the strip sliding away from it. This therefore is equivalent to a lower blank holder force, and as expected, this results in less drawing and thinning of any material (Figure 14). Only deformation takes place, which means that the strip will be shorter than expected – similar to the punch friction being high.

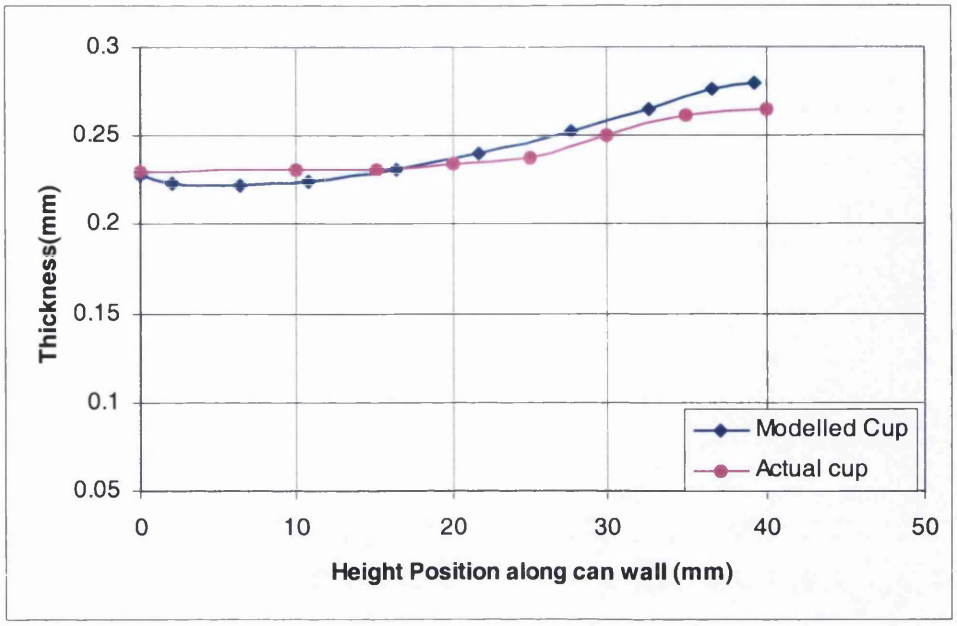

Figure 14: Blank holder friction low

(b) High: -

With the same reasoning, the blank holder friction set high is equivalent to a large blank holder force, which means there is little movement of the strip that is in contact with the blank holder. This will clearly result in extreme thinning of the strip that isn't in contact with the blank holder (Figure 15).

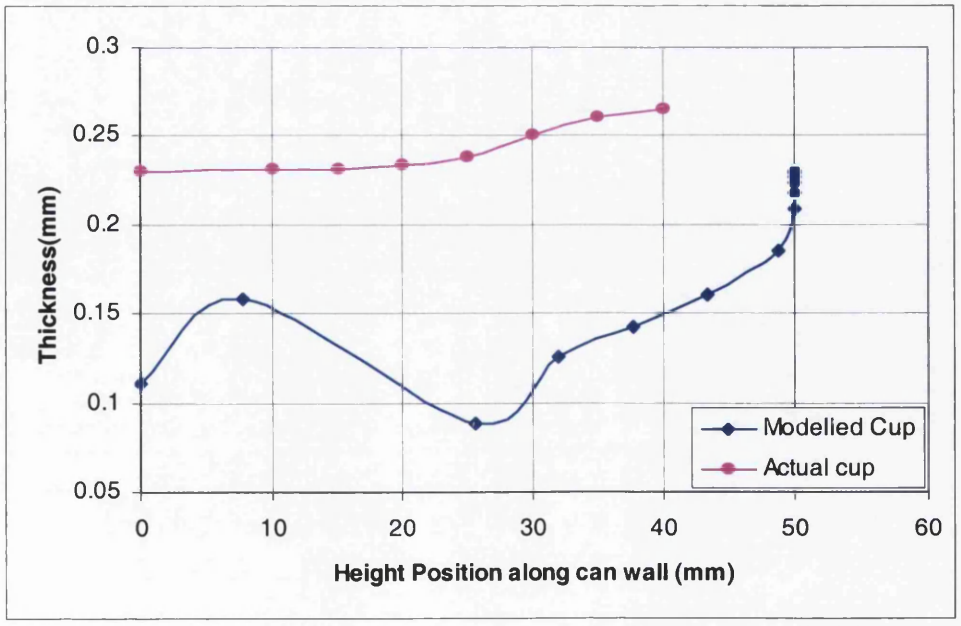

Figure 15: Blank holder friction high

D L Davies dave.davies@orange.net

Friction between sheet and die

Since contact occurs mainly in the same area as the blank holder contact, there is no surprise that frictional changes between sheet and die affect the sheet in a similar manner to the blank holder (Figure 16, Figure 17).

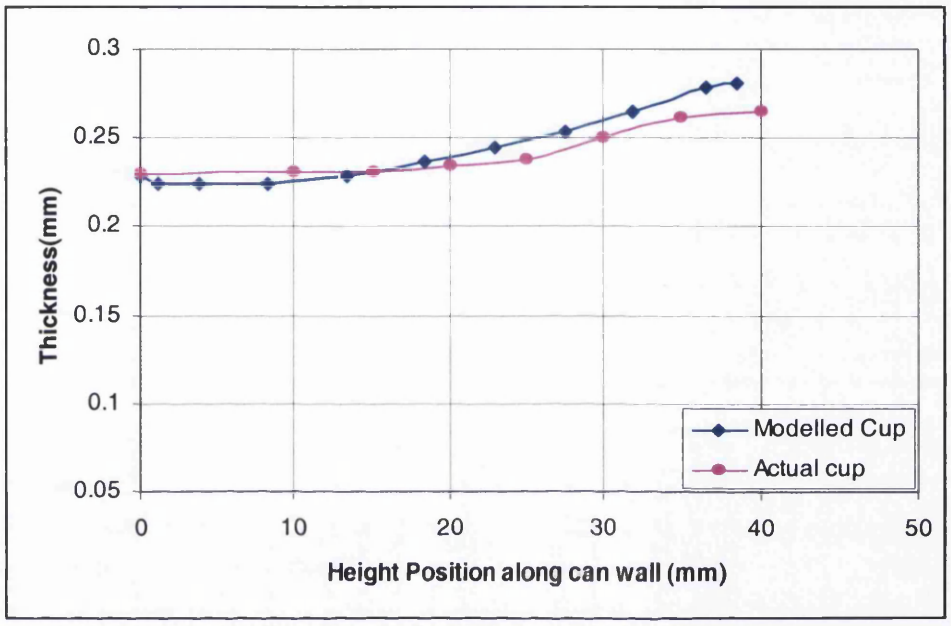

Figure 16: Die friction low

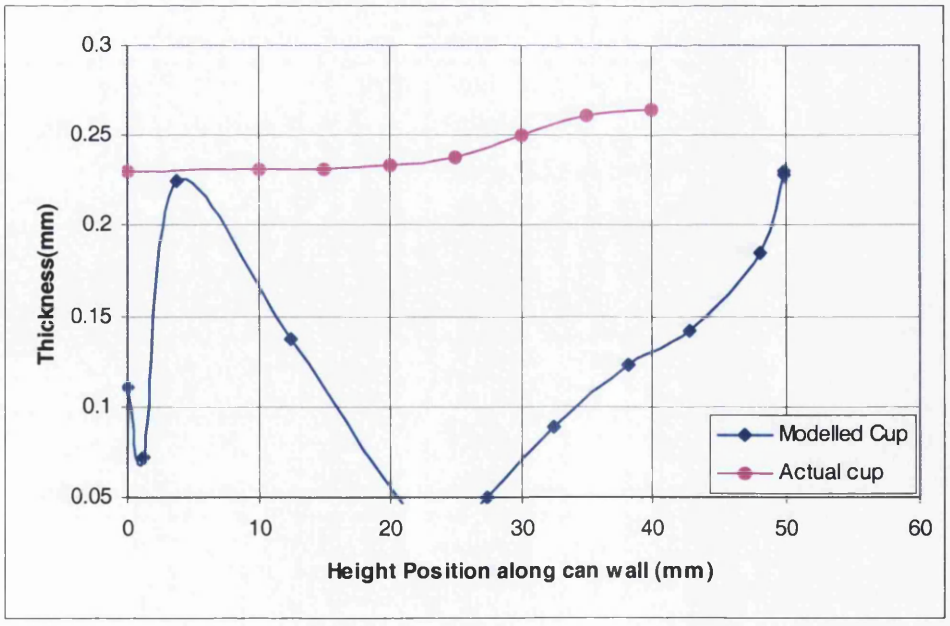

Figure 17: Die friction high

D L Davies dave.davies@orange.net

A summary of the effects the varying friction coefficients have on the thickness profile of the cup can be seen in Figure 19 where the base, low and high wall locations correspond to those indicated in Figure 18

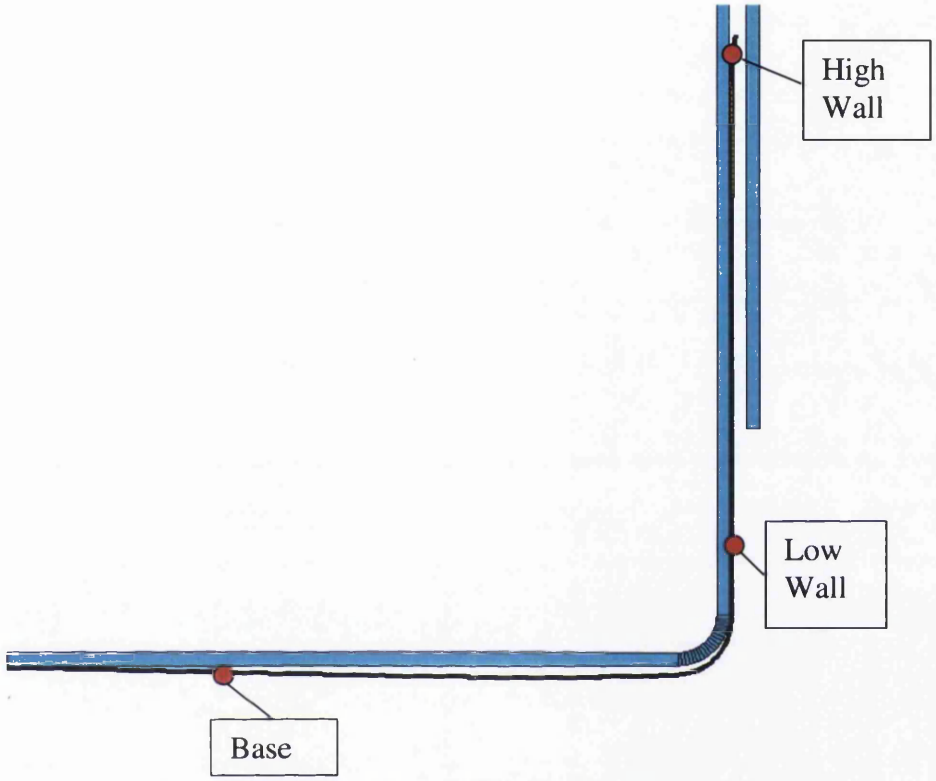

Figure 18: Cupping thickness test areas

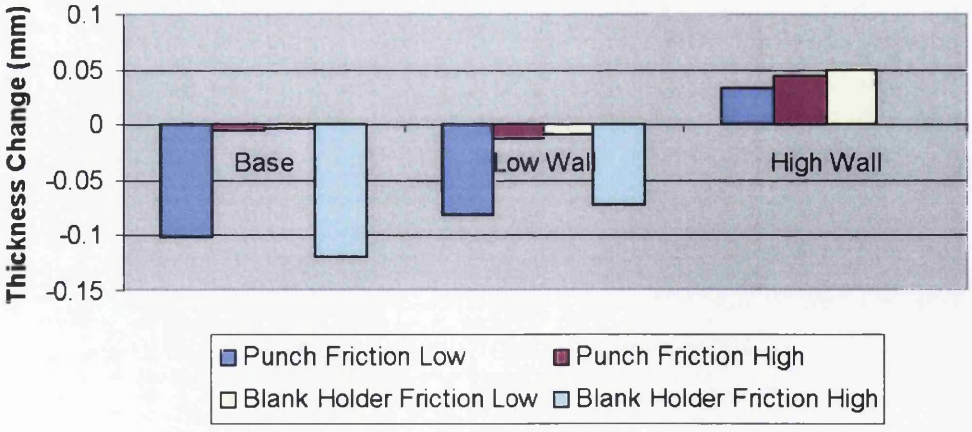

Figure 19: Cupping friction effect on gauge

D L Davies dave.davies@orange.net

3.3.2. Model Development

The early model trials didn't take into account the calculated work-hardening data. The revision of the material model had a significant effect in dealing with the "top-wall over thickening" problem, not only in satisfying the gauge but also its yield stress in comparison to tensile tests taken post cupping and redrawing. The combination of the revised material model and the addition of an extra force imposed during cupping address the "base-thinning" problem.

3.3.2.1.Material Model

The strip material is treated elasto-plastically using Von-Mises' work hardening principle. The hardening data (Table 1) is calculated from combining the theoretical strains at various stages during the process with corresponding tensile test data.

The equivalent strain during drawing is equal to the natural logarithm of the diameter ratios, so for cupping $\ln(136/91) \approx 0.4$, and redraw $\ln(91/66) \approx 0.32$ (Figure 20)

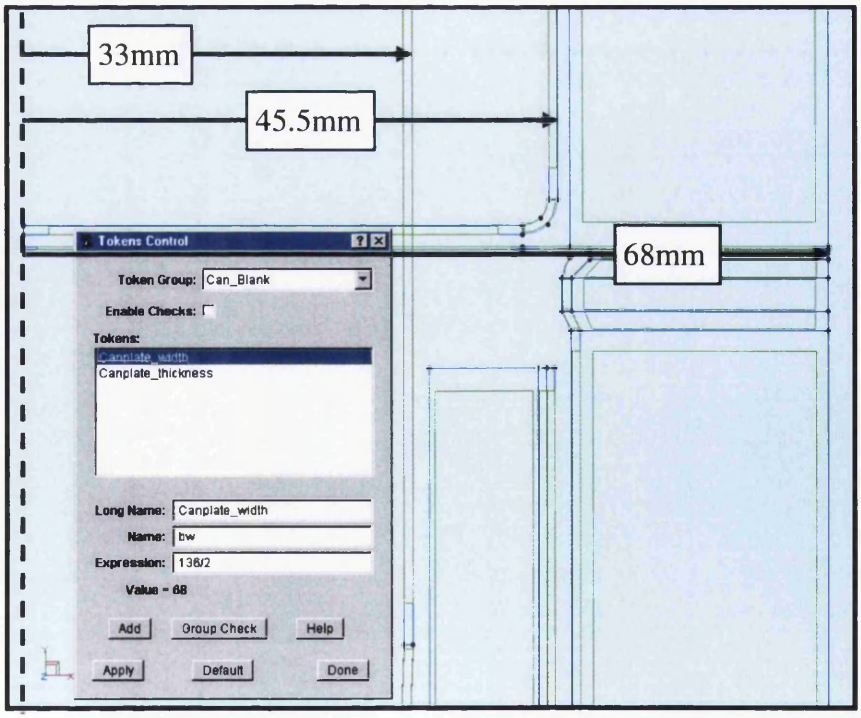

Figure 20: Geometry highlighting blank, cup, and redrawn cup diameter measurements

D L Davies dave.davies@orange.net

Ironing can be considered a plane strain process and so its associated equivalent strain is the natural logarithm of the thickness ratio times 2 divided by square root of 3. E.g. for 35% reduction $\varepsilon \approx 1.15 \times \ln(1/(1-0.35)) \approx 0.5$

Work hardening based on tensile tests performed after several stages						
	Stage	Yield	Part Equivalent Strain		Total Equivalent Strain	
	1st draw	475		0.4		0.4
	Redraw	560		0.32		0.72
Ironing						
	20%	680		0.25		0.97
	35%	700		0.50		1.22
	49%	760		0.77		1.49
	59%	800		1.03		1.75
	67%	850		1.27		1.99
	72%	870		1.47		2.19

Table 1: Work hardening data for can strip material

The tooling however is treated elastically, in particular tooling dies, the properties of which are defined to simulate tungsten carbide. This allows small strains to occur in the dies (Figure 21), which can be enough to allow the material to pass through when the reduction ratio is high.

Figure 21: Ironing ring elasticity

D L Davies dave.davies@orange.net

3.3.2.2.Cupping Vacuum Force

The additional force was placed on the underside of the strip beneath the draw punch (Figure 22), its aim to simulate a vacuous force to prevent the strip base to leave the punch.

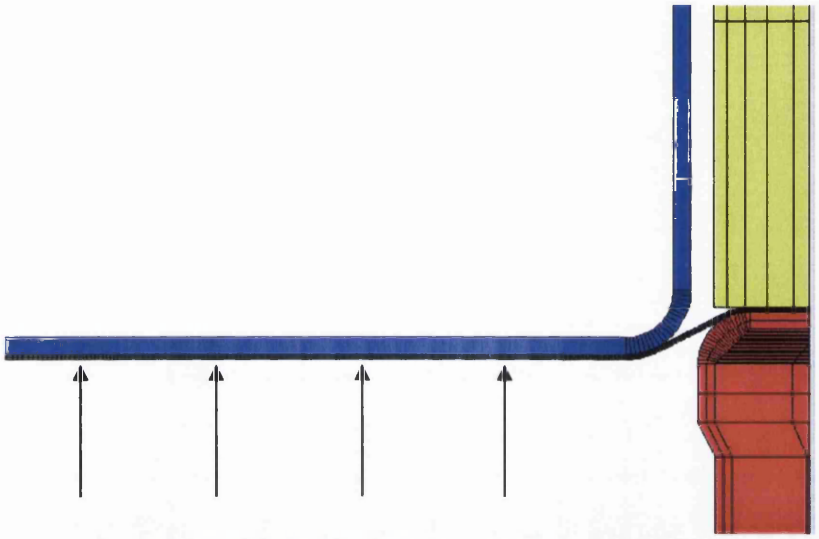

Figure 22: Force on strip simulating vacuum

Note: Due to different geometric properties between the draw punch and the redraw punch the extra force constraint need not be added in the redraw stage (the increased volume in the central region between strip and punch).

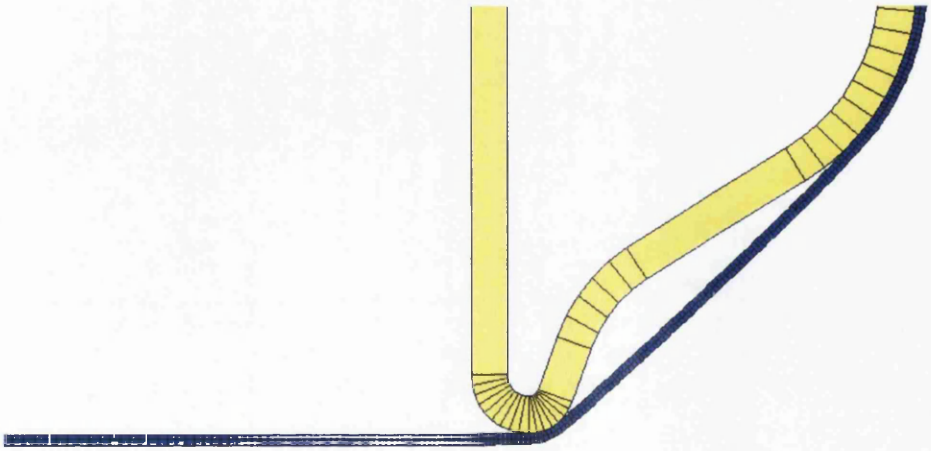

Figure 23: Redraw punch noting large volume above central part of base

3.3.2.3.Friction Coefficients Evaluation

Running the simulation with the above modifications with unknown real friction coefficients, and thus estimated in the model, is illustrated in Figure 24

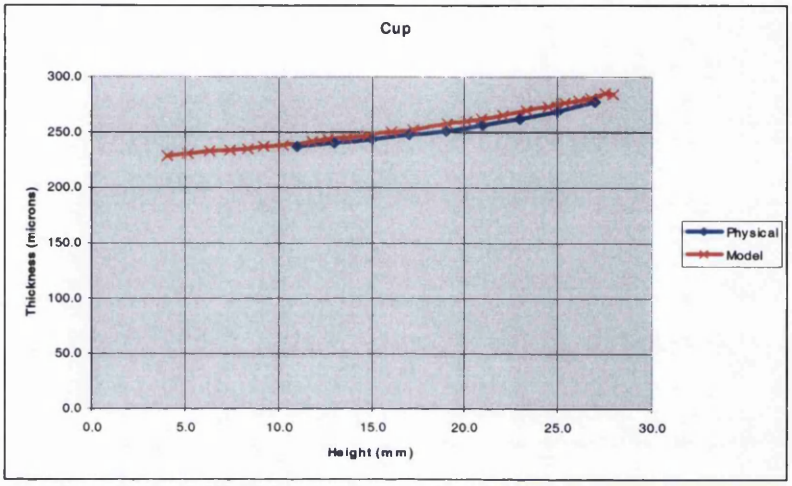

Figure 24: Initial height-gauge profile with 1st estimate of friction coefficients

Although the error is small, the discrepancy may be enough to prevent ironing of the cup, as this process is so precise. In order to achieve the very accurate results for cupping, factorial analysis is utilised, described in detail in the factorial analysis chapter. After applying this developed package to cupping it improves the cup profile noticeably seen in Figure 25

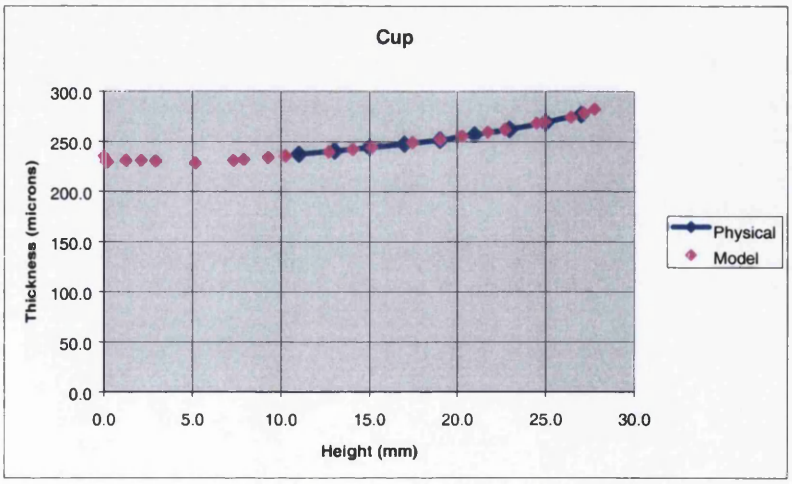

Figure 25: Height-gauge profile, friction coefficients calculated using factorial analysis

D L Davies dave.davies@orange.net

3.3.2.4.Contact Set-up

Most tool contacts are defined by a single slideline, where each slideline is given a set of contact properties such as Coulomb's coefficient of friction. In order to take into account varying lubrications along one tool-piece, namely the redraw punch (Figure 26), the contact is split up into 3 slidelines. This also allows the possibility of distributing the friction coefficients so they tie in with Stribeck's curve [13].

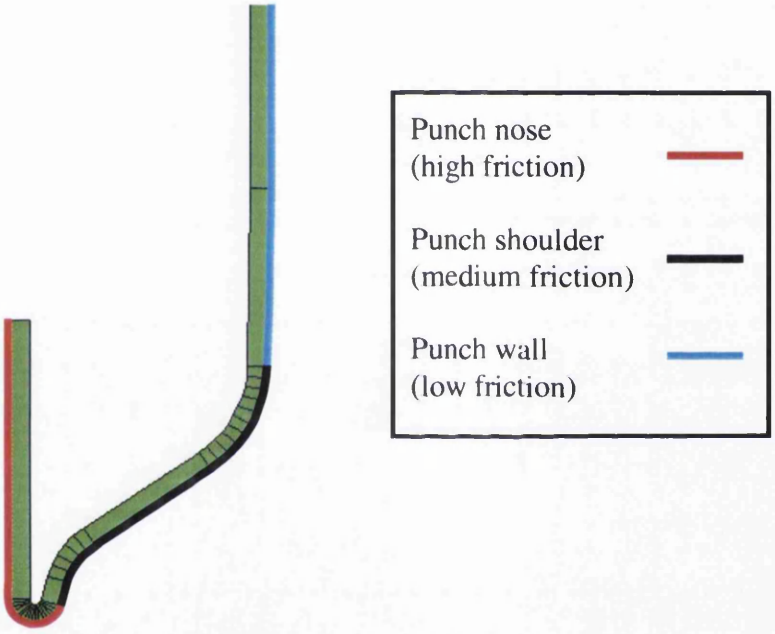

Figure 26: Redraw punch contact line split into 3

Another slideline option is whether to check for element penetration of one surface (either one), or both. Checking both surfaces means that neither surface can overlap any element of the opposite surface by a specified amount, but this scheme is usually considered computationally expensive. For most cases just checking the can strip surface will suffice. Areas where both are needed occur when the can strip is formed around a radius that is small relative to the can's mesh density. This could include the redraw die radius in some cases, but for the present tooling set-up and mesh density it isn't needed. The only area where it is required is during ironing where the mesh

density becomes too low. Due to the stretching of the elements as a result of ironing it is hard to ensure a high enough mesh density, thus both sides are checked in all ironing ring contacts (Figure 27). The issue of the element penetration at the sharp corner within the ironing ring still remains, but is noticeably reduced. Additionally a different element type (F-bar element) has helped, in that it curtails the shearing effect of the element, which helps with convergence in later steps (more unlikely for elements to invert).

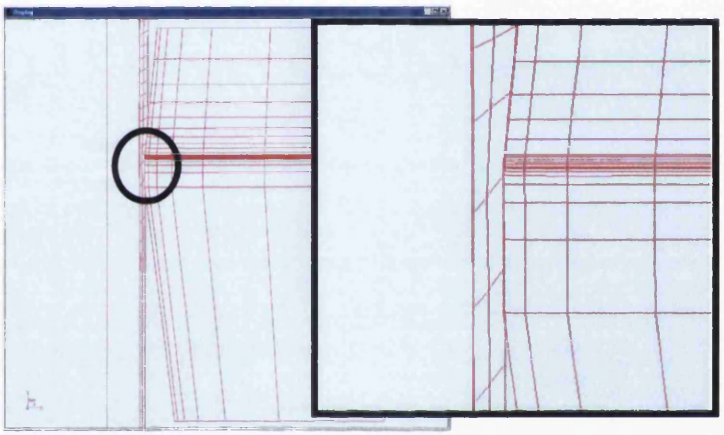

Figure 27: Penetration checked both sides in ironing rings

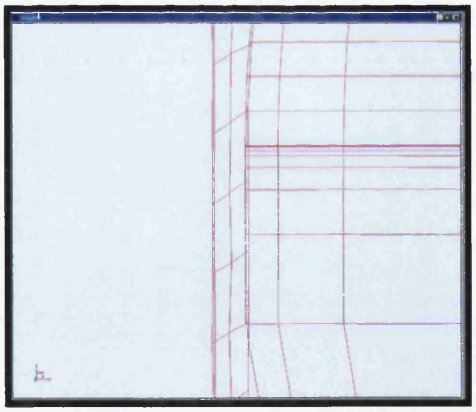

Figure 28: Penetration only checked on strip

3.3.2.5.Mesh Density

The convergence problem that can occur during the ironing process can be totally overcome by having a sufficiently dense mesh (especially rings 3 and 4), which is

dependent on the available computing power. Presently a relatively uniform highly dense initial mesh is used shown below (Figure 29).

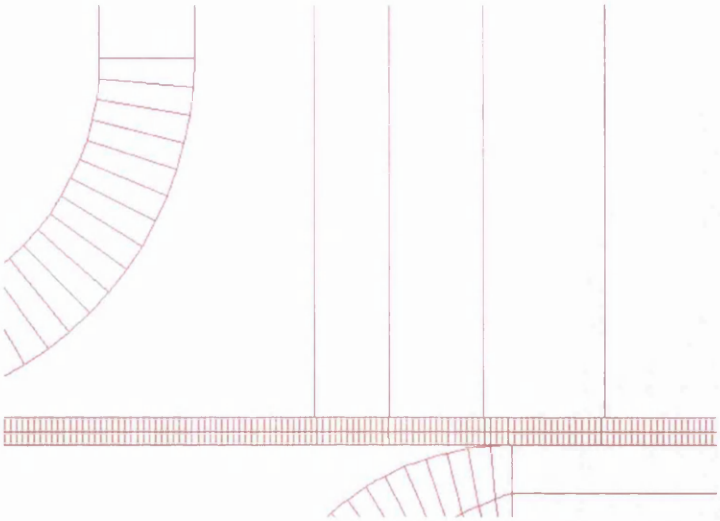

Figure 29: Initial mesh

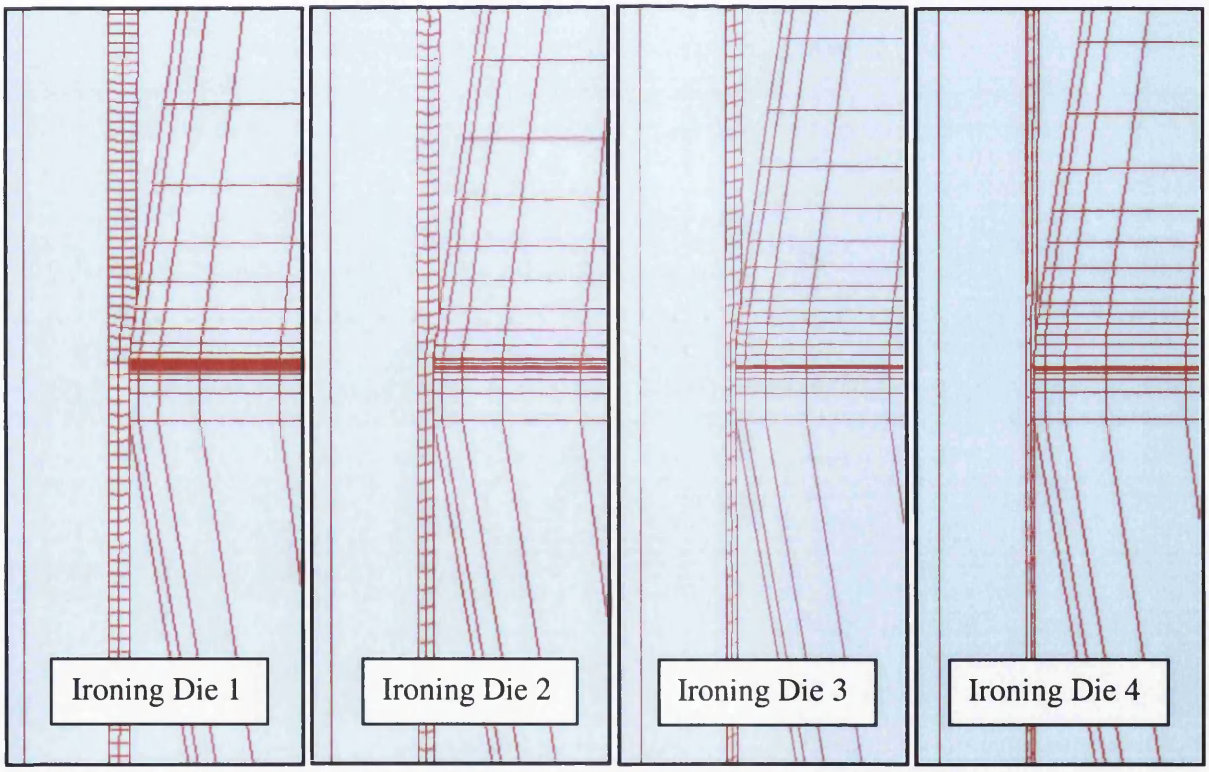

Figure 30: Ironing dies, showing decrease in density at each die

3.3.2.6.Automated Stage Termination

The continuity of the model has been achieved largely due to the addition of an "automated stage termination" piece of code. It is now possible to terminate a stage when a pre-defined point passes through a given plane. The DWI model uses this several times to automate stage transferral when the strip leaves a blankholder or ironing ring. The details of this feature and the associated differences implied to the model can be seen in more detail in Appendix A.i.

3.4. DWI Related Experiments

3.4.1. Chime Wrinkling Hypothesis

3.4.1.1.Ironing Ring Geometry

During simulations of the DWI model setting up the ironing die constraints had a significant effect – enough to warrant an investigation of the ironing ring geometry. Keeping the same ironing ring but changing the constraints, it's possible to understand the role of different aspects of the ring's geometry (Figure 31).

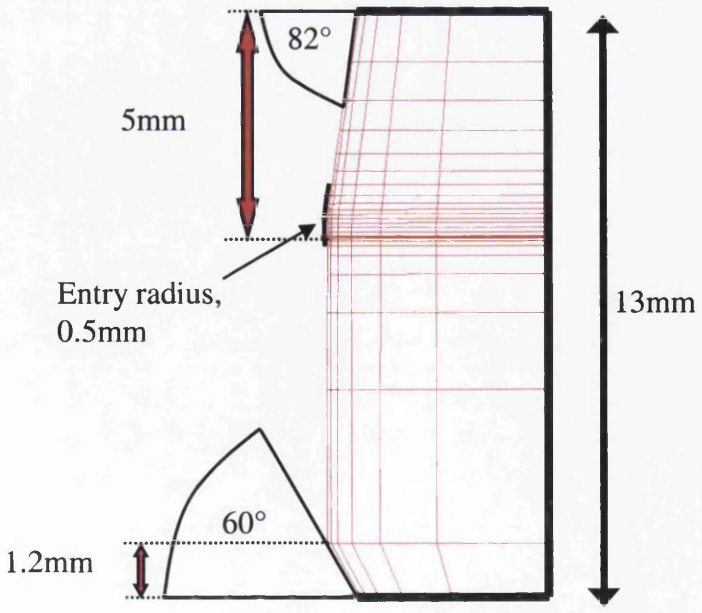

Figure 31: Typical Ironing Die Geometry

All the properties of its geometry are connected to the fact that it behaves in a perfectly elastic manner (with very high Young's modulus – Tungsten Carbide, 620GPa). The top taper length affects how much elastic deformation the die undergoes in the upper region of the deformation area. The top taper angle also affects the amount of elastic deformation in the same area, but it's main purpose is in setting the maximum strain rate possible – maximum because the angle (as measured above), will become larger due to elasticity, and hence the strain rate reduced. The bottom taper length and angle seem to be for purely controlling the amount of elastic deformation of the die in the lower region of the deformation area. The face length then is to provide continuity between the potentially differing amounts of elastic deformation between the upper and lower regions. The entry radius is there to prevent fracturing on entry.

With further work it would be possible to predict how much elasticity occurs and where for any given ring geometry.

3.4.1.2.Ironing Ring Percentage Reduction Threshold

Through simulations it has been noted that sometimes the punch nose loses contact with the strip, and so possible causes for this circumstance were investigated. An area that seems to bear some correlation is that when the ironing % reduction is too high, then the strip would leave the punch nose. To this end the notion of the % reduction threshold was developed.

"% Reduction Threshold" – the ironing % reduction level at which contact is lost between strip and punch nose.

For each tooling set-up there exists a % reduction threshold: -

Threshold = function (Set, IRgeom, Frel),

where,

Set is the strip entry thickness to the ring,

IRgeom the ring geometry,

Frel the relative friction levels, strip/die : strip/punch

Examples

- Given the incoming gauge and ring geometry it is the relative friction levels that govern the threshold
- Fixed friction coefficients and a specified ring geometry yields a maximum entry gauge

3.4.1.3.Tapered Strip in Ironing Ring

Passing a tapered strip through an ironing ring, and taking note of normal contact pressure at the punch nose, the following was observed: -

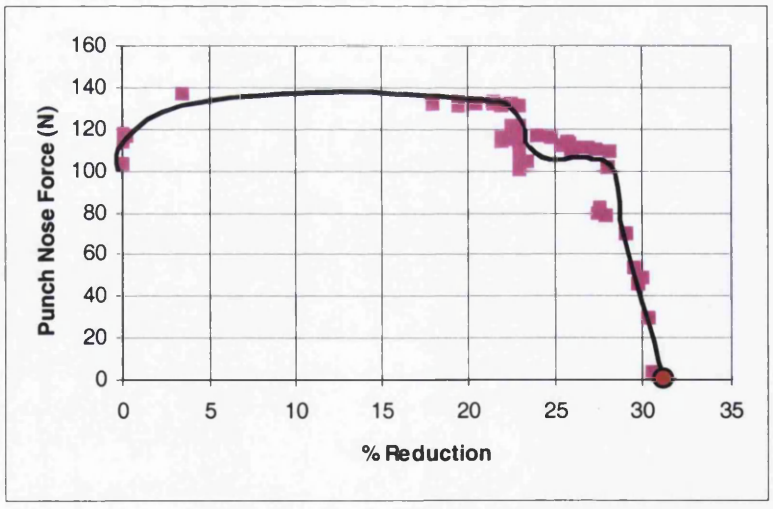

Figure 32: % reduction threshold

3.4.1.4.Chime Wrinkling?

As the DWI model is set-up, the % reduction in the ironing rings is very near its threshold, ≈ 31%. Also noted was, near the threshold the punch nose contact is very sensitive. This prompts the question; under near threshold conditions could small deviations in the circumference cause a strain field around the chime, due to widely varying forces around the circumference?

3.4.2. Doming

In addition to a doming model attached at the end of the DWI model, an independent doming model (A.ii) was made in order to answer a number of questions:-

- How many elements through the thickness of the strip are required?
- What element type is most appropriate for this model?
- For the given dome geometry what is the optimum dome depth with respect to its reversal pressure?
- How does the dome ring pressure affect the forming/reversal pressure of the dome?
- How do the reversal tests compare to the corresponding tests with the DWI model?

3.4.2.1.Element Type and Through Thickness Density

In order to obtain the true solution of the reversal pressure the standard element was used keeping everything else constant other than increasing the number of elements through the thickness, and so using the assumption that the error tends to zero as the mesh density increases. A further two element types were then looked at with a various number of elements through the thickness taking note of the reversal pressure with each simulation.

D L Davies dave.davies@orange.net

Using an implicit code the best way to run a reversal pressure test is to use an arc length load case method. It has the benefit of a different solution when unloading from a bifurcation point, which in this case is the point where reversal occurs. This can then easily be displayed graphically by showing a trace of the movement of any node near the nose of the dome as it varies with the internal pressure applied (Figure 33). The reversal pressure is taken to be the point at which the incremental internal pressure first becomes negative, i.e. when the curve first doubles back on itself.

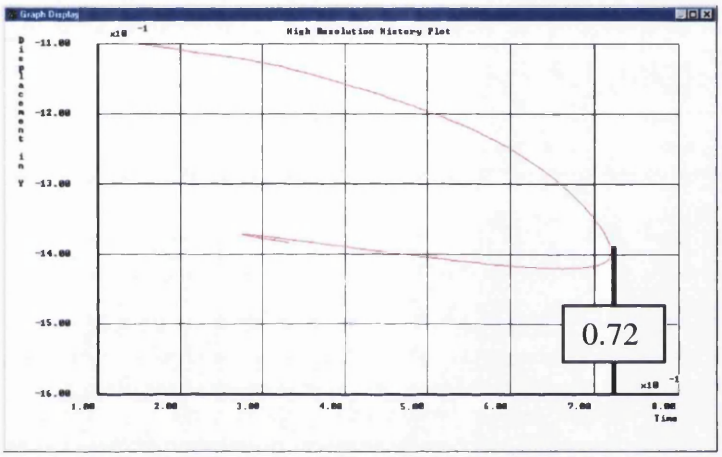

Figure 33: Arc length buckling load curve

Element type	Thickness	PSI(N/mm^2)	
		N/mm^2	psi
Standard element	2	0.843	121
	3	0.723	104
	4	0.720	104
	5	0.720	104
	6	0.733	106
	7	0.732	105
F-bar element	2	0.721	104
Double density	2	0.711	102
Half-density	2	0.795	114
	3	0.733	106
	4	0.736	106
Enhanced element	2	0.725	104
	3	0.733	106
	4	0.728	105

Table 2: Element type and thickness effect on dome reversal pressure

With reference to Table 2, the standard element results indicate the reversal pressure is tending to approximately 0.73N/mm^2 using the default mesh density across the strip as the number of elements through the thickness increases. Also it is noticed that increasing the mesh density across the strip has the tendency of lowering the reversal pressure. Combining these two observations it's a reasonable assumption to say the reversal pressure is tending towards 0.725N/mm^2 (≈102psi). The enhanced element is probably the most accurate, but for the slight edge it has on accuracy over the F-bar element, its computational cost makes the F-bar a better option. A similar argument follows with how many elements to use through the thickness, and so the F-bar element with 2 elements through the thickness is used for the model.

3.4.2.2.Dome Depth

A study into how the dome depth affects the reversal pressure was looked at. This involved using the doming model keeping everything constant other than changing the distance the dome post travels in the dome forming stage, and taking note of the reversal pressure for each test. Additionally for each run the amount of pull-down was noted; pull-down being the distance the can height is reduced as a result of doming the can (Table 3). This measurement will be used later to tie in results with the DWI model for fair comparisons.

Dome depth(mm)	Reversal Pressure (Nmm^{-2})	Pull-down (mm)
10	0.721	2.43
11	0.738	3.02
12	0.764	3.40
12.5	0.768	3.52
13	0.766	3.54
13.5	0.765	3.54
14	0.906	3.66
14.3	0.915	3.78
14.5	0.923	3.91

14.7	0.910	3.78
15	0.917	3.90
15.5	0.770	4.02
16	0.773	4.14

Table 3: Dome depth effect on reversal pressure

It can be seen there are 3 different types of failure with the range of dome depths used. For the shallower dome depths the mode of collapse is a "base" failure (Figure 34), and for the deeper depths the mode is a "nose" failure (Figure 36). Someway between these two modes is a combination of the two, at which the optimum depth occurs, and so is called a "mixed" failure (Figure 35). For deeper domes the reversal pressure increases slightly and proportionally with depth up to the point where the dome depth is too large to be formed with the given tooling. Although these reversal pressures are higher than d=16 they are significantly lower than the optimum dome depth. A summary of the results can be seen in Figure 37.

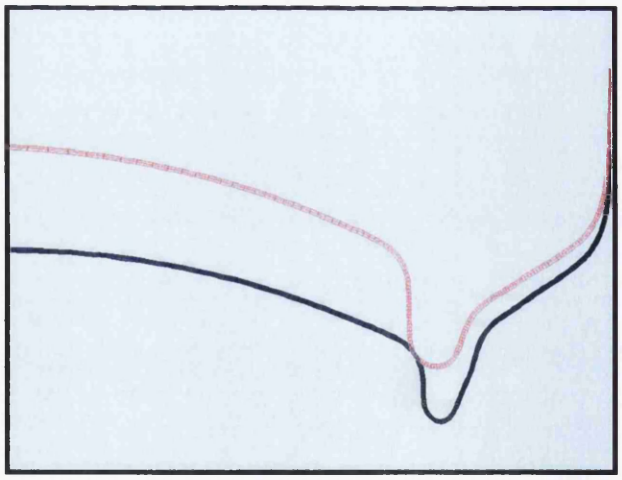

Figure 34: "Base" mode failure

D L Davies dave.davies@orange.net

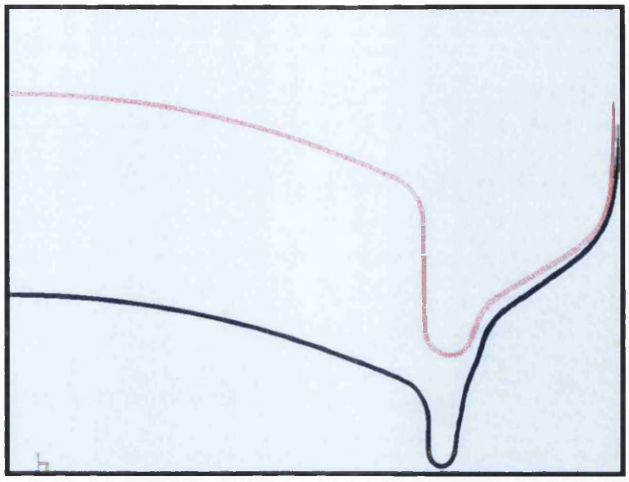

Figure 35: "Mixed" mode failure

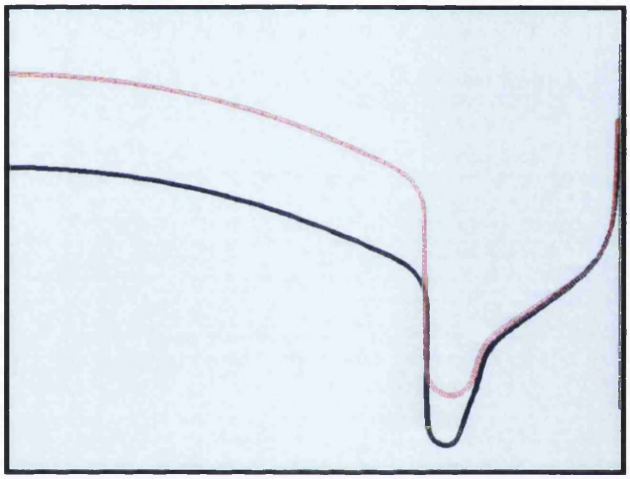

Figure 36: "Nose" mode failure

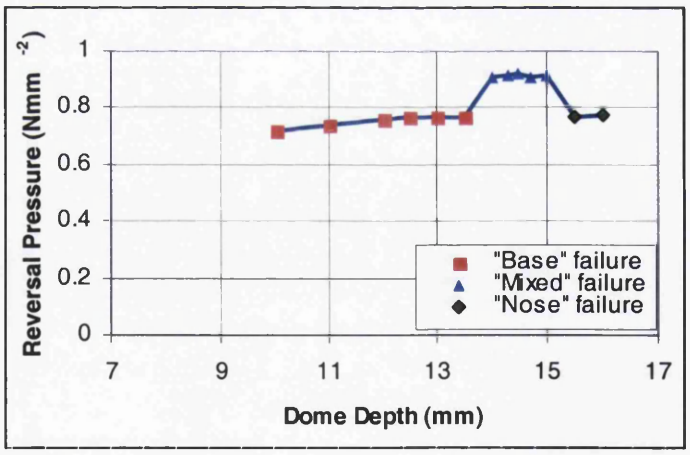

Figure 37: Dome depth effect on dome reversal pressure

3.4.2.3.Dome Ring Pressure

Using the optimum dome depth calculated above for the given tool set-up, the effects of varying the dome ring pressure was investigated. The range of pressures varied from 1 to 6 Nmm^{-2} where $1Nmm^{-2}$ is equivalent to a clamping force of 3177N due to the area over which the pressure is applied to the dome ring. Once again the pull-down was also noted for each test along with the reversal pressure as defined in the above experiments, (Table 4) with the corresponding graphs in Figure 38 and Figure 39.

Ring Pressure (Nmm^{-2})	Reversal pressure (Nmm^{-2})	Pull-down (mm)
1	0.857	6.83
2	0.867	6.19
2.5	0.882	6.07
3	0.899	5.95
3.5	0.834	5.80
4	0.809	5.10
4.2	0.798	4.83
4.4	0.789	4.57
4.7	0.776	4.28
4.9	0.771	4.14
5	0.767	3.91
5.1	0.764	3.63
5.5	0.759	3.46
6	Breaks	0.72

Table 4: Dome ring pressure effect on reversal pressure

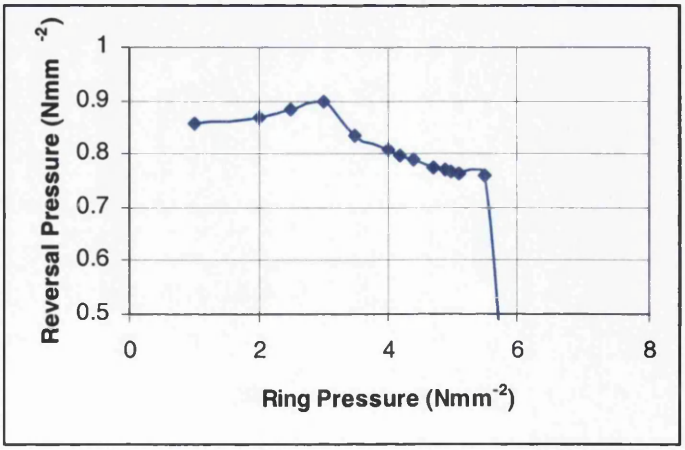

Figure 38: Dome ring pressure vs reversal pressure

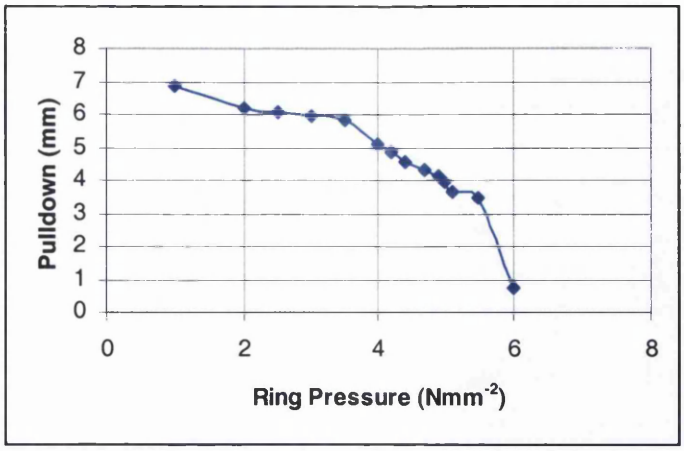

Figure 39: Dome ring pressure vs pull-down

3.4.2.4.DWI vs Doming Model

To compare the two models as fairly as possible, the DWI model is run using the doming parameters as calculated in the doming model achieving the maximum reversal pressure, i.e. dome depth 14.5mm and dome ring clamping such that the pull-down was 5.95mm. Two comparisons can then be carried out to test the differences between the two simulations. The first is to compare the geometry of the formed can base to see if any significant differences exist (Figure 40); the second is to check the calculated reversal pressure of both models.

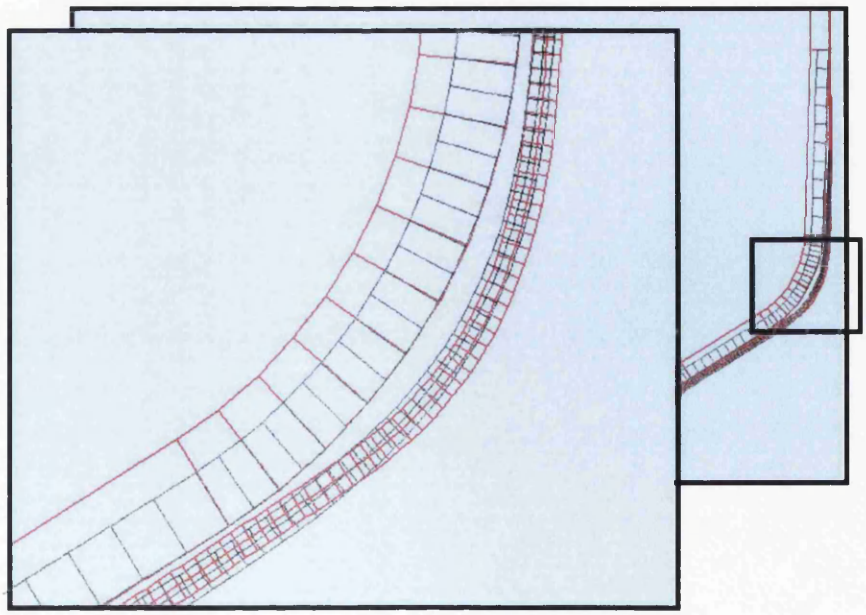

Figure 40: Geometry difference between DWI and doming models at the chime shoulder

D L Davies dave.davies@orange.net

Figure 40 shows the superposition of the two models, DWI and doming, using the same doming parameters (dome depth 14.5, 6mm pull-down), after dome forming and immediately prior to the reversal stage. The red is the Dwi model, and black the doming. Looking at the two in a reasonable scale (top picture), the strip position appears to fit on top of each other exactly. Even when zoomed in on the shoulder of the chime there isn't a large difference that can be noted. If these two strips' material properties were to be re-initialised at this point then the difference in geometry alone would not affect the reversal pressure. This directly implies that if the results of the reversal tests are different then it must be attributed to the difference in the material history and hence the current material state, and not due to the slight difference in formed shape.

A point to note however on the slight difference in geometry is that the DWI model has the shoulder of the chime slightly bulged outward. It is feasible that if this bulge were enough so that the can wall diameter to be less than the maximum diameter at the bulge then it could drastically change the behaviour of the can's integrity in the axial direction. That is to say buckling of the can wall would occur at a lower pressure than that of a straight can wall, and so the DWI model would predict a lower axial strength than the doming model for the same doming parameters.

The cause for this slight geometry difference is obviously to do with the material history prior to the dome forming. One way of displaying the difference between the two is to look at the plastic strains of the material (Figure 41), and it can be seen that it is consistently higher for the DWI (left), and consequently greater work-hardening of the material and more springback at the punch shoulder radius.

D L Davies dave.davies@orange.net

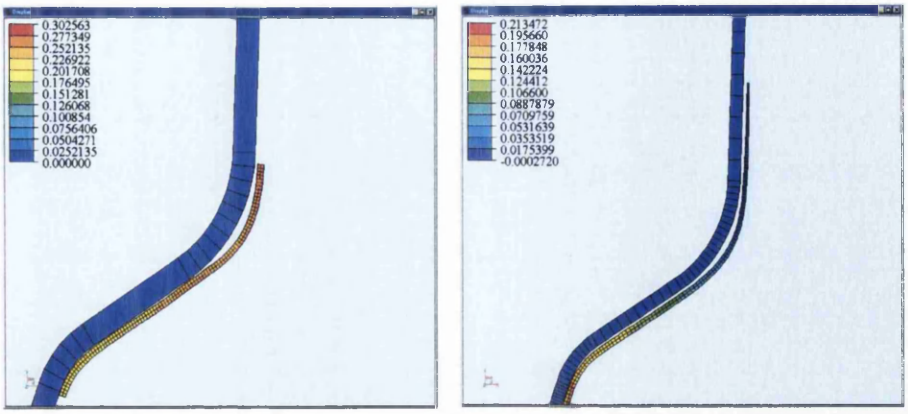

Figure 41: Plastic strain difference between DWI and doming models at chime shoulder

Another measure to compare the two models is to run each with a large variety of parameter settings and comparing the reversal pressures of like settings (Table 5, Table 6). Like settings being essentially when the dome depths are both the same and the pull-down is approximately equal. For the latter, in most cases a combination of test cases may need to be averaged in order to compare like pull-down settings (see example comparison measurement below)

Dome info			Ring pressure		Reveral pressure		Pulldown
Dome travel	Springback	Dome depth	(Nmm^{-2})	(N)	(Nmm^{-2})	(p.s.i.)	(mm)
11	0.1	10.9	2	6354	0.793	114	3.74
11	0.1	10.9	3	9531	0.778	112	3.55
11	0.1	10.9	4	12708	0.764	110	3.45
11	0.1	10.9	5	15885	0.738	106	3.09
11	0.1	10.9	6	19062	0.722	104	1.78
11	0.1	10.9	7	22239	0.753	108	0.57
11	0.1	10.9	8	25416	0.739	106	0.26
11	0.1	10.9	9	28593	0.745	107	0.22
12	0.65	11.35	1	3177	0.86	124	4.2
12	0.1	11.9	2	6354	0.876	126	4.39
12	0.1	11.9	3	9531	0.857	123	4.21
12	0.1	11.9	4	12708	0.838	121	4.02
12	0.1	11.9	5	15885	0.768	111	3.54
12	0.1	11.9	6	19062	0.836	120	2.31
13	0.6	12.4	1	3177	0.934	134	5.02
13	0.1	12.9	2	6354	0.928	134	5.11
13	0.1	12.9	3	9531	0.909	131	4.92
13	0.1	12.9	4	12708	0.871	125	4.48

D L Davies dave.davies@orange.net

13	0.1	12.9	5	15885	0.913	131	3.67
13	0.1	12.9	6	19062	0.875	126	2.51
14	0.6	13.4	1	3177	0.867	125	5.82
14	0.1	13.9	2	6354	0.872	126	5.82
14	0.1	13.9	3	9531	0.908	131	5.61
14	0.1	13.9	4	12708	0.897	129	5.05
14	0.1	13.9	5	15885	0.906	130	3.7
14	0.1	13.9	6	19062	0.819	118	2.70
15	0.6	14.4	1	3177	0.851	123	6.55
15	0.1	14.9	2	6354	0.856	123	6.55
15	0.1	14.9	3	9531	0.899	129	6.31
15	0.1	14.9	4	12708	1.002	144	5.25
15	0.1	14.9	5	15885	0.917	132	3.94
16	0.55	15.45	1	3177	0.845	122	7.36
16	0.15	15.85	2	6354	0.856	123	7.26
16	0.1	15.9	3	9531	0.891	128	7.01
16	0.1	15.9	4	12708	0.830	120	5.78
16	0.1	15.9	5	15885	0.773	111	4.18

Table 5: Doming model reversal results

Dome info			Ring pressure		Reverse pressure		Pulldown
Dome travel	Springback	Dome depth	(Nmm^{-2})	(N)	(Nmm^{-2})	(p.s.i)	(mm)
11	0.1	10.9	3	5160	0.759	109	3.67
11	0.1	10.9	4	6880	0.743	107	3.48
11	0.1	10.9	5	8600	0.784	113	2.83
11	0.1	10.9	6	10320	0.673	97	1.52
12	0.1	11.9	3	5160	0.791	114	4.33
12	0.1	11.9	4	6880	0.777	112	4.14
12	0.1	11.9	5	8600	0.710	102	3.25
12	0.1	11.9	6	10320	0.687	99	1.73
13	0.1	12.9	3	5160	0.802	115	5.01
13	0.1	12.9	4	6880	0.804	116	4.73
13	0.1	12.9	5	8600	0.719	104	3.33
13	0.1	12.9	6	10320	0.690	99	1.83
14	0.1	13.9	3	5160	0.793	114	5.67
14	0.1	13.9	4	6880	0.818	118	5.16
14	0.1	13.9	5	8600	0.753	108	3.81
15	0.1	14.9	3	5160	0.797	115	6.39
15	0.1	14.9	4	6880	0.825	119	5.42
15	0.1	14.9	5	8600	0.756	109	3.95
16	0.1	15.9	3	5160	0.806	116	7.10
16	0.1	15.9	4	6880	0.836	120	5.69
16	0.1	15.9	5	8600	0.766	110	4.32

Table 6: DWI model reversal results

The dome reversal results from Table 5 and Table 6 can be compared by matching the dome depth and then finding a matching pull-down value. In most cases an exact pull-down value doesn't exist and so a weighted average system is utilised in order to compare like with like. For example, the DWI model with 11mm dome travel and 3.67mm pull-down has a reversal pressure of 109psi. This result can be compare with the dome model with 11mm dome travel and the combination of the 3.55mm and 3.74mm pull-down results, 112 and 114psi respectively. Firstly, the dome results must be linearly weighted such that they correspond to a pull-down value of 3.67. In this case the approximation of an equal weighting is sufficient, i.e. 113psi. The results can then be compared to see how the models differ. For this example,

109 / 113 = 96.6%, (i.e. DWI 3.4% lower than doming)

This was done for all the possible comparisons and the results of which can be summarised by the following statistics. The DWI model reversal pressures are a mean average 8.2% lower than the doming results with a 7% standard deviation. In quartile terms, the 1st quartile is 3.6%, median 7.6% and 3rd quartile 13%, and results beyond the 3rd quartile were normally for high reversal values in the doming model.

3.5. Results and Validation

The means by which the DWI model is to be validated is twofold. Firstly by directly comparing the formed cans geometry with the simulated can. This will give a measure of how accurate the final formed can is. This means of validation is made stronger by the fact geometry comparisons are made after each forming stage possible in the process. The 2nd method of validation is to ensure the process is simulated correctly. This is done by outputting a pseudo-force trace that can be compared with an actual force trace of the DWI process.

3.5.1. Profile Plots

Profile plots, which show the gauge at multiple heights from the base, have been compared to real physical data for each stage of the process (Figure 42 to Figure 47). Physical measurements are taken on the straight can wall only, whereas the model can easily give a complete profile from base to its top. This accounts for the cup having data collected above 10mm, and the other stages only having data measured above 25mm due to the height of the chime formed by the redraw punch.

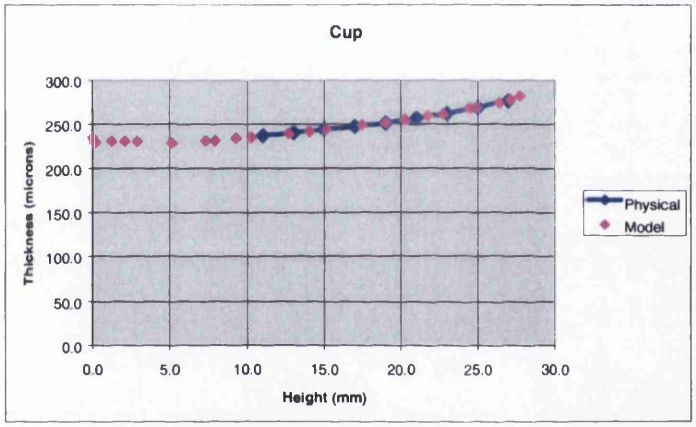

Figure 42: Profile comparison of cup

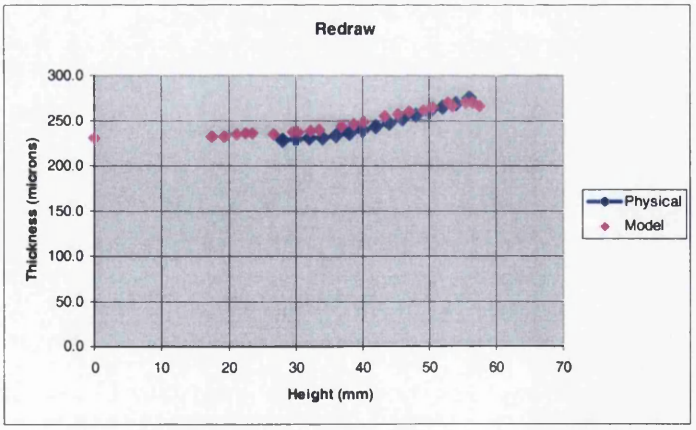

Figure 43: Profile comparison after redraw stage

D L Davies dave.davies@orange.net

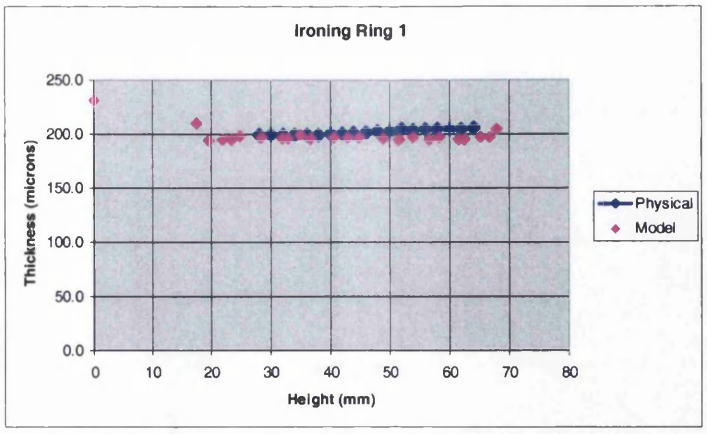

Figure 44: Profile comparison after 1st ironing ring

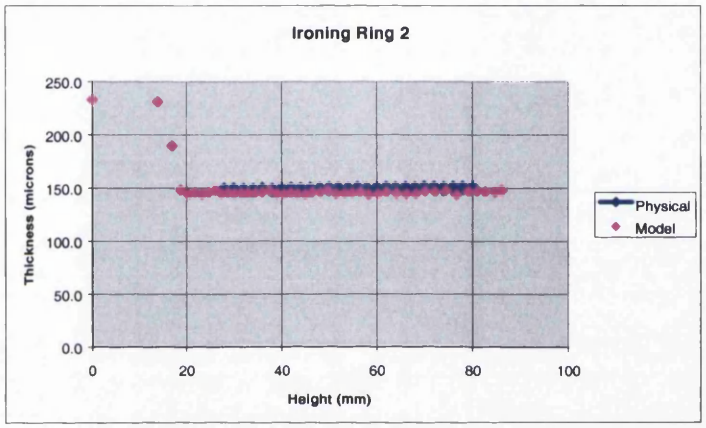

Figure 45: Profile comparison after 2nd ironing ring

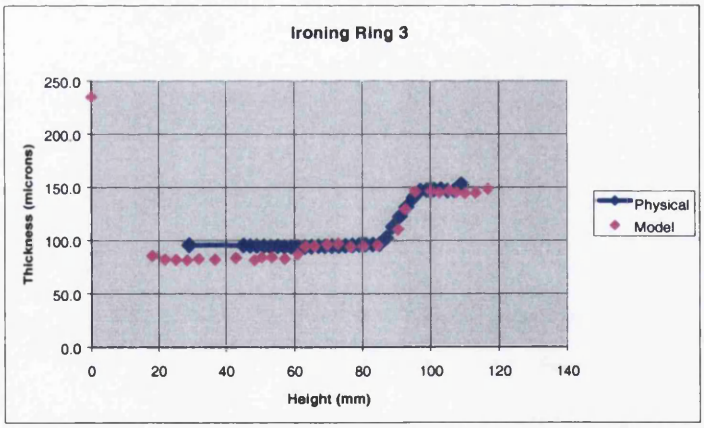

Figure 46: profile comparison after 3rd ironing ring

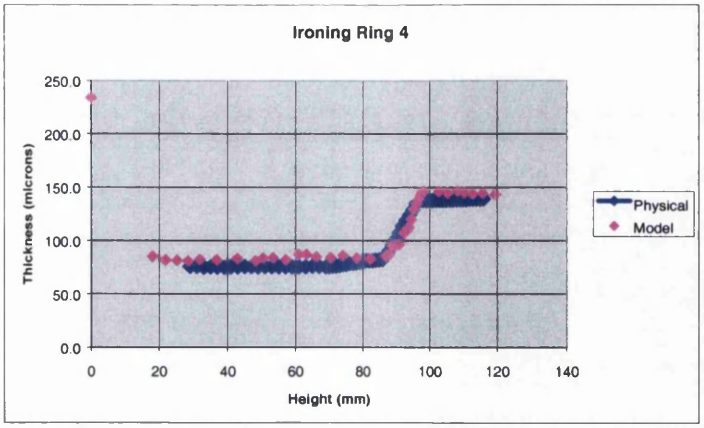

Figure 47: profile comparison after 4th ironing ring

The model closely follows the results of the physical data. Calculating the area enclosed between the two curves over the range existing for the physical data yields a measurement of error. The cupping has very good accuracy, less than 1% error with an increasing amount in further stages, 5% error in the 4th ring. The only area where statistically the error is greater than 5% occurs during the 3rd ring. This can be accounted for by the fact the model has employed tandem ironing (3rd and 4th ring simultaneously), whereas in the experiment the 4th ring was omitted in order to get measurements for the 3rd ring only. Taking this into account and only looking at the height above 67mm (Figure 46) the error is approximately 3%.

3.5.2. Force Trace

In the course of the DWI forming analysis, a force trace (Figure 48) is produced. The force trace indicates the force the punch requires in order to achieve its displacement, and can be thought of as the resistance to motion of the punch. The force trace can be used to identify areas of concern, help with tool spacing for ironing rings, or develop a strategy with ironing reduction ratios to increase efficiency.

D L Davies dave.davies@orange.net

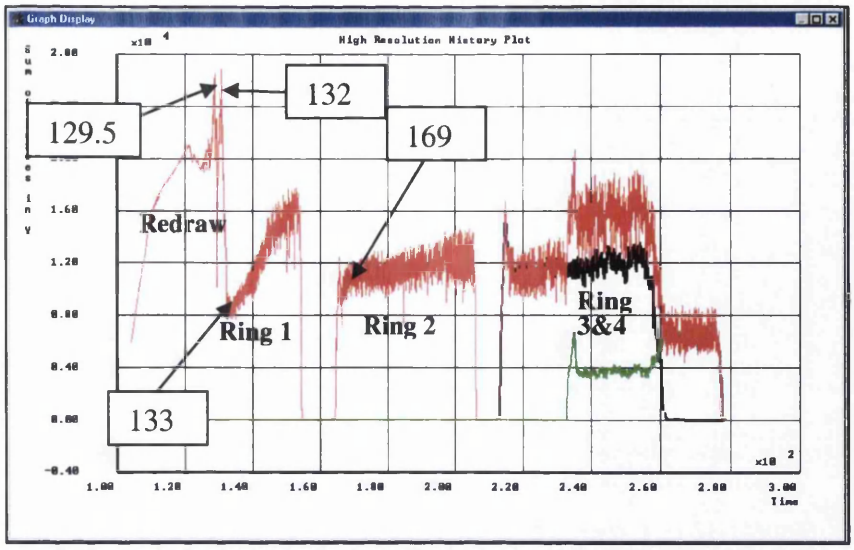

Figure 48: Calculated force trace for redraw punch in body maker

The higher the ironing ratio, the greater the resistance and thus the higher the force. This is illustrated in the 1st ironing ring where due to the increasing can wall thickness after the redraw stage (Figure 43), the ironing ratio increases as the can passes through it. This explains the significant gradient during the 1st ironing ring force trace only, and not in any of the other ironing rings since the ironing ratio in the subsequent ironing stages is equal from the top to the bottom of the can wall (Figure 44 - Figure 47). The slight gradient in the 2nd ring is purely attributed to the work hardening of the material.

The red line of Figure 48 is the sum of all reaction forces, and so is a measure of the force on the punch. The black and green lines are the components of the 3rd and 4th rings respectively. This section demonstrates the employment of tandem ironing.

As a comparison, during the forming of the cans to be validated, the force trace of the punch in the body maker is recorded. The measured trace has much noise and variability, but when smoothed (Figure 49) using a moving average, the key features of the trace can be seen and parallels those seen in Figure 48.

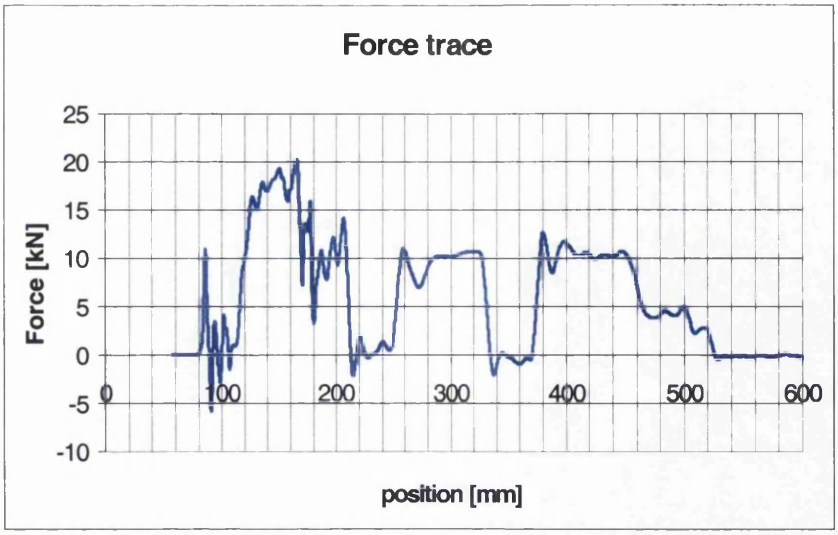

Figure 49: Smoothed measured force trace of redraw punch in body maker

The timings seen in Figure 48 identified by the arrows correspond to Figure 50 to Figure 53. These figures show what is happening at the corresponding times and help describe the some of the features of the force trace.

The peak at 129.5 is caused by the onset of ironing in the redraw die just prior the release of the blank holder (Figure 50) at which point there is an immediate drop in force. This quickly starts rising again though due to the combination of the increasing ironing ratio in the redraw die as well as the initialisation of ironing in the 1st ring. This force reaches a peak near 132 at which time the material is about to leave the redraw die (Figure 51).

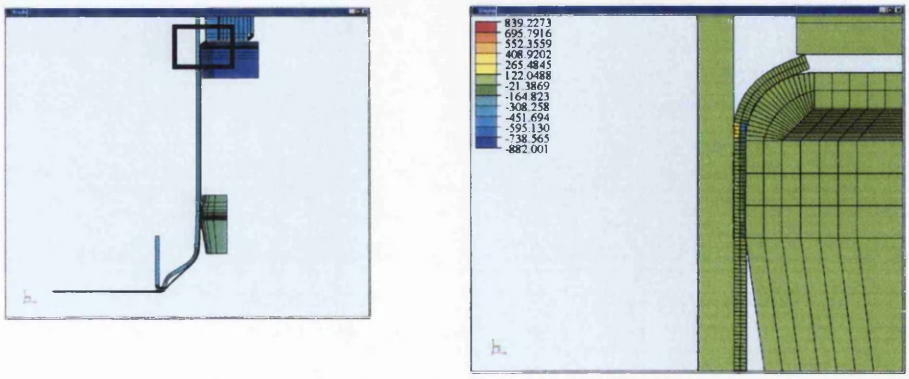

Figure 50: First peak in redraw section (time=129.5)

D L Davies dave.davies@orange.net

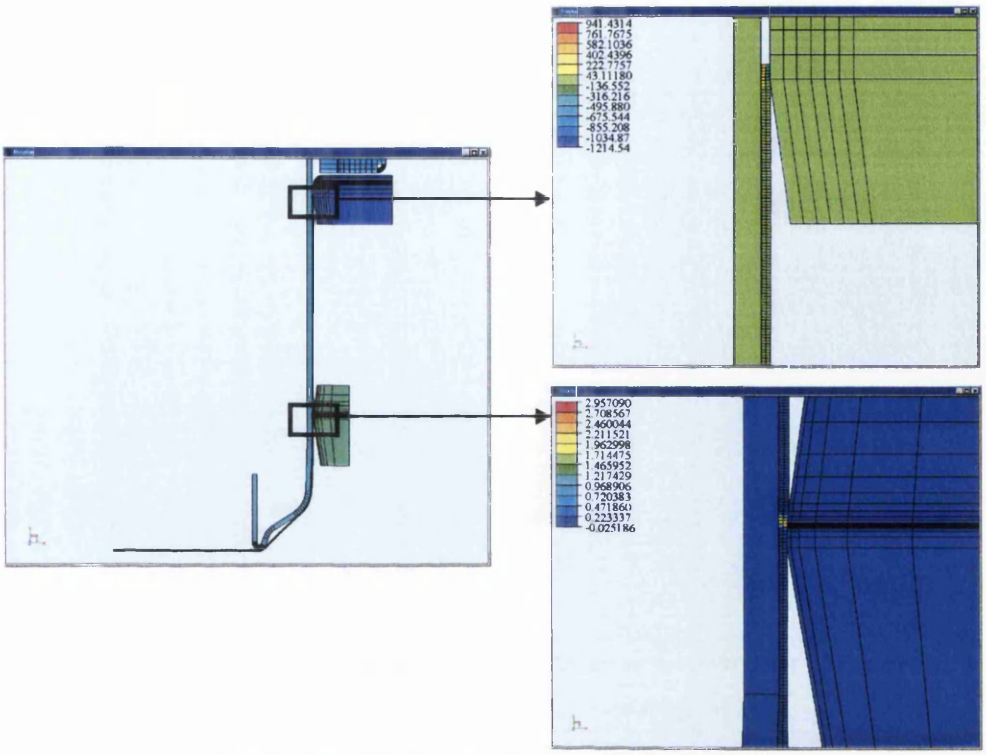

Figure 51: Second peak of redraw section (time=132)

The sudden drop in force is due to material leaving the redraw die where ironing was occurring. The force at 133 (Figure 52) is exclusively the resistance to the ironing in the 1st ring. As explained above this resistance increases during this stage due to the can wall being thicker towards the top and hence an ever increasing ironing ratio. However, after this stage the wall thickness is fairly uniform, such that in subsequent ironing stages the ironing ratio will remain constant for that stage (Figure 53).

D L Davies dave.davies@orange.net

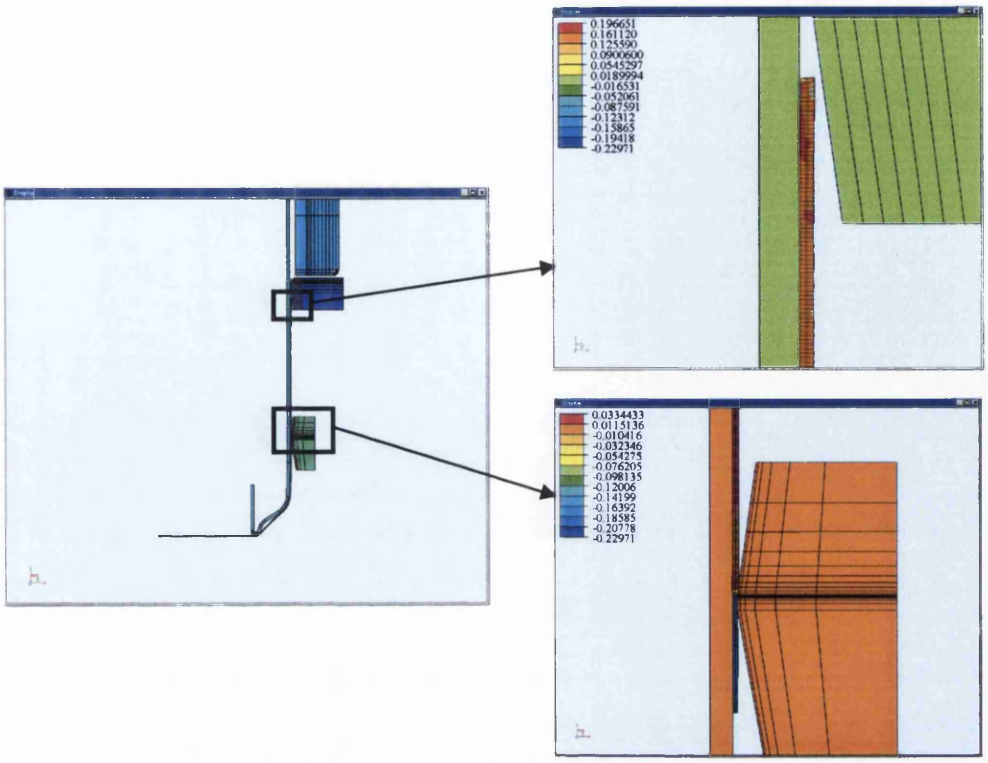

Figure 52: Start of slope of 1st ironing ring section (time=133)

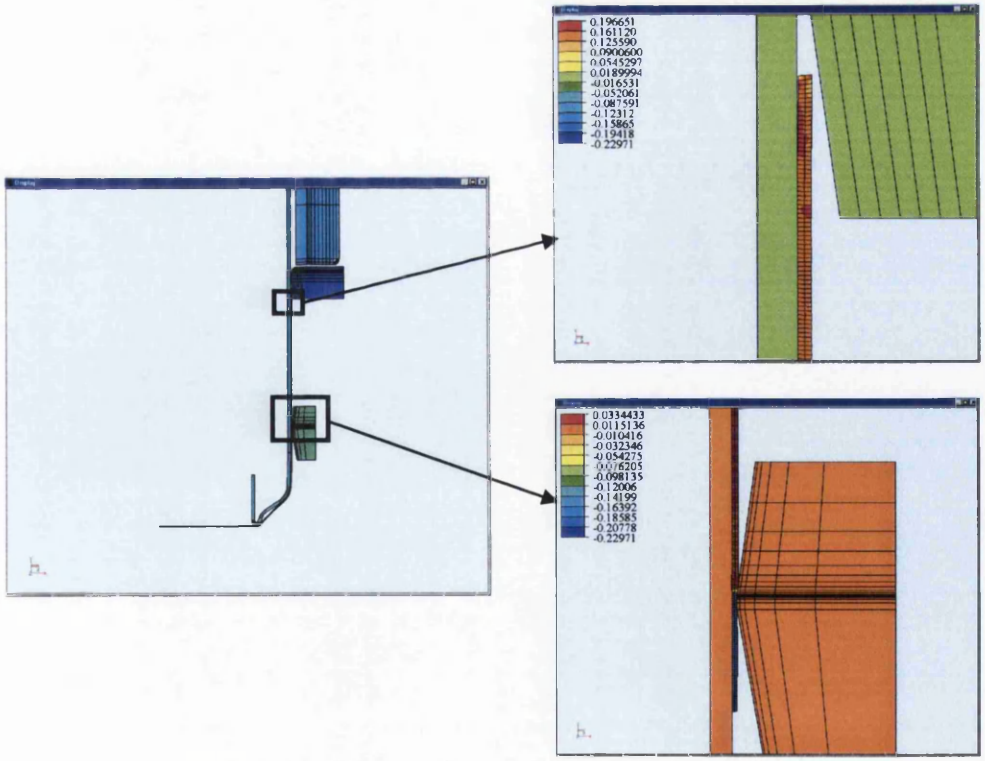

Figure 53: Start of 2nd ironing ring section (time=169)

4. FACTORIAL ANALYSIS

4.1. Introduction

Here's an illustrative example to explain what factorial analysis is and what its uses are. The following will work through and explain how a 3-level factorial analysis of some given data is made, but first the idea of what factorial analysis is in a very simple case is described, with the help of Figure 54.

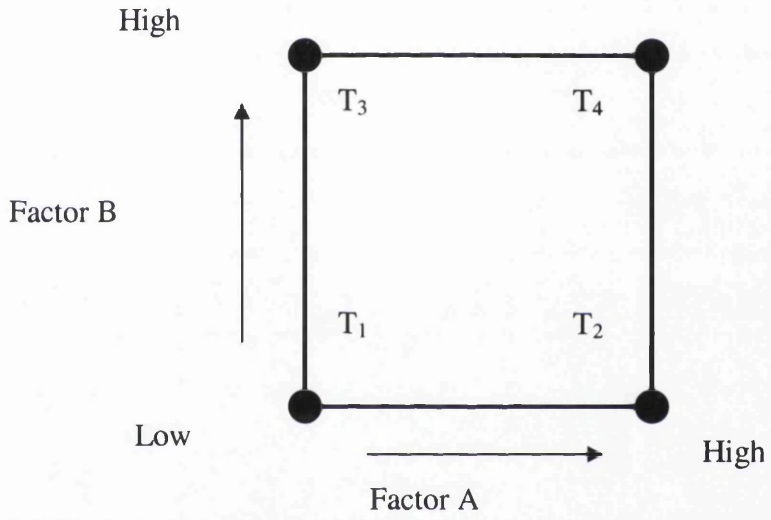

Figure 54: Basic illustration of factorial analysis

Where factor A, B are two control parameters, e.g. factor A maybe thickness and B weight. T_i's are correspondingly the output response value, e.g. T_1 is the temperature, say, corresponding to the input data of factors A and B both being low.

So in table form the above illustration is shown in Table 7 below.

Factor A	Factor B	Response
Low	Low	T_1
High	Low	T_2
Low	High	T_3
High	High	T_4

Table 7: Basic factorial analysis data table

D L Davies dave.davies@orange.net

Now in this case there are two numbers that will be generated from the data in the table. Note two corresponds to the number of factors, namely A and B, and so these two numbers correspond to the effects of A and B.

These "effects" are worked out by averaging all the response values corresponding to a factor being high and comparing that with the average of all the response values corresponding to the factor being low. For example A's effect is worked out by taking the difference between the average response values when A is high, T_2 and T_4, and the average response values when A is low, T_1 and T_3, i.e.

$$A'sEffect = \tfrac{1}{2} \times (T_2 + T_4 - T_1 - T_3)$$

An interpretation of what this value is, is the gradient of how the response typically changes as A goes from low to high. So if A is large and positive (negative) then it means that on average as A goes from low to high the response value will increase (decrease) significantly.

Similarly then for factor B,

$$B'sEffect = \tfrac{1}{2} \times (T_3 + T_4 - T_1 - T_2)$$

The only real difference between this example and a 3-level factorial analysis, is that there's an extra input value each factor could take, i.e. factor A could be low, medium or high instead of just low or high. This extra input value turns this analysis tool into a non-linear trend finder.

The uses for a 3-level factorial analysis are: -

- Scientific interpretation of results
- Finds trends – linear and non-linear

- Generates a model for predicting (interpolating)

4.2. Worked Example

Figure 55 and Table 8 show the geometry of a punch that is being investigated parametrically to see what effect each parameter has on the dome reversal pressure.

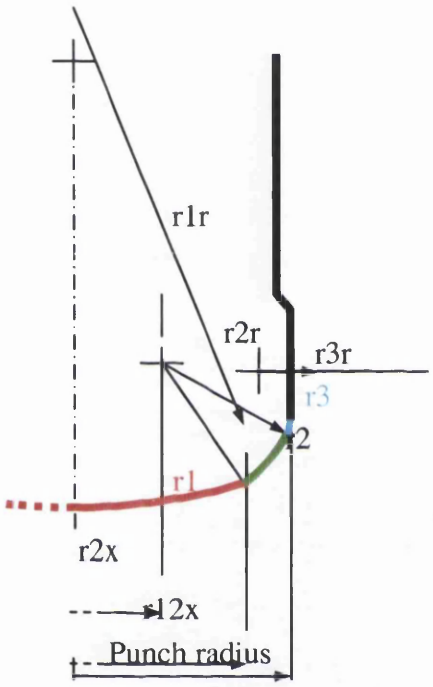

r1r - radius r1

r12x - x coord of shoulder

r2r - radius r2

r2x - x coord of r2's centre

Figure 55: Three-radius punch with parameters highlighted

		Factor	High(h)	Low(l)	Mid(m)
Radius 1	r1r	A	1.75	1.55	1.65
Radius 2	r2r	B	0.95	0.75	0.85
Rad 2 centre	r2x	C	0.62	0.55	0.60
Shoulder x	r12x	D	1.75	1.55	1.65

Table 8: Worked example factor data information

So there are in total 81 experiments to do to cover all possibilities. A sample can be seen in Figure 56,

D L Davies dave.davies@orange.net

A r1r	B r2r	C r2x	D r12x	Dome Reversal(psi)
.	.	.	.	.
	.	.	.	.
h	h	l	l	419
l	l	m	l	461
m	l	m	l	438
h	l	m	l	378
l	m	m	l	453
.	.	.	.	.
.	.	.	.	.

Test conditions

Response

I.e. r1r = 1.55 r2r = 0.85 r2x = 0.6 r12x = 1.55

Figure 56: Worked example sample data

The idea now is to break up the analysis into parts.

- Split results up for each factor
- For each factor, split the results up for each case
- Calculate the average response for each case

Example: Results can be split according to factor B

Factor B has three cases; low, medium & high with corresponding averages 399, 420, 380 p.s.i. Table 9 is a summary table breaking down the results into the primary effects (effects A to D) which can also be seen graphically in Figure 57

Factor	A	B	C	D
Low	425.3	399.2	399.9	417.1
Medium	399.4	420.0	401.4	407.0
High	374.2	379.9	397.7	374.8
Average	399.7	399.7	399.7	399.7

Table 9: Worked example summary data for main effects

D L Davies dave.davies@orange.net

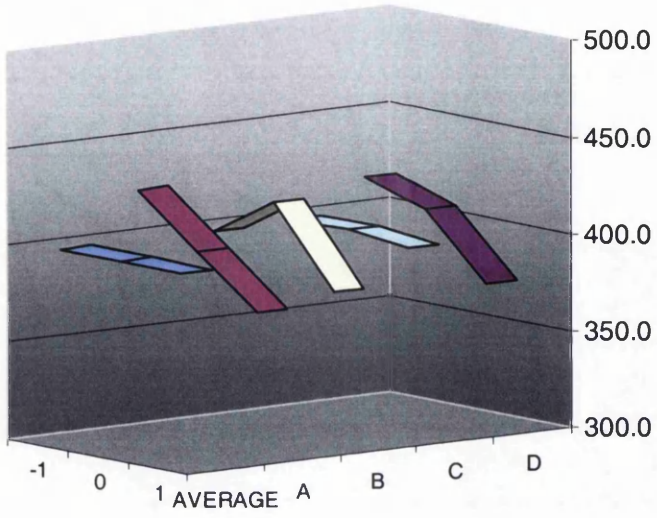

Figure 57: Graphical interpretation of primary effects

4.2.1. Interaction Effects

So far only the effect of how each parameter independently changes the response has been considered – something that could be done just by paying close attention to the results as you get them. Something more subtle than this though is the concept of "interaction effects". An interaction effect measures the dependence of a factor upon one or more other factors. For example, by changing factor A, say, the response value may become far more sensitive to factor B, in which case there must be an interaction effect between A and B. As before there is a formula that calculates this interaction effect.

In general each main (primary) effect in a k-level factorial analysis will have k cases. For this example each main effect has 3 cases (low, medium & high). But interaction effects will have k^{i+1} cases, where i corresponds to an i^{th} order interaction. For this example each 1^{st} order interaction (B & D for example) has $3^2 = 9$ cases.

It's of value to see visually what's going on to understand more clearly what an interaction effect is.

D L Davies dave.davies@orange.net

Figure 58 is a graph showing how the response (p.s.i.) changes as A goes from low to high under the three cases of additionally B being low, medium & high.

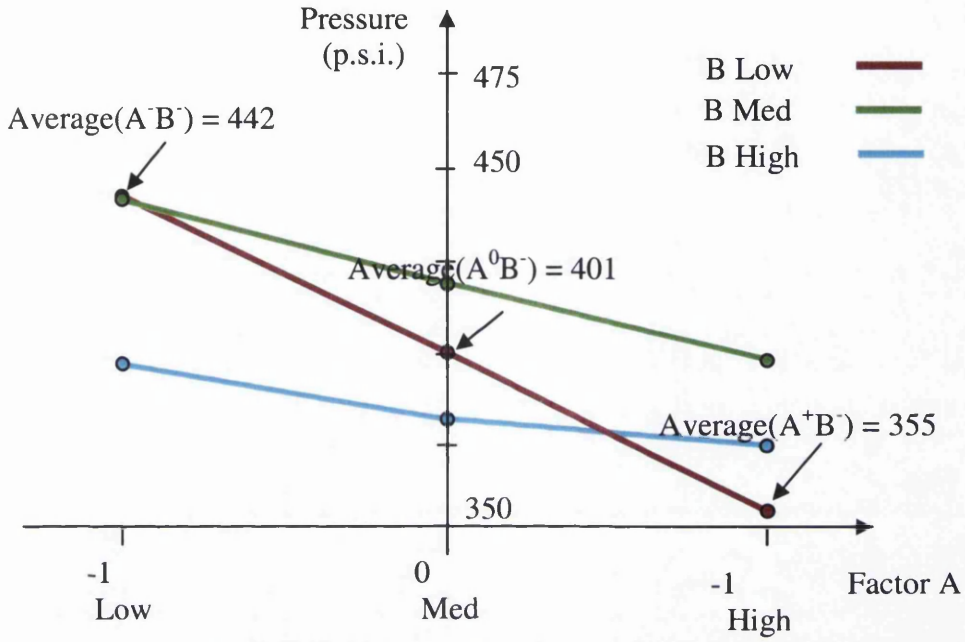

Figure 58: Interaction effect AB; variance of factor A as B changes

Alternatively this could be thought of as 2-D surface in the 3-D system, reversal pressure against A and B (Figure 59).

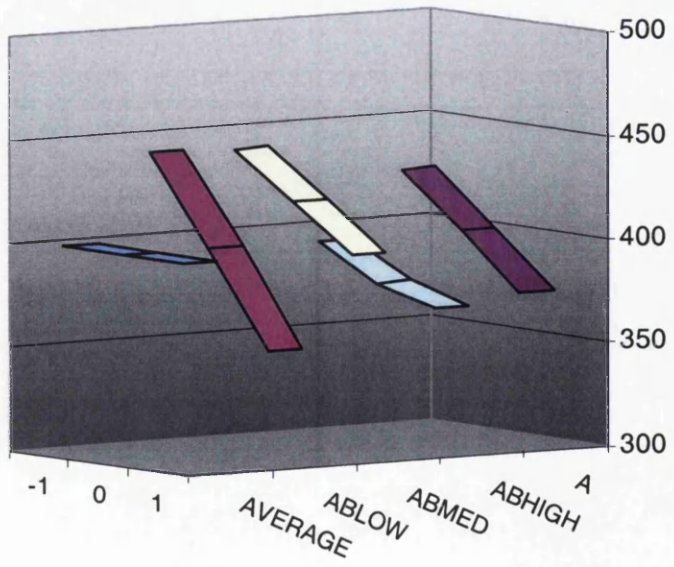

Figure 59: Interaction effect AB in graphical form; reversal pressure vs A,B

D L Davies dave.davies@orange.net

All there is left to show is how to calculate this interaction effect. The final model just simply adds up all the main effects and all possible interaction effects depending upon the initial data.

To show how to calculate an interaction effect the following test data in Table 10 used

Test Data			
A	**B**	**C**	**D**
r1r	**r2r**	**r2x**	**R12x**
1.6	0.8	0.61	1.75
	Rescale (-1,1)		
-0.5	-0.5	0.5	1

Table 10: Worked example test data

And the interaction effect being calculated is the AB interaction effect. Firstly the effect of A being –0.5 is evaluated (Figure 60), and likewise B = -0.5 (Figure 61) comparing it against the average response value, approx. 400 p.s.i..

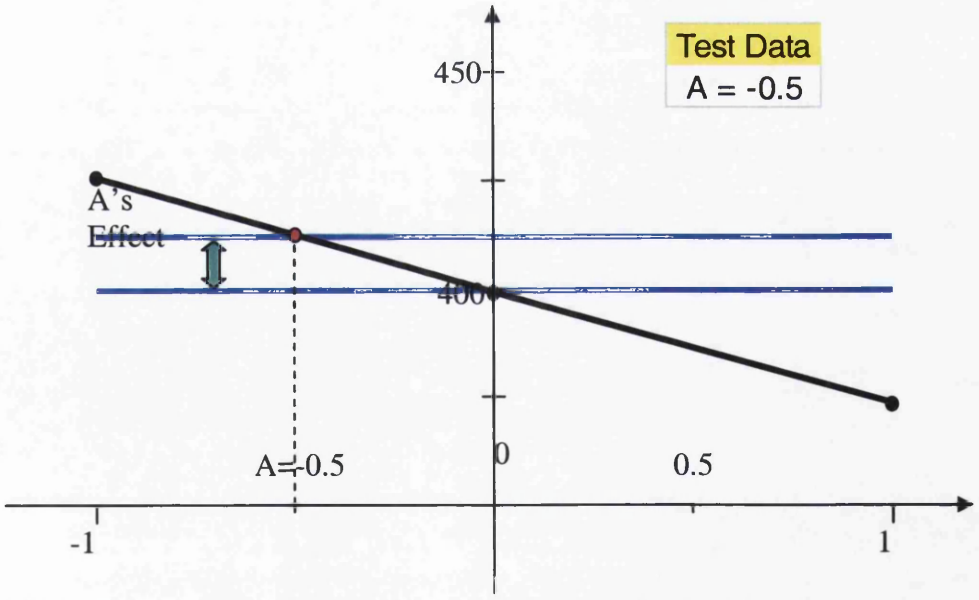

Figure 60: Graphical representation of main effect A, highlighting value at A=-0.5

D L Davies dave.davies@orange.net

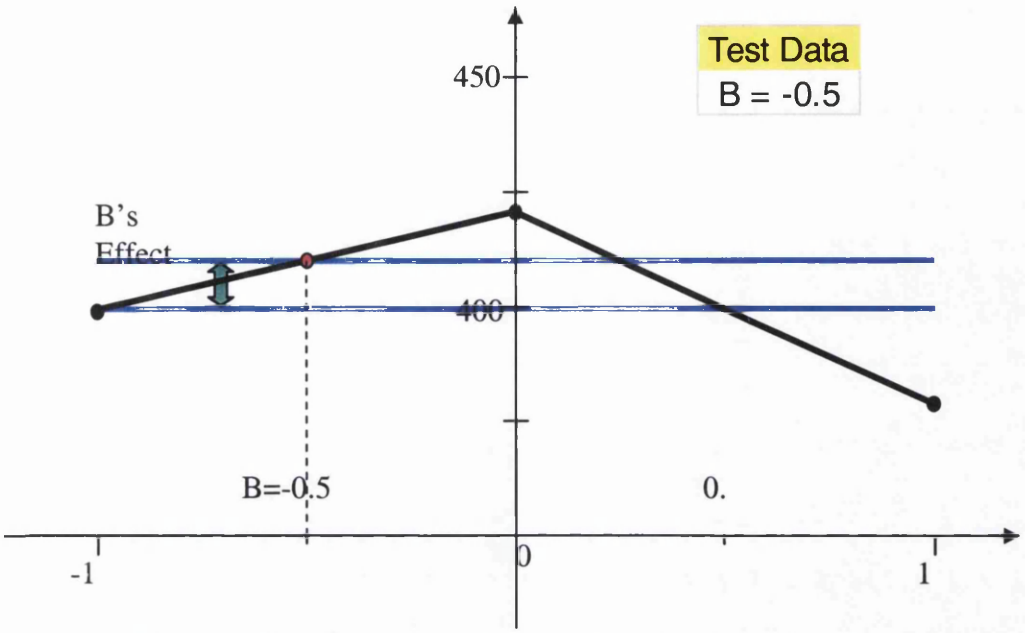

Figure 61: Graphical representation of main effect B, highlighting value at B=-0.5

Now combining these effects (Figure 62) and comparing with AB interaction surface (Figure 63) at A,B=-0.5, then the AB interaction is found.

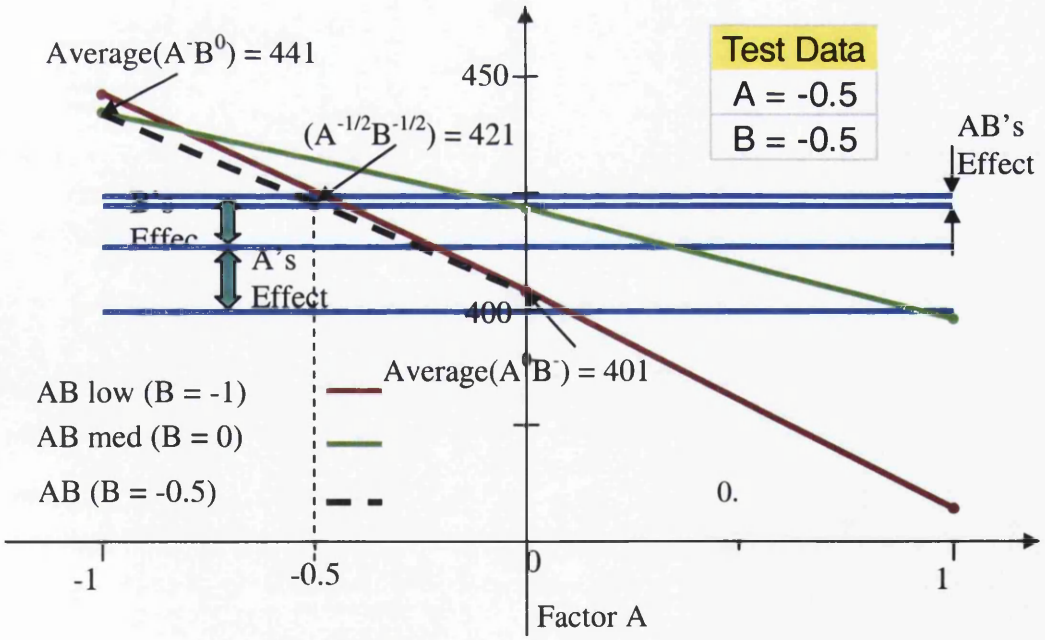

Figure 62: Graphical representation of interaction effect AB

D L Davies dave.davies@orange.net

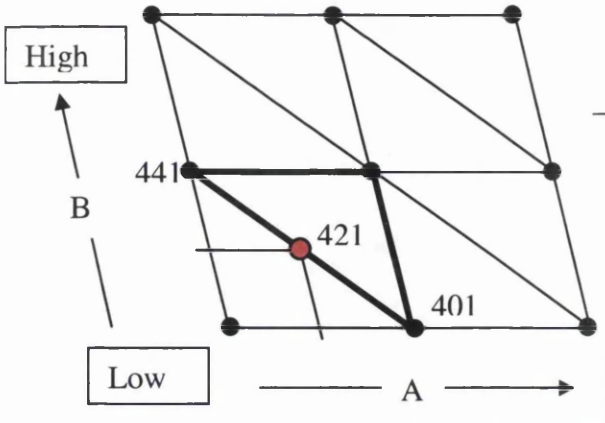

AB's effect =
–(Average + A's effect + B's effect)
+ AB(-0.5,-0.5)
–(399.7 + 12.7 + 9.9) + 421
= –1.4

Figure 63: Calculation of interaction effect AB

So the general rule for assembly is:-

- Start with average response of all tests (399.7)
- Compensate with main effects
- Fine tune with interaction effects (NB higher order interactions yield more accuracy)

For this test data Table 11 lists all the contributions as follows,

Factor	Constant		A	B	C	D
Contribution	399.7		12.7	9.9	-0.1	-24.9
Factor	AB	AC	AD	BC	BD	CD
Contribution	-1.4	-0.5	4.6	8.5	-1.6	1.0

Table 11: Factorial analysis contributions for example test data

And so the predicted dome reversal pressure under this proposed test is the sum of the vaues in the table = 407.9

This whole process is automated within an excel file, and the modelling window for this experiment is shown below in Table 12.

D L Davies dave.davies@orange.net

	Test Data		
A r1r	B r2r	C r2x	D r12x
1.6	0.8	0.61	1.75
	Rescale		
-0.5	-0.5	0.5	1
Response (psi)	407.9		

Table 12: Factorial analysis excel model

All that needs to be done is to substitute the actual test data values directly under the variable name and excel outputs the response instantaneously.

4.3. Factorial Analysis Applied to the DWI Cupping Process

Using the same principles as demonstrated above, factorial analysis can now be applied to the cupping process (Figure 64) to determine the friction coefficients and blankholder pressure required to simulate the process accurately.

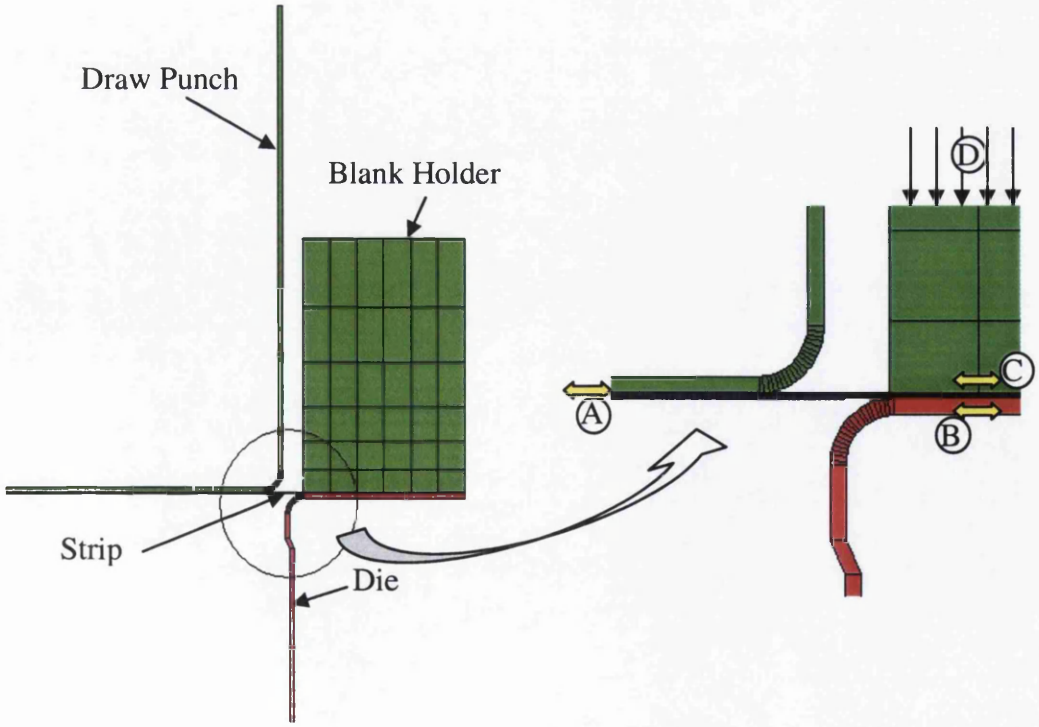

Figure 64: Cupping geometry set-up highlighting parameters used in factorial analysis

D L Davies dave.davies@orange.net

In this case the parameters under investigation are the three friction coefficients and the blankholder pressure. Whereas the previous example only had one response value (reversal pressure) for each parameter configuration, this experiment has 3 response outputs. So a *three-level*, *four-parameter* factorial analysis is performed for *three* different responses, the response being the gauge at three different areas of the simulated cup; the base, the low wall and the high wall (Figure 65,Table 13).

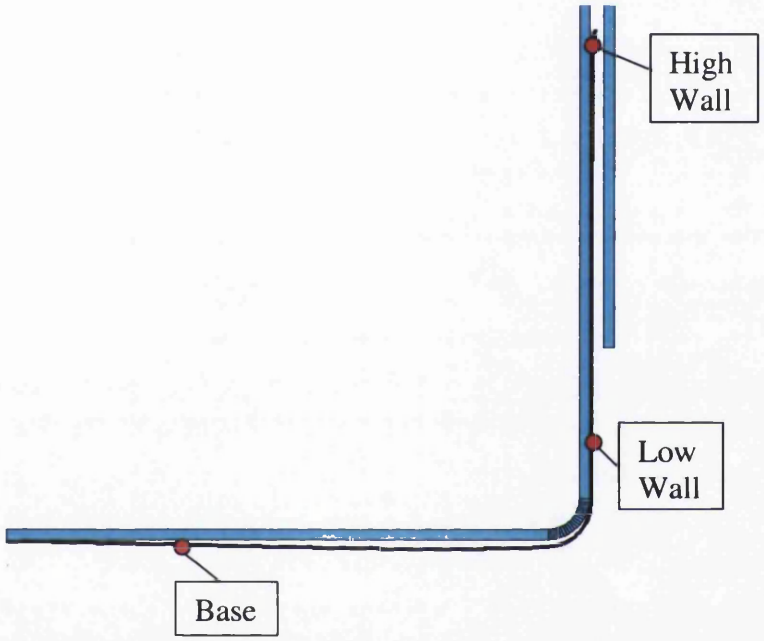

Figure 65: Response values for factorial analysis; gauge at base, low wall and high wall

Input factors				Output responses
Friction coefficients			Blank holder pressure	Thickness
Punch	Draw die	Blank holder		
Factor A	Factor B	Factor C	Factor D	
Low				Base
Medium				Low Wall
High				Top Wall

Table 13: Factorial analysis input/output information

For each response value a corresponding factorial analysis model will be generated, so immediately there will exist a predictive tool to see the effects of varying friction coefficients have on the thickness profile of the cup. In addition to this, developments

have been made to the factorial analysis model by writing it within the MATLAB code. The developments yielded several advantages and additional features:-

- Old model was multi-linear; new model is non-linear
- Old model interaction surfaces were multi-triangular planes; new model describe the surfaces using bi-cubic interpolation
- New analytical post-processing programs written to investigate the model designed to answer engineering questions of interest

All the data is entered into a spreadsheet containing all the test cases with the corresponding responses in their respective rows, an excerpt of which can be seen in Table 14.

	Punch	Die	Blankholder		Gauge of strip after cupping			
			Friction	Force		Base	Low wall	High wall
Low	0.05	0.05	0.05	1.167				
Medium	0.15	0.15	0.15	3	Physical	0.230	0.230	0.265
High	0.25	0.25	0.25	4.5	Data			
	0.15	0.25	0.15	1.167		0.223	0.222	0.290
	0.25	0.25	0.15	1.167		0.223	0.221	0.290
	0.05	0.05	0.25	1.167		0.228	0.224	0.290
	0.15	0.05	0.25	1.167		0.228	0.224	0.290
	0.25	0.05	0.25	1.167		0.228	0.224	0.290
	0.05	0.15	0.25	1.167		0.221	0.224	0.290
	0.15	0.15	0.25	1.167		0.226	0.223	0.290
	0.25	0.15	0.25	1.167		0.225	0.222	0.290
	0.05	0.25	0.25	1.167		0.200	0.206	0.290
	0.15	0.25	0.25	1.167		0.220	0.219	0.290
	0.25	0.25	0.25	1.167		0.222	0.219	0.290
	0.05	0.05	0.05	3		0.225	0.225	0.287
	0.15	0.05	0.05	3		0.228	0.224	0.288
	0.25	0.05	0.05	3		0.228	0.225	0.287

Table 14: Cupping strip thickness data

For convenience the factor data is re-scaled (Table 15) such that the lowest value is taken as –1 and the highest as 1 using a simple cell formula performed within the same spreadsheet

D L Davies dave.davies@orange.net

-1	-1	-1	-1
0	-1	-1	-1
1	-1	-1	-1
-1	0	-1	-1
0	0	-1	-1
1	0	-1	-1
-1	1	-1	-1
0	1	-1	-1
1	1	-1	-1
-1	-1	0	-1
0	-1	0	-1
1	-1	0	-1
-1	0	0	-1
0	0	0	-1
1	0	0	-1
-1	1	0	-1
0	1	0	-1
1	1	0	-1
-1	-1	1	-1

Table 15:Rescaled input data

The highlighted square has formula

=IF (H9<>0, IF (B9=0.05, -1, IF (B9=0.15, 0, 1))," "),

which means

Check cell is non-empty

If cell value is 0.05 (low), then output –1

Elseif cell value is 0.15 (med), output 0

Else output 1

The results are set-up in the following way (Figure 66) to make cutting and pasting data into the MATLAB factorial program easier. The buttons have macros assigned to them such that they cut the relevant data into clipboard memory.

D L Davies dave.davies@orange.net

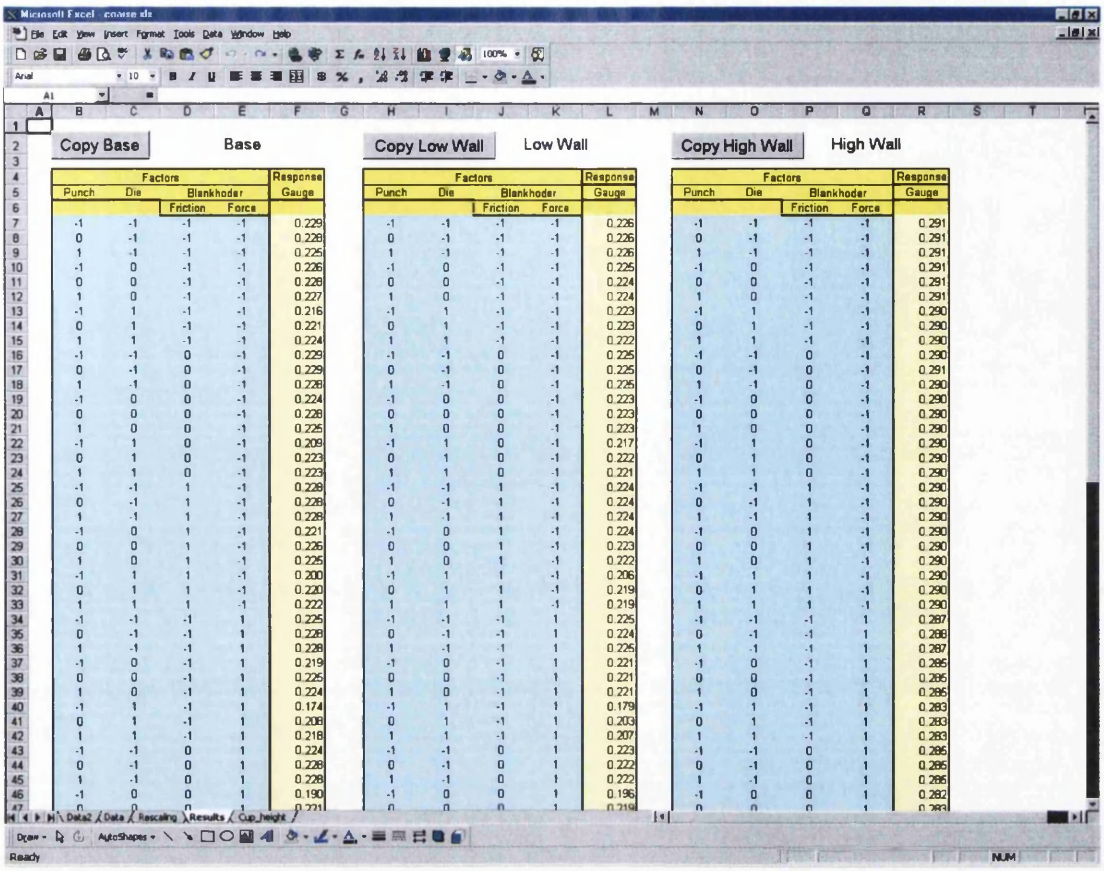

Figure 66: Cupping data results layout

Setting up the FA model is now easy. For example, taking the high wall data (click on "copy high wall"), simply type "fact" in the MATLAB window and paste in the data as prompted (Figure 67).

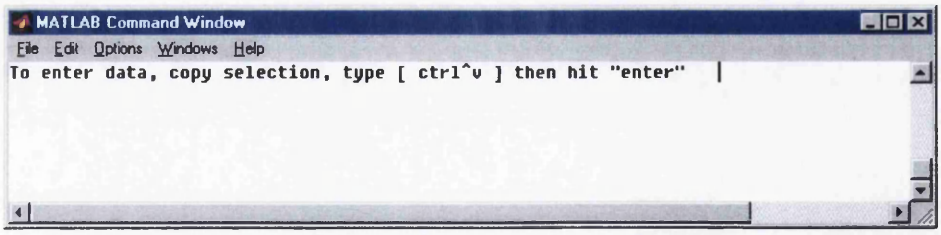

Figure 67: MATLAB data insertion window

The factorial analysis package (chapter 4.4) generates a model for each response output, and each model in this case will have 7 graphs (Figure 68) associated with it,

which describe the parametric effect of each factor as well as their interactive effects. For example, the results for the top wall gauge: -

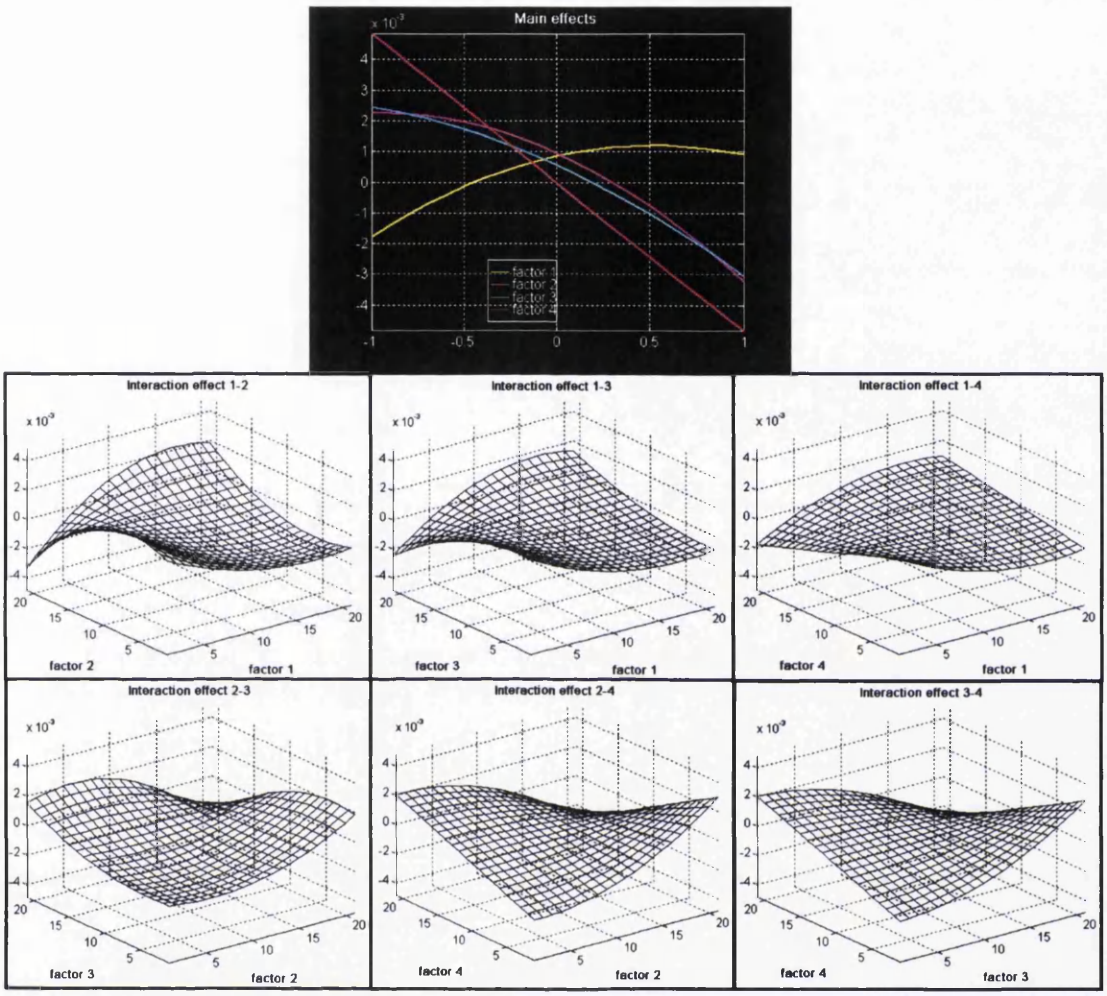

Figure 68: Main and interaction effect graphs for high wall gauge

With the further use of interrogation programs (chapter 4.4.1) it is then possible to calibrate the friction levels to achieve the physical data gauge curve. Recall the motivation for using this tool. The idea is to be able to simulate the cup forming accurately, which means the thickness profile of the cup must be correct, ie the thickness of the cup along the height of the cup (Figure 11). Using an initial estimate for the friction coefficients and the blankholder pressure the profile (Figure 69) is obtained. Although fairly accurate, not accurate enough to be able to model the

further forming process as described in the DWI chapter (3). But running the model using the information obtained using the factorial analysis programs the profile (Figure 70) is obtained. It is noticeably more accurate and as such resulted in the possibility of simulating the remainder of the DWI process.

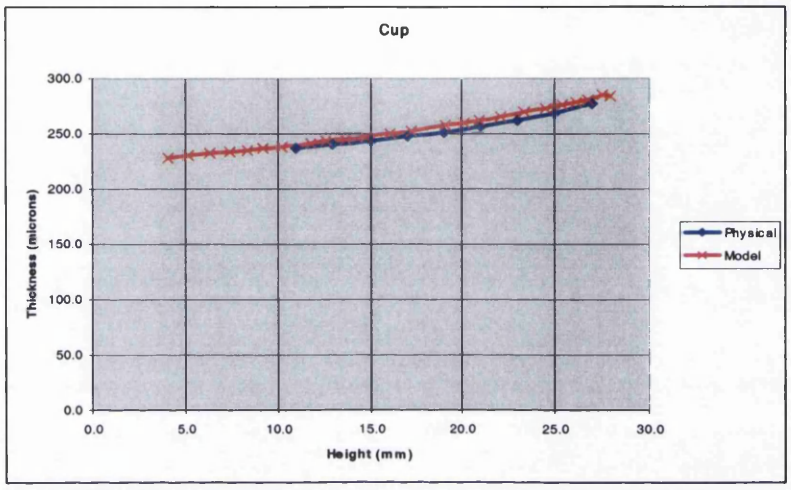

Figure 69: Initial height-gauge profile with 1st estimate of friction coefficients

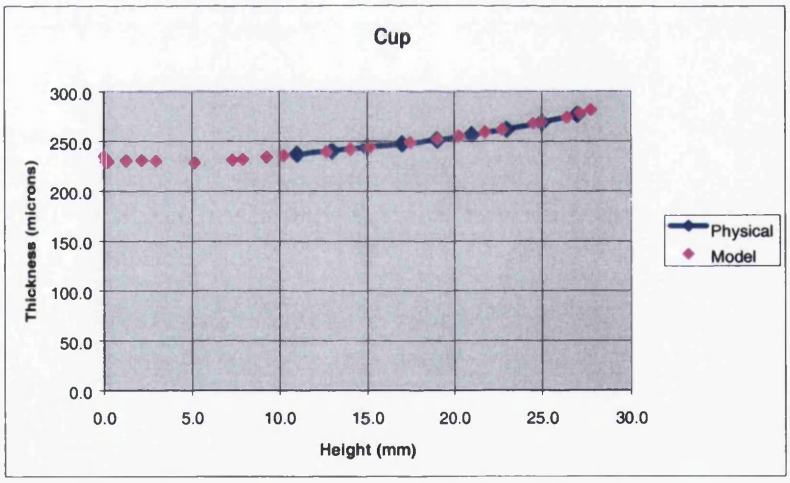

Figure 70: Profile plot of cupping using fact anal settings

4.4. Factorial Analysis Package

As described in the worked example (4.2) where the analysis is performed on an Excel spreadsheet using multiple cell reference formulas and if subroutines, the MATLAB version created carries the same principles. It splits up the data according to factors, calculates averages, main effects and interaction effects. The worked

example pays close attention to the theory that is needed in order to understand notions such as interaction effects and with sufficient literature to enable interpretations of interaction surface diagrams.

The MATALB version uses the same theory behind the scenes, but is a developed factorial analysis package that will benefit both established and non-users of factorial analysis. It is designed to be user friendly for people who have little or no experience with FA who just seek an answer (optimality), but also helps those who can interpret interaction diagrams to clarify what really is happening within the system being analysed.

4.4.1. Programs

The package is made up of a number of MATLAB m-files (C-based programs): -

Fact.m

Value.m

Ivalue.m

Mvalue.m

Fmodel

Max3fact.m

Max4fact.m

Tmodel.m

Multiopt.m

all of which can be seen in Appendix B.i.

4.4.1.1.Fact.m

This program is the workhorse for all the FA work. The input for the function is the data to be analysed, and its output is the variables that define an interactive FA model.

It works out all the main and interaction effects and stores and compiles them in such a way that a model is set up of similar fashion to the spreadsheet worked example (above). The difference is that the spreadsheet model was purely written for that example. Many hours work had made one model that specifically interpolated any given input data. Whereas this program can create any model in seconds and also then has the ability to answer more questions using the other post processing programs.

4.4.1.2.Value.m, Ivalue.m, Mvalue.m

Value.m uses the model set up from fact.m to work out the contribution of any factor input with any value within the range of the original input data. I.e. it answers questions such as, what contribution will factor B give at a value 0.4*max value?

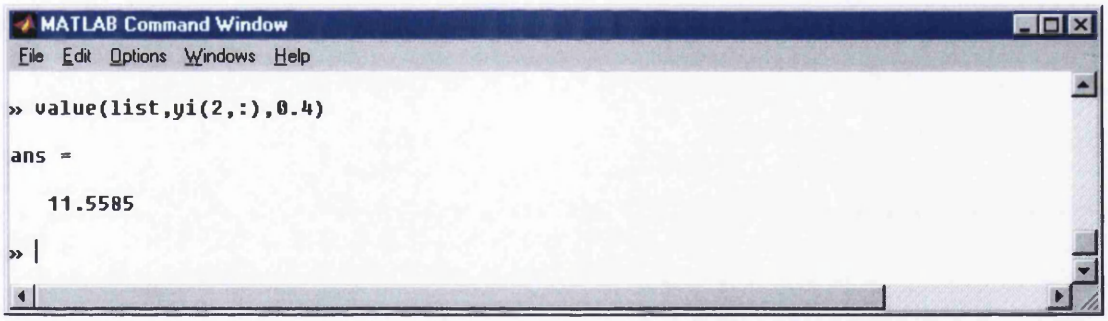

Figure 71: Factorial analysis value.m example

Where,

list = [-1 0 1], the levels input into the model,

yi(2,:), where the 2 corresponds to factor B,

0.4, the value of B based on the scale defined by "list"

The answer, ans, 11.5585, is the expected difference to the average set-up response by setting factor B to 0.4*max value. In this case the response is the reversal pressure used in the worked example (1.2), where the average response was 399.7psi. So the

interpretation of this result would be if factor B is set to 0.89 (see 1.2), then it can be expected that the reversal pressure would be 411.3psi (399.7+11.6).

Ivalue.m uses the model set up from fact.m in the same way. Only this function works out contributions of interaction effects, i.e. given two factors with two arbitrary values within their restricted range, Ivalue outputs its contribution.

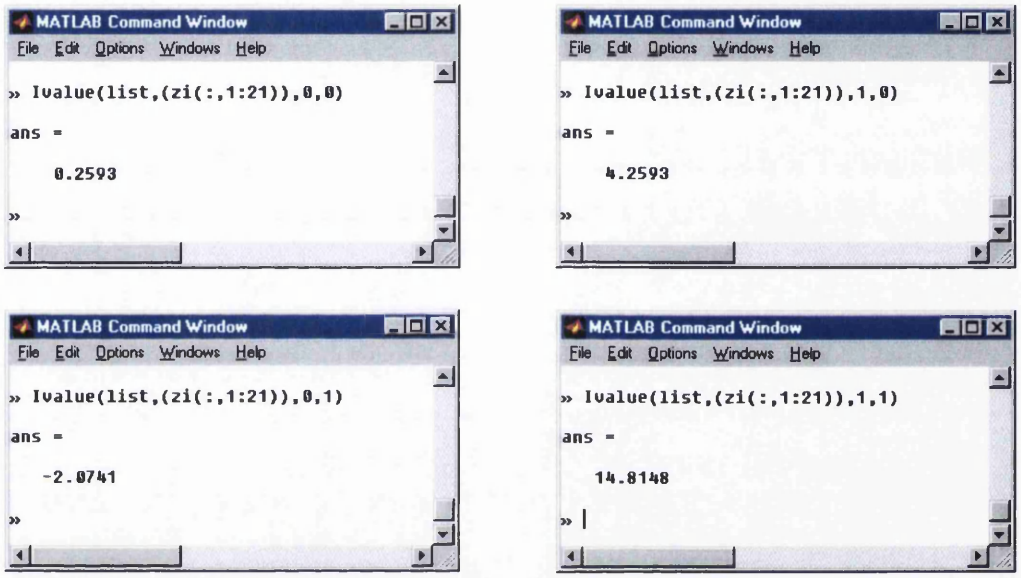

Figure 72: Factorial analysis Ivalue example

Figure 72 is a good example to show that interaction effects are non-linear and how the sensitivity of one factor changes as another one does. It shows the value of interaction affect AB at four values of A and B, A=0 B=0, A=0 B=1, A=1 B=0, A=1 B=1. This shows that when A=0 increasing the value of B toward 1 has a negative effect on the response, yet conversely when A=1 increasing the value of B toward 1 has a positive effect on the response. Once again these figures are from the worked example (4.2), so this means when radius r1r (factor A) = 1.65 (0), increasing radius r2r (factor B) from 0.85 (0) to 0.95 (1), it's expected that the reversal pressure will lower by 2psi. Similarly, when r1r = 1.75, increasing r2r from 0.85 to 0.95, it's expected that the reversal pressure will increase by 10psi.

Both these functions are essentially a lookup table taking values from the main interaction graph or the interaction surfaces, and so obvious trends and dependencies can be seen easily without having to observe the values accurately.

Mvalue.m recursively uses Value and Ivalue to add up all the contributions to obtain the predicted response to any given input data. I.e. with input values for all factors, mvalue outputs the model prediction under those conditions

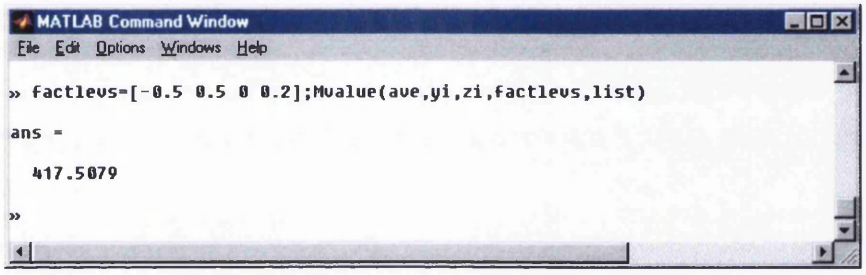

Figure 73: Factorial analysis mvalue example

Figure 73 means the factorial analysis model predicts when r1r, r2r, r2x, r12x = 1.6, 0.9, 0.6, 1.67, then the reversal pressure will be 417.5psi.

4.4.1.3.Fmodel.m

Fmodel simply calls on Mvalue after prompting the user for factor input levels – so this function would be of use to anyone interested in answering questions like, 'what would happen if the tooling was set up in this way?' without actually having to perform the potentially expensive physical operation.

For example if factors A to D with respect to the cupping model (1.3) are [-0.5 0.5 0.25 0.3] then the model predicts the wall thickness at the top of the cup is 0.2824mm (Figure 74)

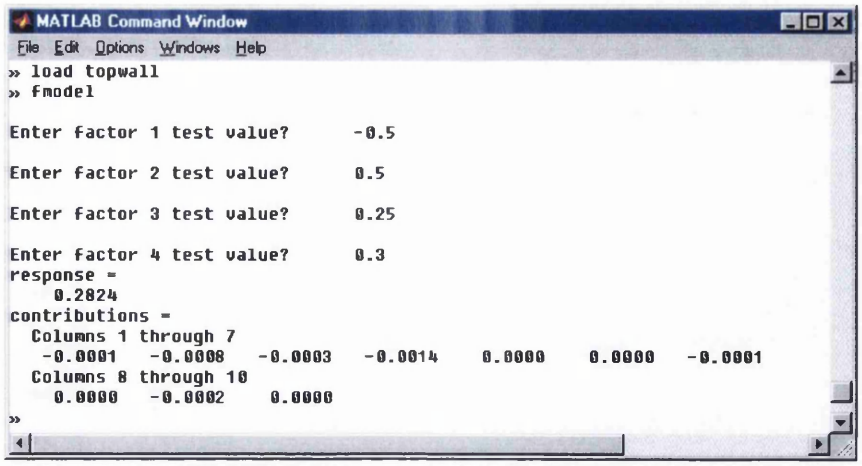

Figure 74: Factorial analysis fmodel example

4.4.1.4.Max3fact.m, Max4fact.m

Max3fact.m uses loops to find the 3 factor inputs required obtaining the 'best' response. It checks the response value for all possible combinations of factor inputs to within a given step size. E.g. if factor A, say, lies between –1 and 1, the step size may be 0.1 and so all permutations with A set to k*0.1-1, k being a whole number between 0 and 20 will be worked out. 'Best' is predefined in the program depending on what you want your optimality condition to be – e.g. the lowest (cheapest) response.

Similarly this can be extended with slight alterations to any number of factors, e.g. 4 which is precisely program max4fact.m.

4.4.1.5.Tmodel.m

With the same objective as the max3fact program, in that the program recursively searches for the optimal input, there are a few differences. Firstly due to the nature of the search algorithm it is unlikely that this will check all possible factor combinations – this program ceases after a given number of loops, whereas the other checks all permutations to within a set step size. This means that if the step size is small then

the number of loops required to check all may be arbitrary large – this could take an impractical length of time to compute.

The other difference is, and hence the name of the program (t for target), is that the response value desired to be searched for is set as an input to the function. In that sense this program acts like an inverse of the model, i.e. using the desired response as an input tmodel works out what factor level values are needed to obtain it. Additionally the program outputs an error graph with a corresponding plot that displays the factor levels for each iteration (Figure 76). The program could be used to answer questions such as, what is the best set of input factors (friction coefficients and blankholder force) in order to obtain a high wall thickness of 0.29mm? (Figure 75)

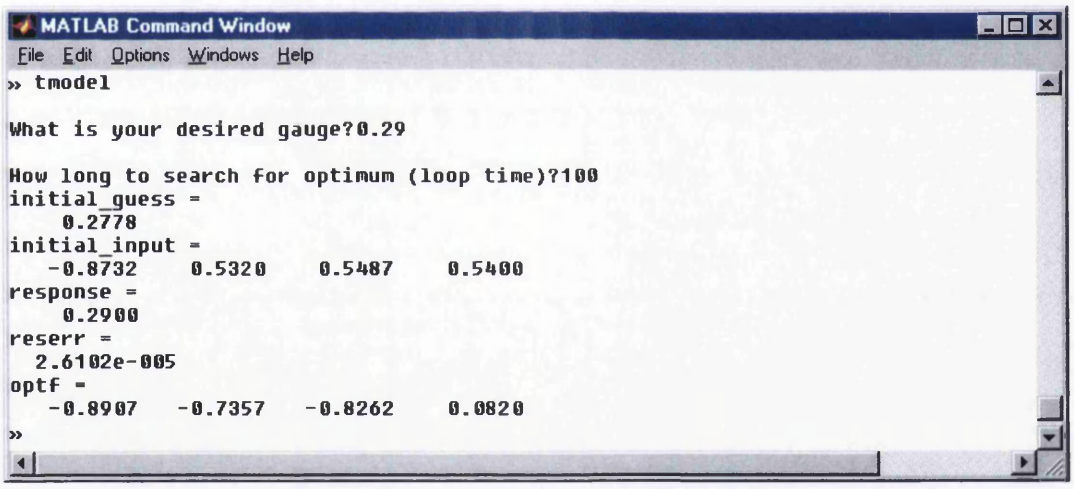

Figure 75: Factorial analysis tmodel example

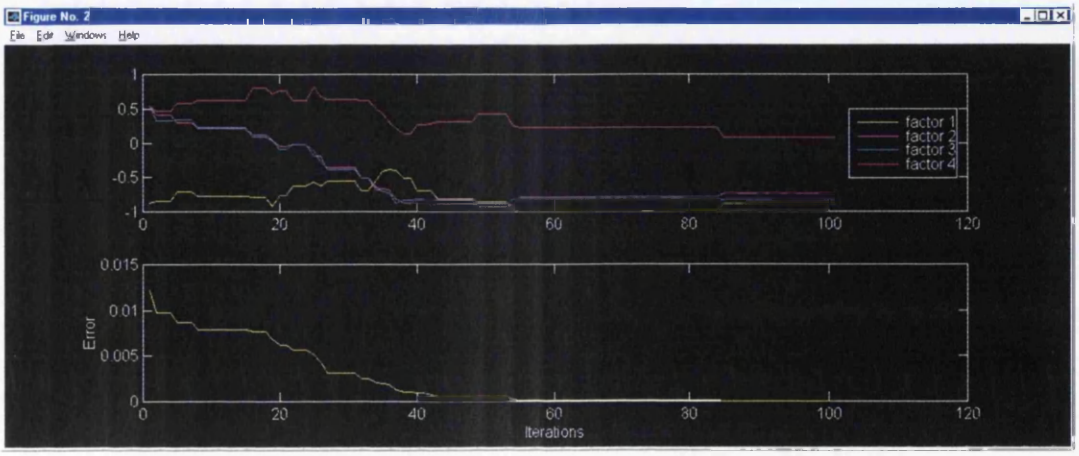

Figure 76: Solution convergence and error plot for tmodel example

D L Davies dave.davies@orange.net

4.4.1.6.Multiopt.m

As the name suggests this model has the capability of optimising more than one response value. This is of use when the system being modelled has more than one output response. E.g. one output may be time and the other profit – a single optimiser for profit could suggest a solution that may be impractical in terms of time, and similarly an optimiser for time needn't maximise profits. There is a need for compromise between the two.

This program switches between different models (in that the response data is different) finding the 'best' input to satisfy all the models. Best in this sense is like that in tmodel, only there is a target response for each model – for each trial input, mvalue (model value) calculates the relevant responses, compares each against its target response and the error is calculated in a least squares sense. I.e. for each model response the discrepancy is squared and then all values summed, with the lowest value being the optimal solution.

So this program is ideal in trying to find out the required set-up in order to obtain a particular cup profile as desired (Figure 77). As with the tmodel program there is a similar error convergence graph (Figure 78).

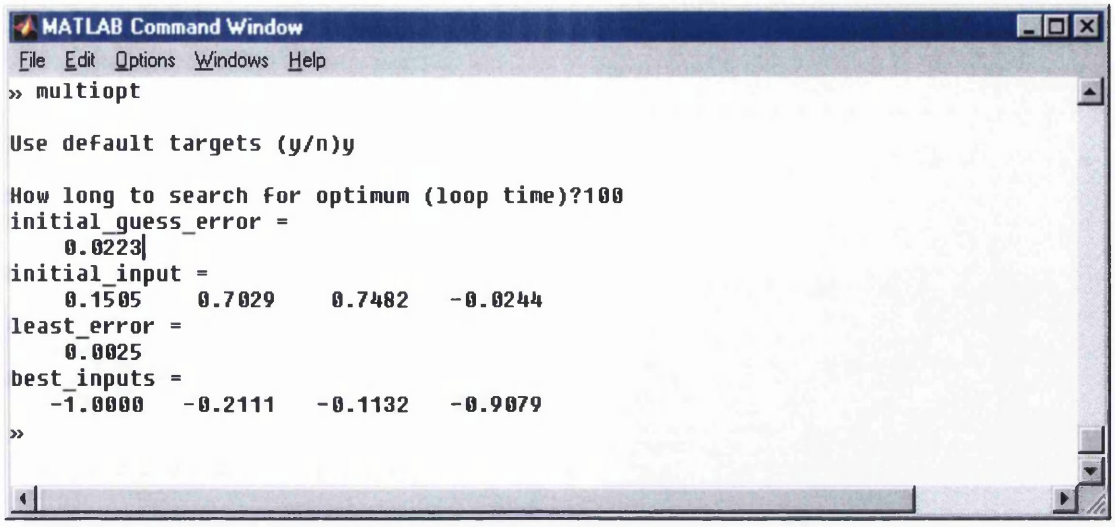

Figure 77: Factorial analysis multiopt example

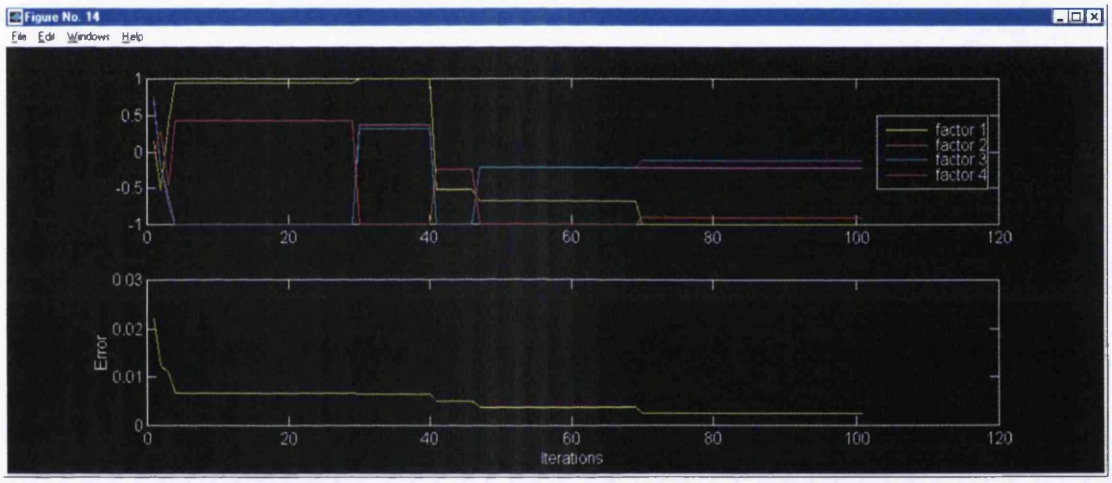

Figure 78: Solution convergence and error plot for multiopt example

D L Davies dave.davies@orange.net

5. EMBOSSING

5.1. Introduction

The embossing of cans is a secondary forming process designed primarily to enhance the aesthetics of the can; although it can be done to improve the structural integrity of the can, similar to the way can beads improve its panelling performance. The availability and knowledge of what shapes and designs can be embossed with various materials is very limited if not non-existent.

The aim of this work is to be able to simulate the embossing of arbitrary designs primarily applied to can preforms, although not exclusively, to check its feasibility of production and to help design the tooling dies required to emboss such a design. The work includes a model that simulates the embossing of an arbitrary design created by the user on an adjoining self written software package. To make this work useful there must exist confidence that the FE code simulates the embossing process realistically.

An attempt to validate some embossing work was done via an existing embossing tool set. The design of the tool set is a sequence of squares with several parameters defining them, e.g. square size and differing corner radii. The idea of this tool set was to develop understanding into the embossing process by comparisons with the squares with slightly differing parameters. Although the idea seemed good in that it's systematic, and it does highlight some features, there are more fundamental features with the process that completely outweigh the effects of the changing parameters looked at. It's also these fundamental features of the process that made validation of this model inappropriate as will be explained in detail later.

Consequently the means by which embossing is to be validated is with another embossing experiment. It involved the creation of sets of male/female tooling dies, designed to emboss small flat strip samples (≈40mm x 95mm). The design of the dies removes the issues that were present in the can embossing experiment, yet still keeps the forming features that existed with it. The prime advantage of the experiment is its repeatability and good control of all boundaries and constraints.

5.2. Modelling of Embossing Arbitrary Design

As a first attempt of embossing arbitrary designs a flat strip is modelled between two rotating tooling dies, male and female (Figure 79). The strip is also pulled through independently at a linear speed equivalent to the rotational speed of the dies at the area of contact. This ties in with practice as the can is rotated at an angular speed equal to the female die with an external force (vacuum under base) independent of the die. Moreover, due to the freedom the can wall has during embossing the deformation behaviour can be expected to be similar to that of a flat strip.

Figure 79: Flat strip embossing with "CORUS" design

D L Davies dave.davies@orange.net

Later models that will cover a curved can wall will use the same principles as in this model, only with different can material properties and geometry, with the stresses and plasticity undergoing embossing very similar.

The model is set-up such that arbitrary embossing designs can be modelled. Ultimately with the idea, given an embossing design in bitmap (bmp) form, the required tooling will automatically be generated as desired (Figure 80). As an intermediate step some self-written MATLAB code (B.ii) was made acting as an interface between user-created design and die tooling geometry.

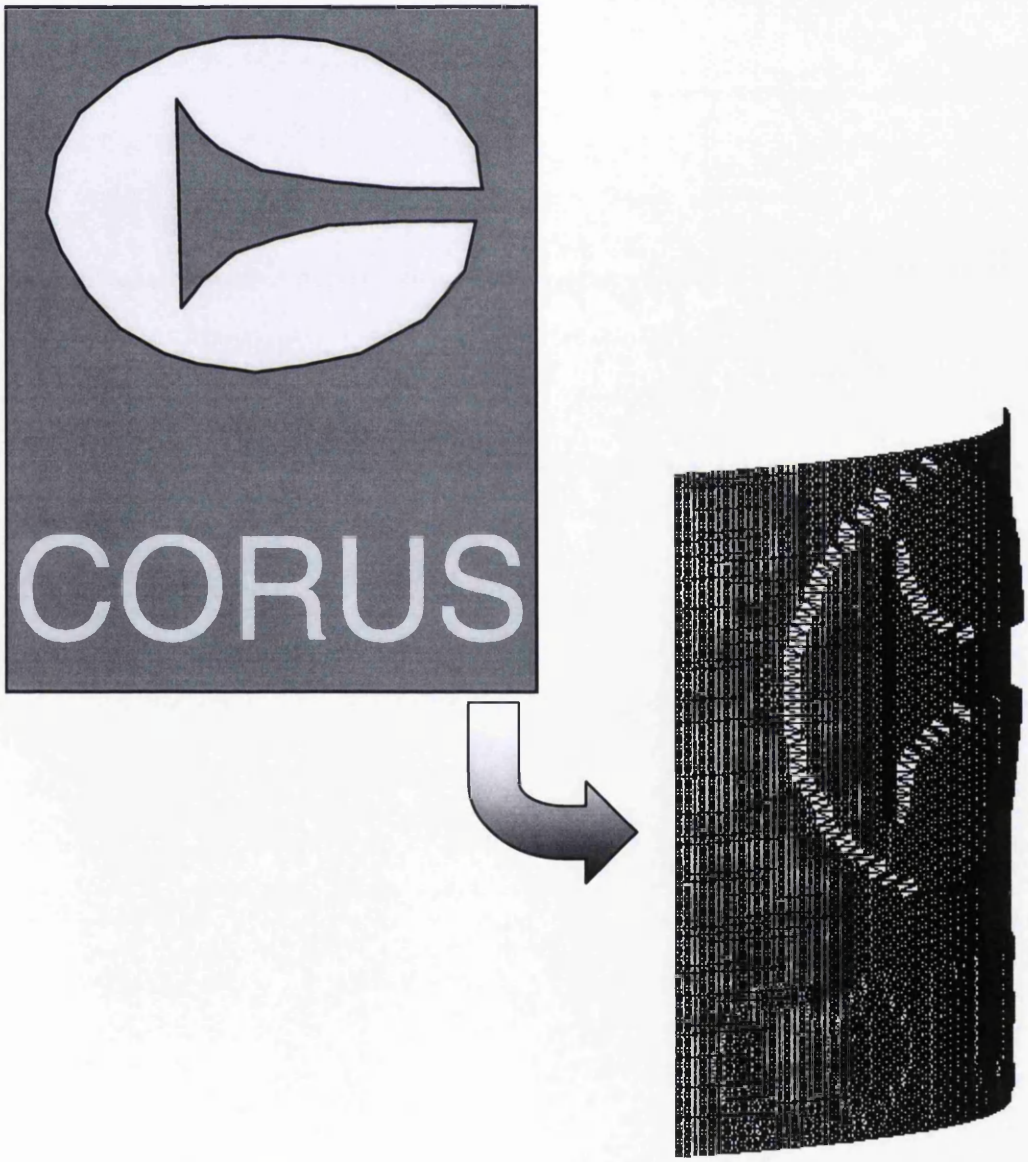

Figure 80: Example of bitmap to embossing tooling transfer

D L Davies dave.davies@orange.net

The principle of this work is to take the co-ordinates of a smooth cylindrical male die, and manually adjust the radial components of particular nodes (Figure 81).

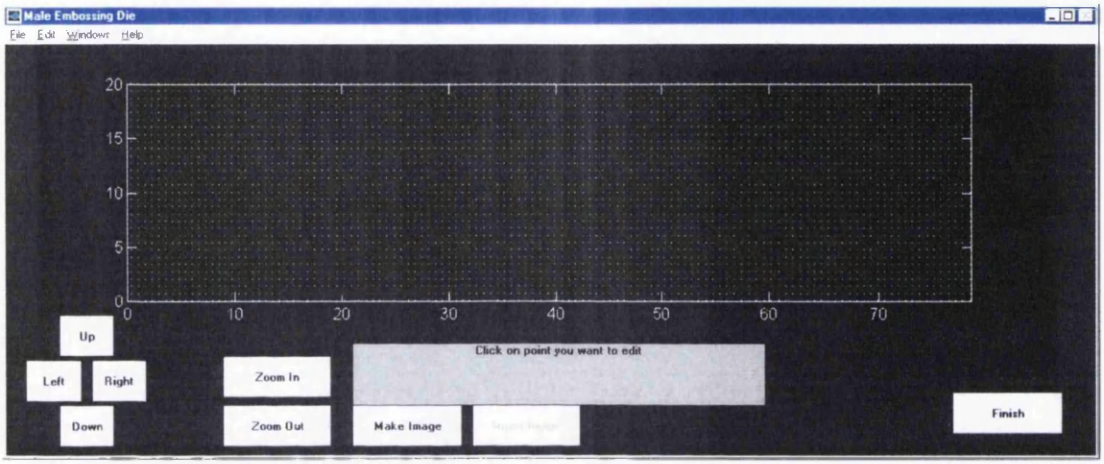

Figure 81: Surface co-ordinates of male embossing die with no radial adjustments

The code is written such that the user has the option of either selecting a particular node then adjusting its radial component, or make an image. The "Make Image" option opens a window where multiple points can be adjusted thus making a whole image first before deciding where on the die it is placed (Figure 82, Figure 83).

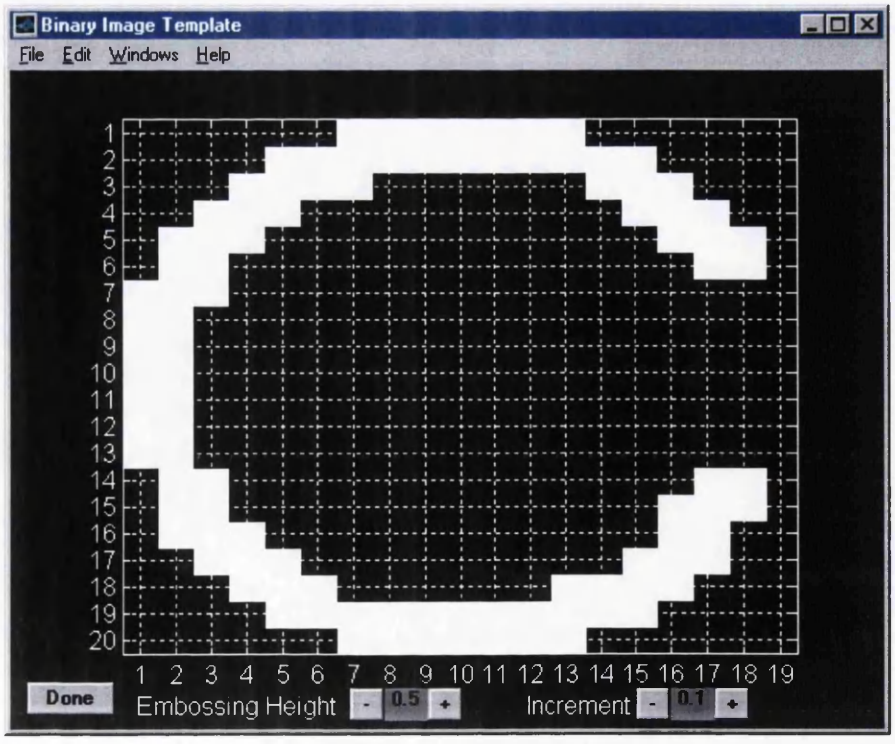

Figure 82: Embossing Image Generator

D L Davies dave.davies@orange.net

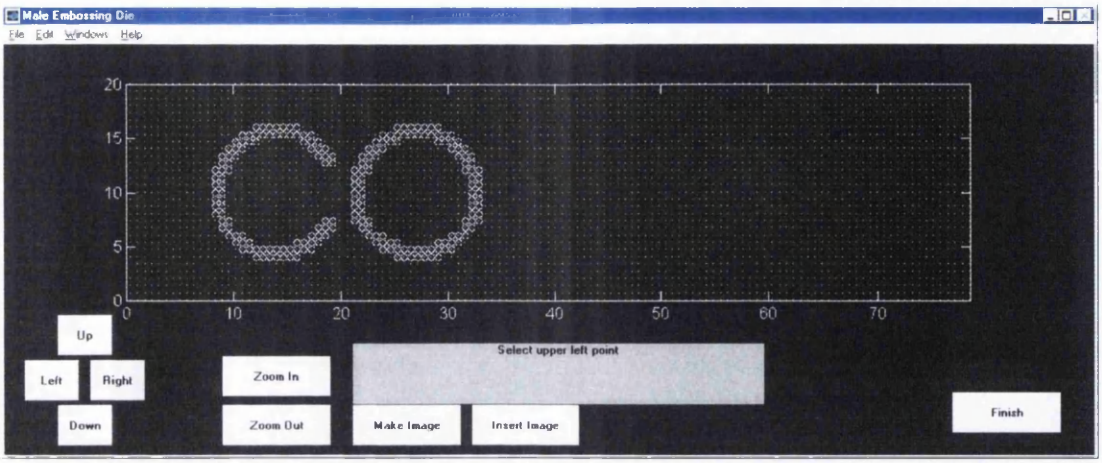

Figure 83: Surface co-ordinates of male embossing die with "C O" radial adjustments

5.3. The Embossing Process

The process involves two cylindrical dies, male and female, and a trimmed can (pre-necking) that is placed over without the female die. The male die has its design radially outwards from it and correspondingly the female radially inward but slightly larger to allow for the thickness of the material. The male die is supported by two arms, top and bottom, whereas the female is only supported from above and so allowing the can to be placed over the female from below. The can is supported at its base by a plate and is help in place by a vacuous force. The embossing of each can involves the automatic placement of the can over the female die, the male moving in toward the female die to a specified gap between the two. Then all three components, male die, female die and can, are mechanically rotated at the same angular speed exactly one rotation, with the male die obviously in the opposite direction.

D L Davies dave.davies@orange.net

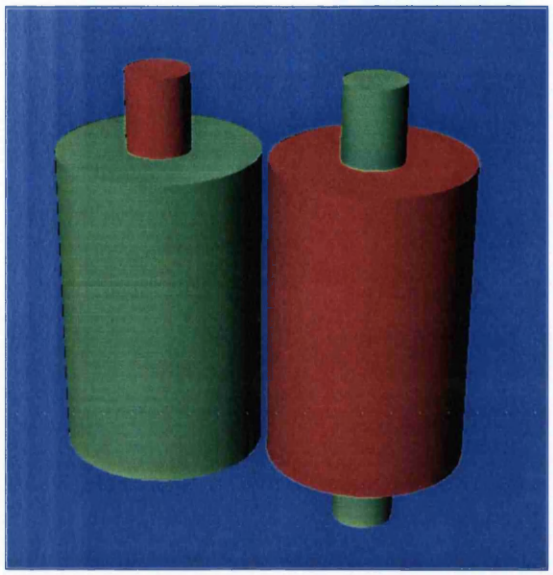

Figure 84: Schematic of embossing tooling

5.3.1. Problems With Embossing Set-up

There are a few issues with the embossing process that makes it a difficult process to simulate. Some of the problems relate only to the tooling set-up of the "squares" embossing where others are a more general problem with the process. The tooling dimensions used with the "squares" are such that certain phenomena occur under some conditions, such as double embossing and/or surface scratching to the can. The double embossing (the result of slipping) may also occur in other embossing tooling set-ups under certain conditions. In addition another more fundamental problem with the process is due to the support of the dies.

5.3.1.1.Die Support

As can be seen above in Figure 84 the male die is supported from top and bottom and so making the die sturdy and is unlikely to deviate during the low forces encountered during embossing. In contrast the female die is only supported from above in order to allow the can to be placed over the die before it is to be embossed. So when

significant forces are present, i.e. when embossing, the lack of support on the bottom of die allows it to slightly angle away (Figure 85).

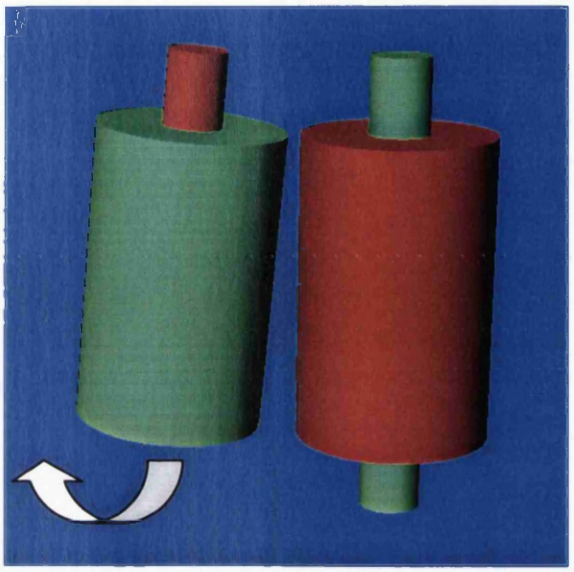

Figure 85: Angling of female die when embossing

Although the angle of deviation is likely to be very small in this case its effect was great enough to outweigh other differences that were being investigated and can be seen in the measured results to follow.

5.3.1.2.Double Embossing

As described above the can is supposed to rotate one revolution in the same time as the female and male dies. But due to the base of the can slipping relative to the base it is held by, it is possible that the can may rotate less than the tooling dies. If in addition the embossing design is at the beginning of the rotation (Figure 87), and so therefore also at the end of the rotation, then it's possible that the design may be printed twice into the can at slightly different location due to the slippage.

D L Davies dave.davies@orange.net

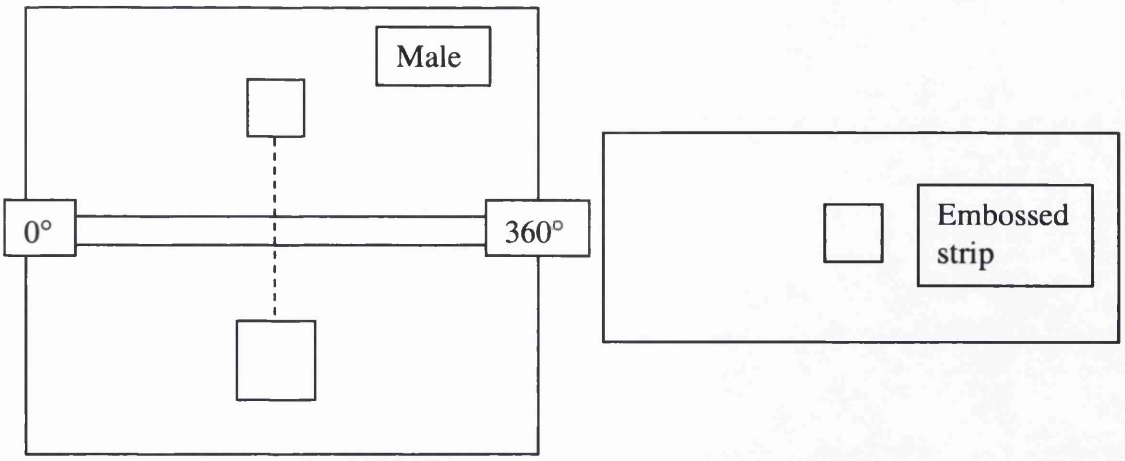

Figure 86: Schematic of "square" embossed without slipping

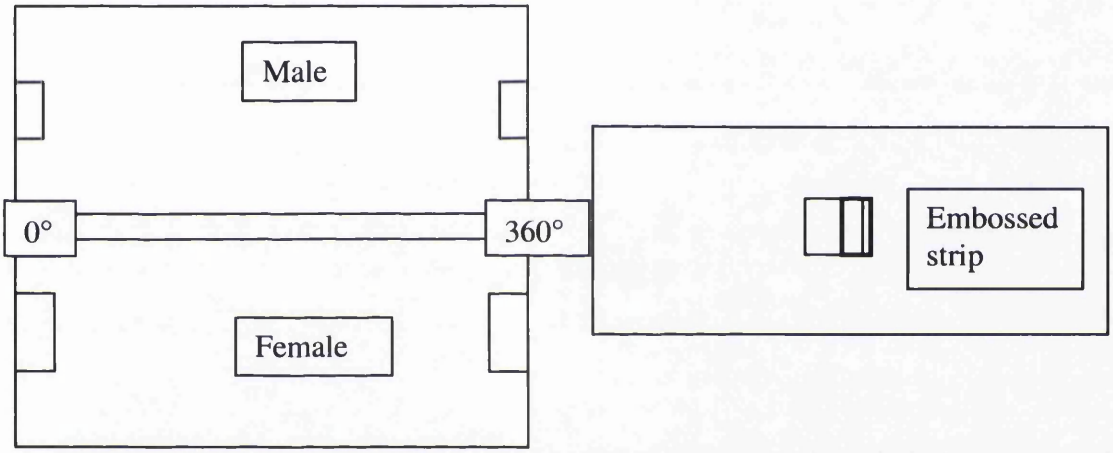

Figure 87: Schematic of "square" embossed with slipping resulting in double embossing

In the case of the "squares" embossing this may be explained by the tooling dimensions and in particular when the tooling gap between male and female becomes sufficiently small. The dimensions to note are the male, female and can diameters.

Just prior to the embossing the male die moves toward the female die making the tooling gap 2mm less than its starting position, the tooling gap being the infimum distance between the flats of the male and female dies. I.e if the initial tooling gap is 2.6mm the effective working tooling gap is 0.6mm when embossing.

D L Davies dave.davies@orange.net

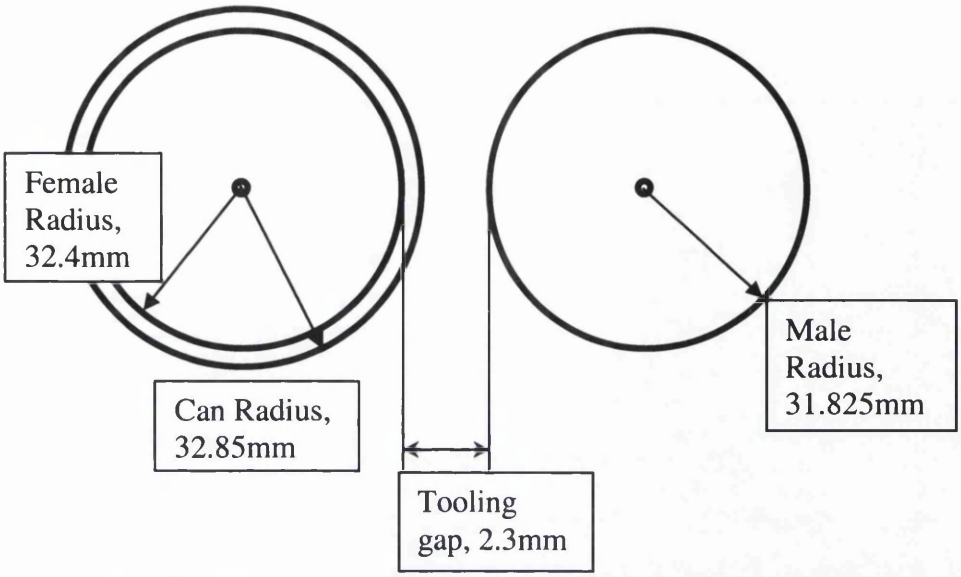

Figure 88: Schematic of typical tooling dimensions for embossing in plan view

With reference to Figure 88 the first thing to note is that the male diameter is smaller than the female diameter. An obvious consequence is that the male diameter is therefore smaller than the can diameter. Combining that with the fact their angular speeds are the same means that whenever the male die is in contact with the can there is an induced tangential frictional force applied to the can wall due to a difference in linear speed at the area of contact (Figure 89).

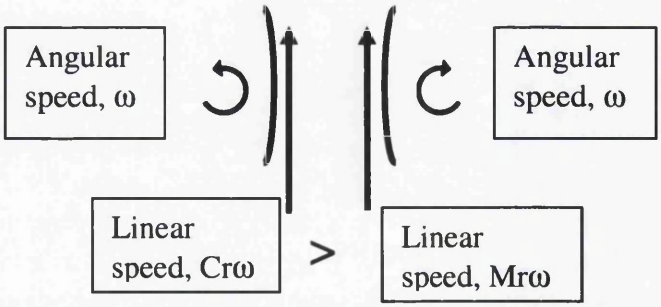

Figure 89: Linear speed differential at contact area during embossing

So if the tooling gap is small enough the male is in contact with the can wall at all times which may explain the reason there's scratching on the top of the can wall for deep embossing (tooling gaps less than 2.45mm(0.45mm)). It's also plausible that

this could be the main cause for double embossing due to the amount of slipping caused as a result of different linear speeds of male die and can wall.

The main causes then for scratching, slipping and so double embossing are the diameter mismatch between male die and can, and when the effective tooling gap while embossing is smaller than the difference between female radius and can radius.

A suggestion for new tooling dies would be to make the male diameter slightly larger than the female die, so enabling the possibility that Mr = Cr and thus the problem of different linear speeds during contact being negated.

I.e. choose Mr such that it's likely that Mr = Cr

Also limit the effective tooling gap to prevent continual contact and displacement between male die and can wall. The effective tooling gap in this case is 2mm less than the initial gap as explained earlier. So in this case limit the tooling gap such that:-

Tooling gap $\geq 2 + Cr-Fr$

5.4. Squares Pattern Embossing

5.4.1. Modelling the "Squares" Pattern

The set-up of the model can be seen in the model's appendix (A.iii), which contains all the specifics of the model, although the general layout of the model and some plots are shown below (Figure 90 - Figure 96). It is set up parametrically such that all geometry is defined by a large number of variables that define the tooling. However, the assumptions used make the system a perfect one in that the tooling dies are rigid and so in particular the female die will not have the degree of freedom to angle away as it does in reality. Also the symmetry constraints used deny the possibility of slippage of the can relative to the dies and so double embossing could never occur.

So although the model does simulate an embossing process it doesn't behave in the exact way of the tooling design it was designed to do, and as such no direct comparisons are made with physical measurements in order to validate the model. Either the physical process would need to be altered, namely in movement of the female die, or modification of the model to allow for such movement, in which case would require significantly more computing power.

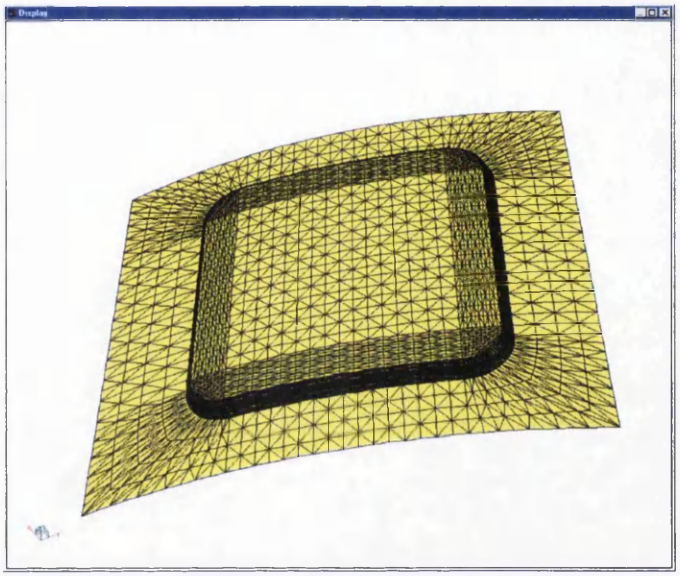

Figure 90: Mesh used for the embossing "squares" model

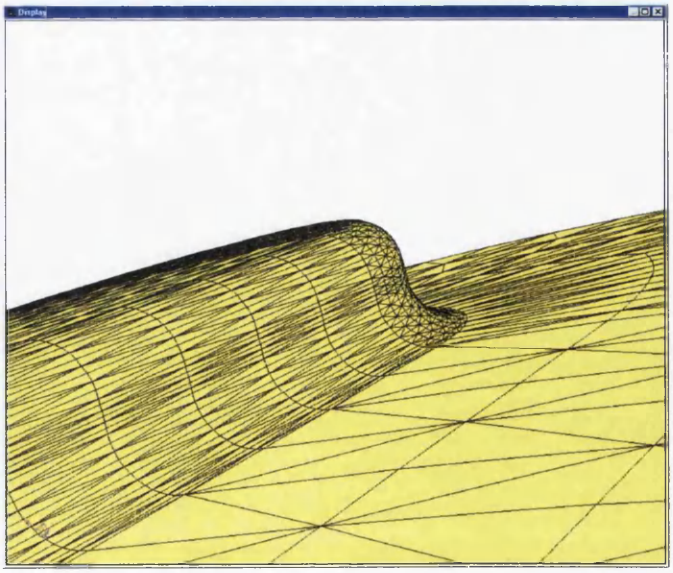

Figure 91: Side view of embossing mesh featuring the blended edge radii

D L Davies dave.davies@orange.net

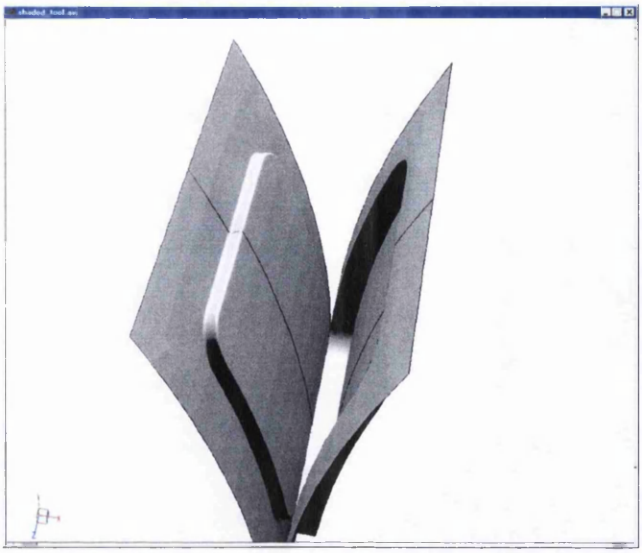

Figure 92: Aerial view of the simulated tooling dies

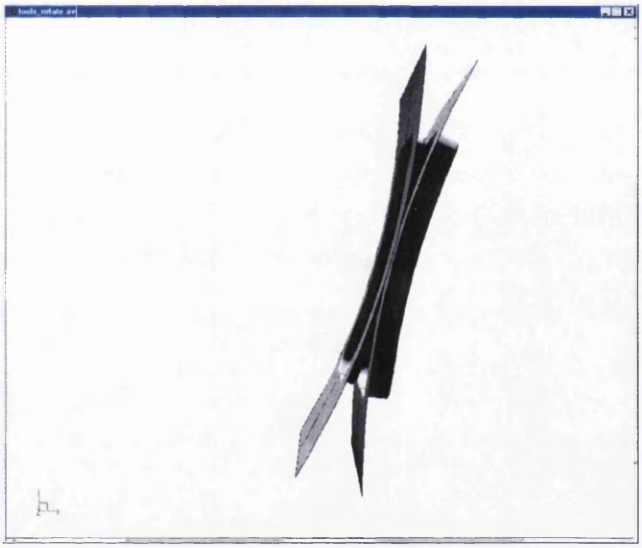

Figure 93: Side view of simulated tooling dies

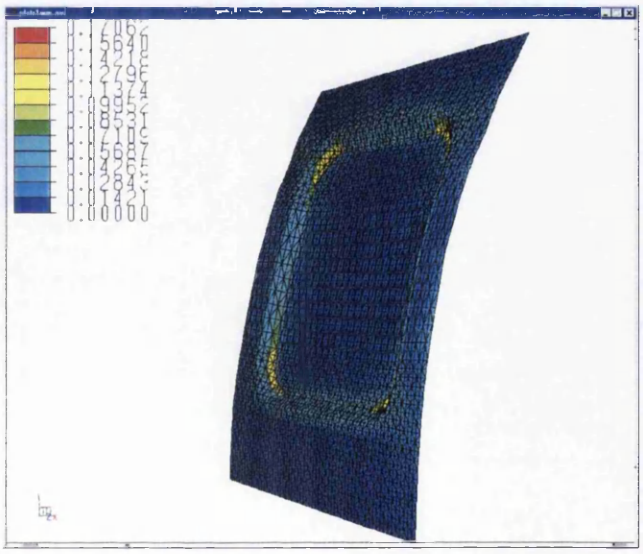

Figure 94: Inside layer of embossed can wall; scale plastic strain

D L Davies dave.davies@orange.net

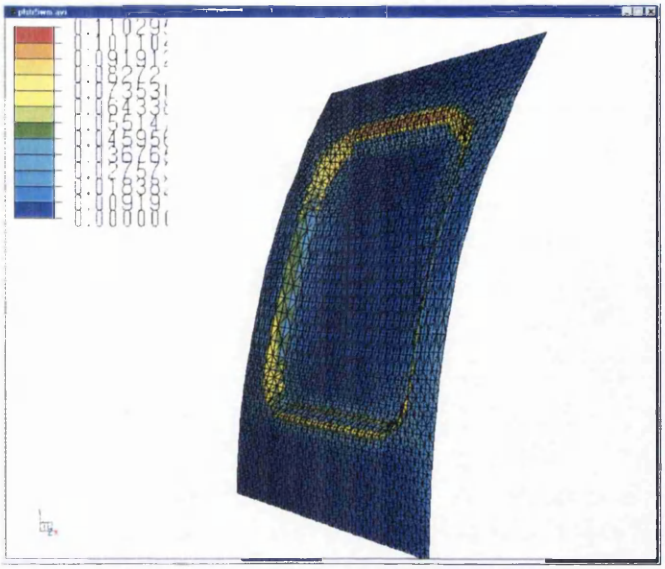

Figure 95: Outside layer of embossed can wall; scale plastic strain

Figure 96: Embossed can wall

5.4.2. Embossed "Squares" Measurements

Taking a preformed can before its necking stage made to the "Scanmap" specifications (as in DWI model), it was then embossed with the "squares" embossing design with a tooling gap of 2.3mm (0.3mm)(heavy embossing). The resultant can was then analysed by taking a trace of the can in several positions using contracer equipment. The design of embossing containing 3 x 8 squares, 12 of which are 5mm

D L Davies dave.davies@orange.net

and the remaining 12 10mm. Each square was measured in two directions, top to bottom and around the can circumference (Figure 98-Figure 102).

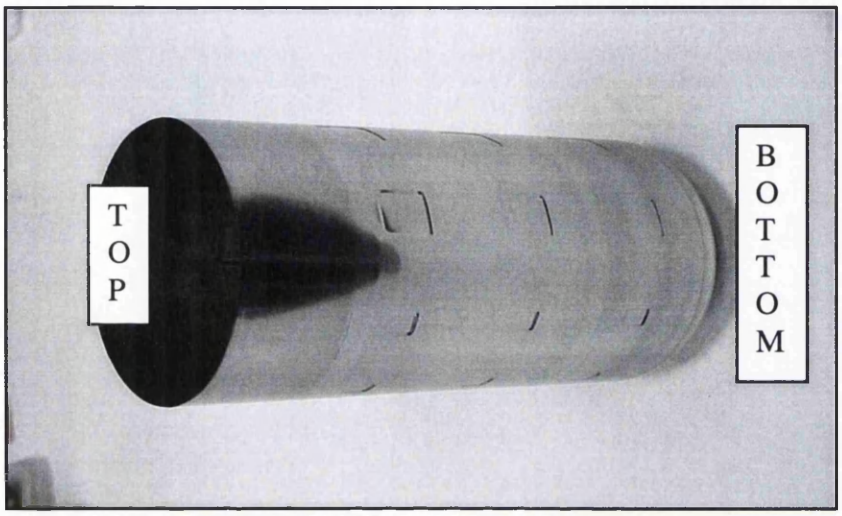

Figure 97: Photo of embossed can with squares design

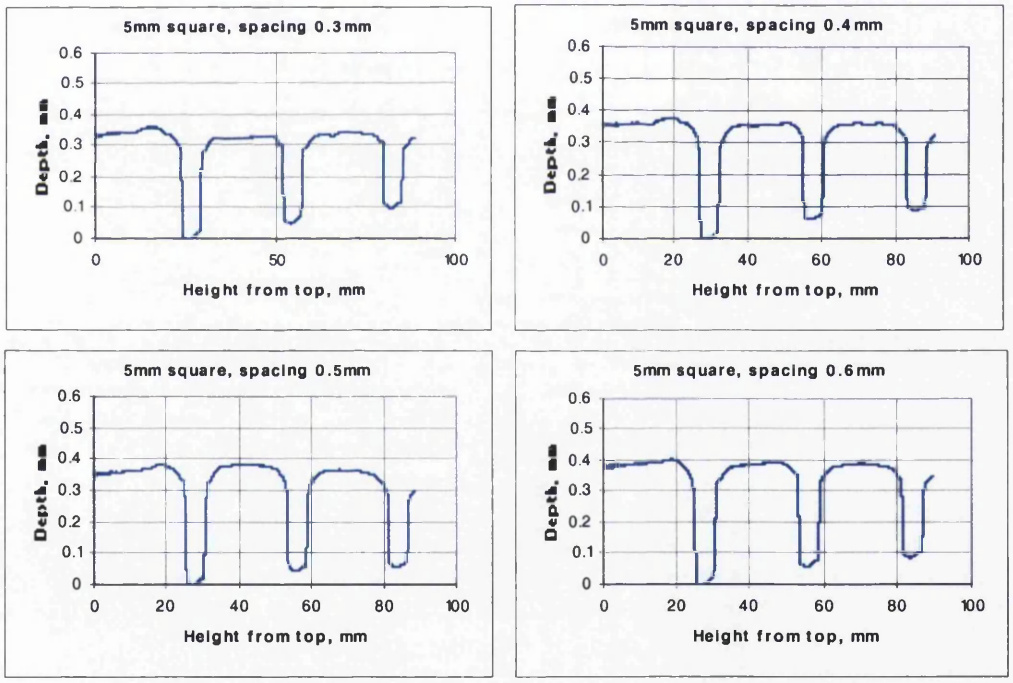

Figure 98: Contracer measurements of 5mm squares in axial direction

D L Davies dave.davies@orange.net

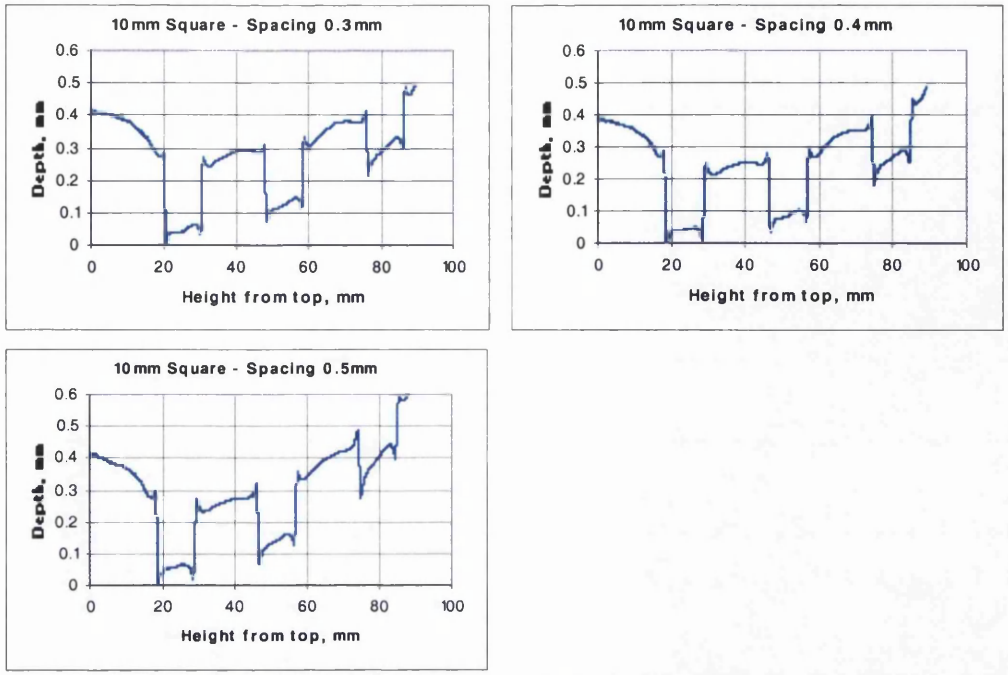

Figure 99: Contracer measurements of 10mm squares in axial direction

Whereas the traces along the length of the can be plotted directly, the radial traces benefit from a transform that essentially takes away the curvature of the can and so the effect of embossing can be seen more clearly. Without this transform the curvature of the can makes it harder to assess features such as embossing depth, and an example of a typical radial trace can be seen in Figure 100.

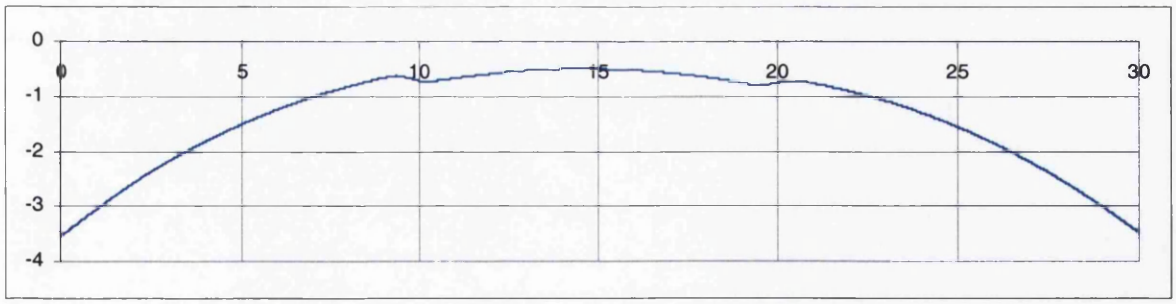

Figure 100: Contracer measurement of 10mm square, spacing 0.4mm around circumference

D L Davies dave.davies@orange.net

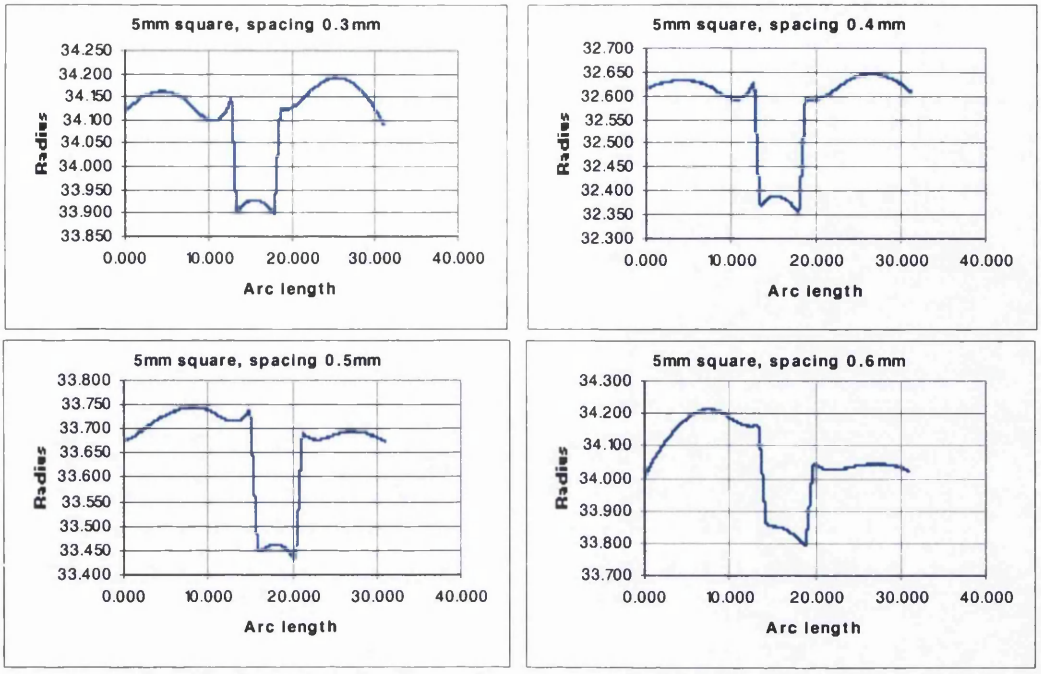

Figure 101: Contracer arc length measurements for 5mm squares

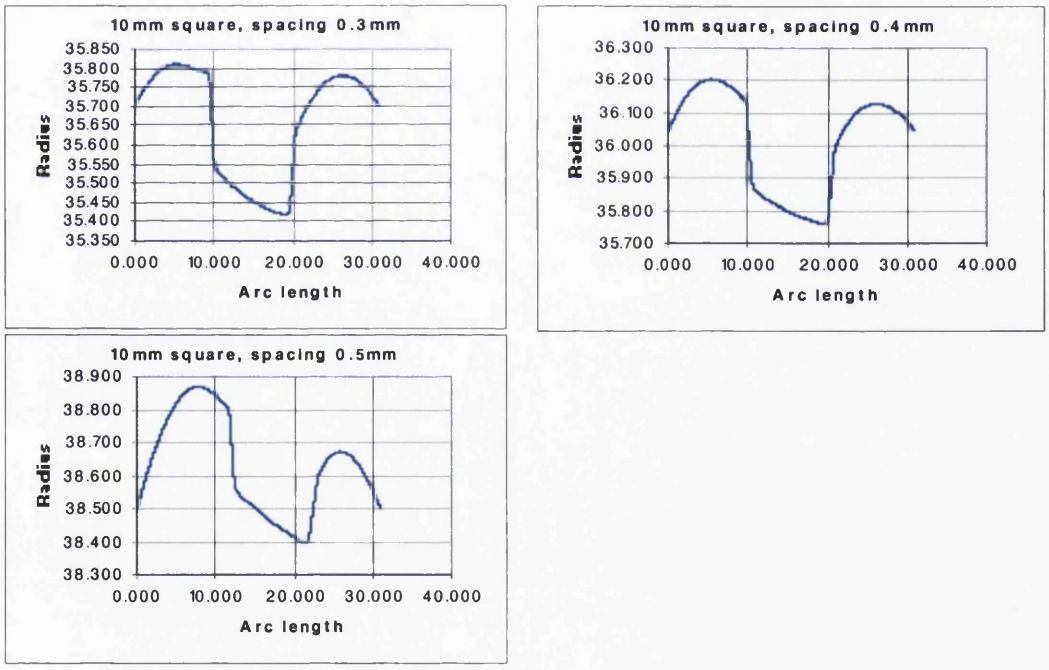

Figure 102: Contracer arc length measurements for 10mm squares

D L Davies dave.davies@orange.net

5.4.3. Discussion and Explanation

5.4.3.1.Close-up Geometry

To get an understanding of what happens during the forming of the embossed squares, and the features created, e.g. spikes, it is beneficial to look closer at the geometry of the tooling set-up. Without this closer inspection it is intuitively hard to begin to understand what stresses are present, where they act, and so ultimately the resultant stress, and in turn the springback that can be expected. The latter, which is important in the resultant geometry is caused in this case by the complex interaction of local tensions and differing stresses in the concave and convex part of the strip. This springback and its varying nature plays the critical role in the formation of the spikes as seen in figures above (Figure 98 to Figure 102).

Using Figure 103 as reference, two plasticity estimates (one for convex and concave) can be generated, which when combined gives a measure of the "spike" value – a value that corresponds to the nature of springback as described above.

Angle α can then be calculated in at least one of two ways, analytically or recursively.

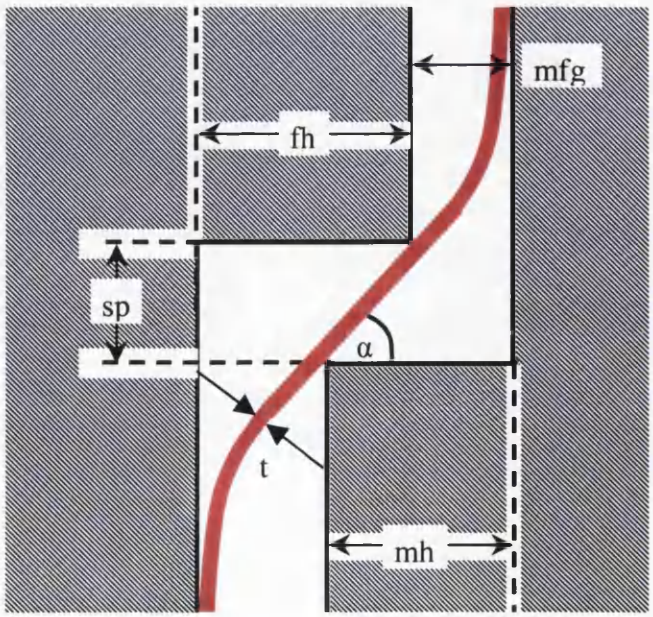

Figure 103: Male and female embossing profile schematic

D L Davies dave.davies@orange.net

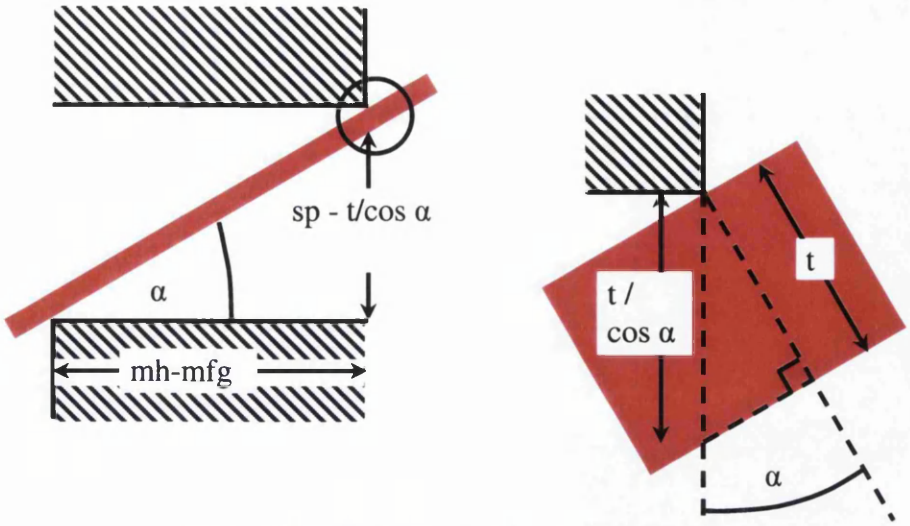

Figure 104: Male-female angle α calculation

Analytical method

$$\tan\alpha = \frac{\left(sp - {}^{t}/_{\cos\alpha}\right)}{mh - mfg}$$

$$(mh - mfg)\sin\alpha = sp\cos\alpha - t$$

$$(mh - mfg)^2 \sin^2\alpha = sp^2\cos^2\alpha - 2spt\cos\alpha + t^2$$

$$(mh - mfg)^2 - t^2 = \left(sp^2 + (mh - mfg)^2\right)\cos^2\alpha - 2spt\cos\alpha$$

$$\left(sp^2 + (mh - mfg)^2\right)\cos^2\alpha - 2spt\cos\alpha + t^2 - (mh - mfg)^2 = 0$$

$$\cos\alpha = \frac{2spt \pm \sqrt{4sp^2t^2 - 4\left(sp^2 + (mh - mfg)^2\right)\left(t^2 - (mh - mfg)^2\right)}}{2\left(sp^2 + (mh - mfg)^2\right)}$$

$$\cos\alpha = \frac{spt \pm \sqrt{sp^2(mh - mfg)^2 - t^2(mh - mfg)^2 + (mh - mfg)^4}}{sp^2 + (mh - mfg)^2}$$

$$\cos\alpha = \frac{spt \pm (mh - mfg)\sqrt{sp^2 - t^2 + (mh - mfg)^2}}{sp^2 + (mh - mfg)^2}$$

Noting from the geometry that in all meaningful and realistic cases that (mh-mfg)>t>0 then the positive root must be taken to obtain a meaningful answer, else (mh-mfg) > t (given), thus

D L Davies dave.davies@orange.net

$$\sqrt{sp^2 - t^2 + (mh - mfg)^2} > sp$$

$$\cos\alpha_{-} = \frac{spt - (mh - mfg)\sqrt{sp^2 - t^2 + (mh - mfg)^2}}{sp^2 + (mh - mfg)^2} < 0$$

But α lies between 0 and π/2, so cosα > 0

So the negative root is not the one desired

$$\alpha_{+} = \arccos\left[\frac{spt + \left(mh - mfg\sqrt{sp^2 - t^2 + (mh - mfg)^2}\right)}{sp^2 + (mh - mfg)^2}\right]$$

Eq 1: Analytical solution for α

Recursive method

$$\tan\alpha_{n+1} = \frac{sp - t/\cos\alpha_n}{mh - mfg}, \qquad \text{with } \alpha_0 = \pi/4$$

Eq 2: Iterative solution for α

Example, with fh=0.85, mh=0.95, mfg=0.45, sp=2, t=0.2,

using Eq 1

α_+ = 1.2287rad (70.3965°),

or using the recursive formula Eq 2

$\alpha_0 = \pi/4$

α_1 = 1.2875

α_2 = 1.1996

α_3 = 1.2384

α_4 = 1.2248

α_5 = 1.2301

$\alpha_6 = 1.2281$

$\alpha_7 = 1.2289$

$\alpha_8 = 1.2286$

$\alpha_9 = 1.2287$

5.4.3.2.Plasticity Estimates and "Spike" Value

The angle α defined above is a crucial part to how the plasticity estimates are to be defined. Intuitively the angle has a significant role in how the strip will be deformed/embossed, but exactly what the role is unclear even after some deliberation. Below, is defined the concept "proj", strongly dependent on α, and is the distance between the edge of the male sidewall including strip thickness to the projected point the strip would meet the female flat based on angle α. This concept is then used to define the convex plasticity estimate, and α is used indirectly once again to define the concave plasticity estimate. The two estimates are then combined to define the "spike" value. It is called such due to the phenomenon seen in the contracer measurements above (Figure 98-Figure 102). It is proposed that this feature is a result of springback, the nature of which is a complicated function of the geometry used. The idea is is that the spike value is a related measure of this springback, and is defined to be the ratio of convex:concave plasticity estimates.

D L Davies dave.davies@orange.net

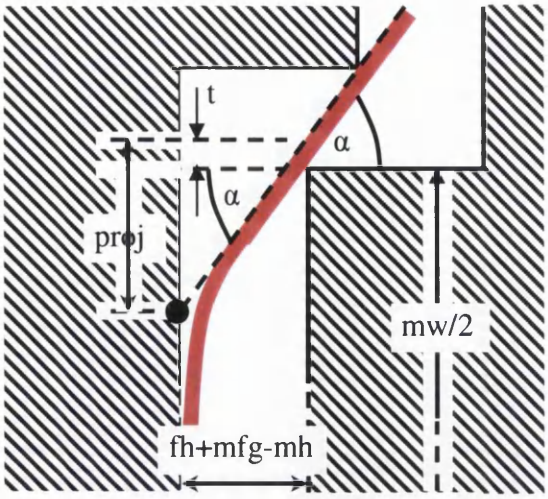

proj := distance from edge of male tool including strip thickness to projected distance based on angle α

Figure 105: Definition of the proj concept

It makes logical sense that for sufficiently large α, proj(α) is big enough such that no plastic deformation occurs on the convex side of the strip. Clearly the converse is true also and so it is evident there exists a bifurcation proj* such that no plastic deformation takes place under the condition proj > proj*, and conversely when proj < proj* plastic deformation does take place. However, for most realistic tool set-ups proj will be large enough to allow plastic deformation occur, so what is needed is a measure of how much plasticity is likely to occur. In particular localised plastic deformation in the convex part of the strip, and this is more likely to occur when the length of the flat of the male square becomes larger. Also it's clear to see from the above description of proj that it's inversely proportional to localised plasticity.

$$\therefore \gamma := \frac{mw/2}{proj(\alpha)}$$

Eq 3: Convex plasticity estimate

Similarly a measure of the plasticity potential on the concave surface can be estimated: -

D L Davies dave.davies@orange.net

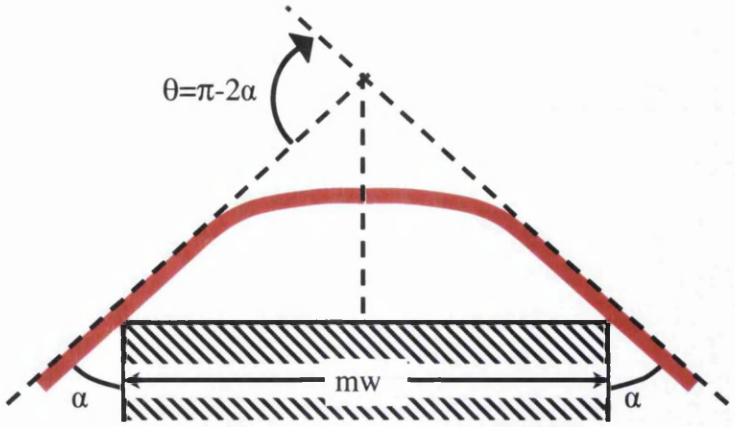

Figure 106: Concave plasticity estimate

The contributing factors to the plasticity are length of male die flat, mw, and the angle θ. As mw increases the plasticity potential decreases because there is more room in which to bend the same angle. Likewise, as θ increases the plasticity potential increases because the same amount of room is available in order to bend a greater angle. Thus the concave plasticity potential estimate is defined as,

$$\omega := \theta/mw$$

Eq 4: Concave plasticity estimate

Now the spike value can be defined as the ratio of the plasticity estimates

$$\psi := \gamma/\omega$$

Eq 5: Spike value definition

From Figure 105 it can be seen that

$$\tan\alpha = \frac{proj(\alpha) - t}{fh + mfg - mh - t/\sin\alpha},$$

$$\therefore proj(\alpha) = t + (fh + mfg - mh - t/\sin\alpha)\tan\alpha$$

Eq 6: Proj(α) formula

$\psi = \{mw/2 / proj(\alpha)\} / \{(\pi-2\alpha)/mw\}$, using Eq 3, Eq 4 and Eq 5

$$\therefore \quad \psi = mw^2 / (2(\pi-2\alpha)proj(\alpha))$$

Eq 7: Spike formula

5.4.4. Flat Strip Embossing

The purpose of this experiment is to validate an embossing process that resembles the above embossing of squares onto can walls. It involves the designing and production of tooling dies to emboss squares similar to the ones used in embossing the can walls, only this time it will be small strips of tinplate (0.22mm) embossed. In this way if this experiment can be simulated and validated then there are enough similarities to the other embossing processes to provide confidence that the other models are also realistic in their predictions.

The simplified tooling gives a strong advantage in that the process is easily repeatable, has little variation and the constraints and boundary conditions are well defined and controlled. Whereas the squares in the can embossing varied a large number of parameters (4 spacings, 3 edge radii, 4 corner radii, 2 square sizes) on only 24 squares, this experiment only focuses on differing square sizes (4 male, 3 female) with an implied spacing difference. E.g. female square size 9.6mm, male 7mm, implies a spacing of 1.3mm.

5.4.4.1.Experimentation

The general tooling dimensions can be seen in Figure 107 to Figure 110. The range of dimensions and spacings between and male and female dies were chosen such that the forming of the embossed 0.22mm strip was similar to the embossing of the can walls. In particular the spike feature that was noted for the 10mm square of the can is

wanted to be found with this experiment, and also to cover the range of square sizes such that this feature no longer exists.

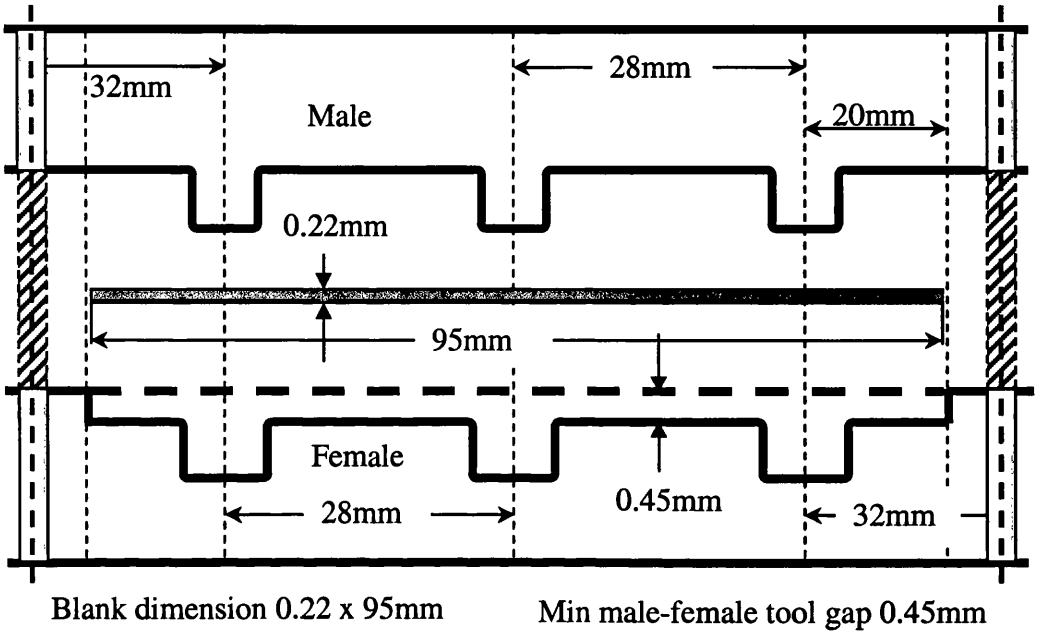

Figure 107: Flat strip embossing tooling template; side elevation

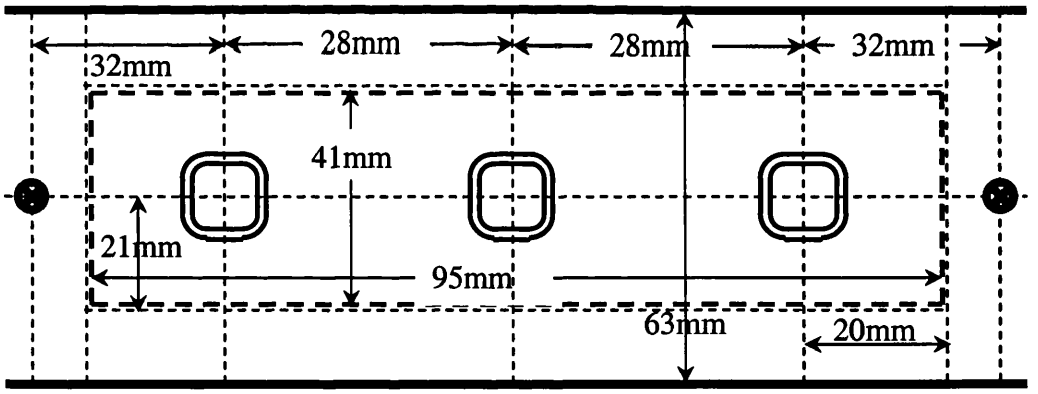

Figure 108: Flat strip embossing tooling template; plan view

Four male, and three female tools were made, with the only difference between them being the nominal square size. The various square dimensions are listed in Table 16 below, along with the combinations that are to be tested.

D L Davies dave.davies@orange.net

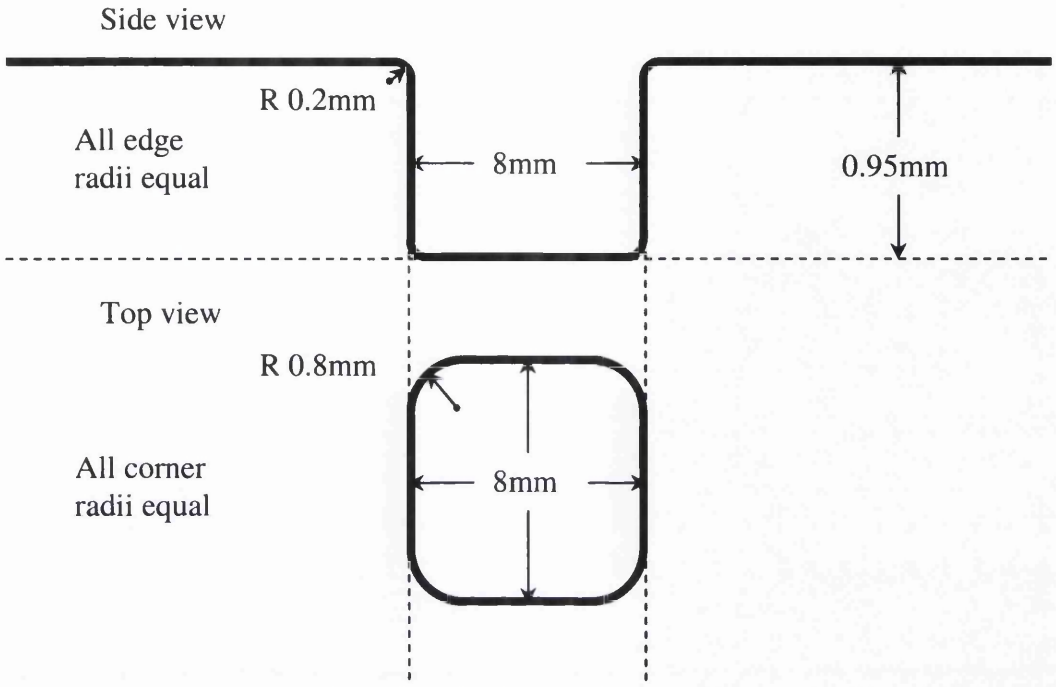

Figure 109: Profile of male die square

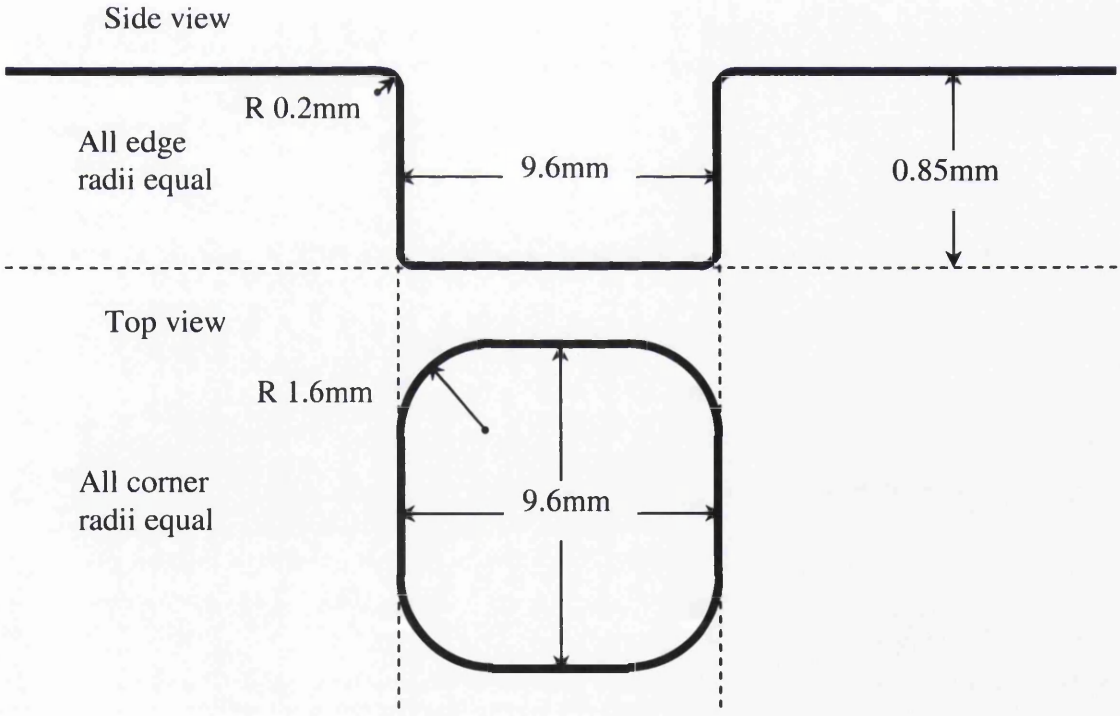

Figure 110: Profile of female die square

Combination	Male square dimensions, mm				Female square dimensions, mm		
	5	7	8	8.8	5.8	7.8	9.6
1	5				5.8		
2	5				7.8		
3	5				9.6		
4	7				7.8		

5	7	9.6
6	8	9.6
7	8.8	9.6

Table 16: Flat strip tooling sets and combinations

The press used for the experimentation was a manual press (Figure 111) working on the principal of a vice. Noting the recess is deeper than the thickness of the strip means that the amount of force applied to tooling isn't critical to the forming provided the force is enough for the male die to come in contact with the female die. The reasoning for the recess is to take away the importance of how much force is applied by limiting the travel of the male die. After the male die comes in contact with the female any additional force applied results in no extra force being applied to the strip since there will be minimal strain compression of the female die. Its purpose then is to easily control accurately the tooling overlap during embossing, i.e. the embossing depth. This makes the process of embossing the strips a repeatable and fair experiment, and takes off the need for an accurate press machine.

D L Davies dave.davies@orange.net

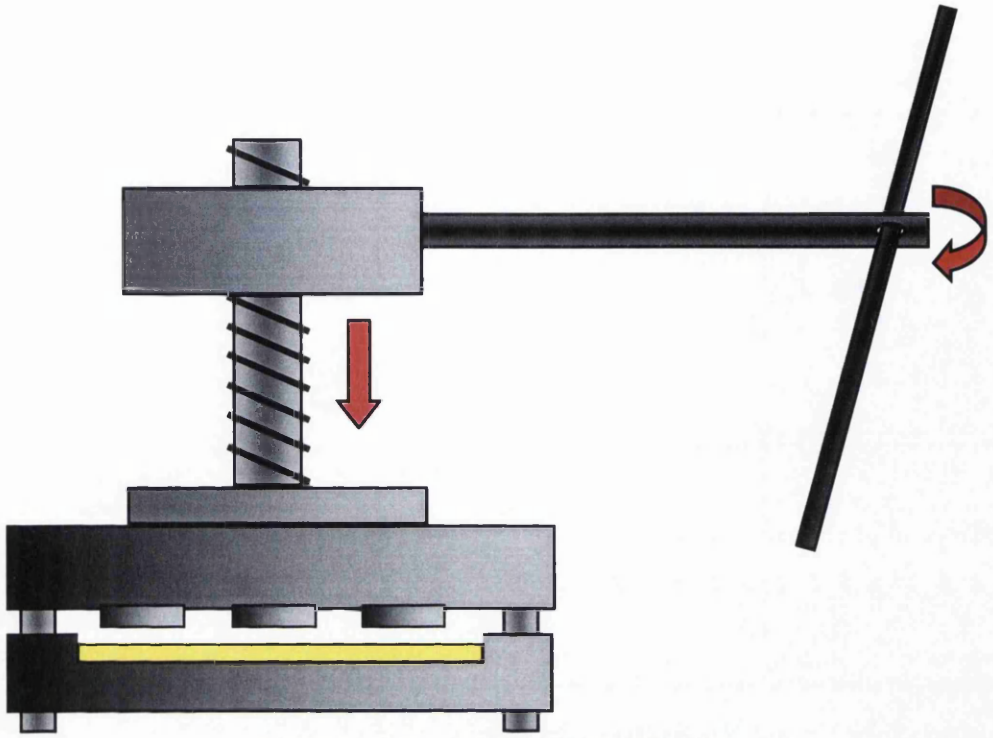

Figure 111: Schematic of embossing press

Also due to the symmetry of the tooling the embossing of the squares can be expected to be symmetrical about the two central axes (Figure 112). This symmetry only holds during the forming because of the constraints and boundary conditions of the system, namely the rigidity and support of the female die.

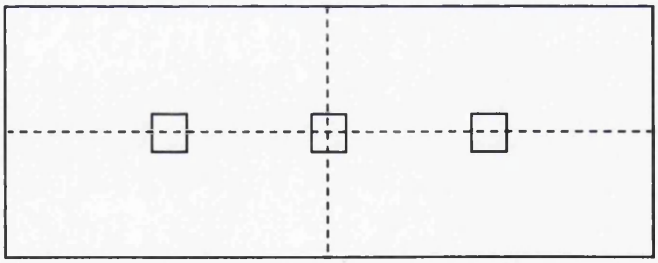

Figure 112: Quarter symmetry of strip and tooling

The symmetry is utilised further when modelling this experiment as only one quarter of the system needs be analysed with the appropriate boundary conditions in place on the lines of symmetry. The boundary conditions are no movement away from the boundary and no rotation about the lines of symmetry.

D L Davies dave.davies@orange.net

Post forming, the embossed samples are scanned using a SVET apparatus to create a surface mapping of the samples. Due to the nature of symmetry present the scan was only taken over the centre square to midway toward an adjacent square. The SVET has the capable resolution of 2.5 microns in all dimensions. Before measuring the samples, a test case was done to check to see if this resolution would be sufficient. The test case was on one of the male tool dies, as the dimensions of which are all known, and the results were so accurate that they even picked up a small fault (a scratch) on the die. As a consequence the SVET was deemed sufficiently accurate and as such was used for the measuring of samples.

5.4.4.2.Simulation

The details of the model can be seen in the modelling appendix (A.v). The aim of the model is to obtain validation of the process. The means of validation are in simulating the "spike" features when they occur, the general displacement distribution, the magnitude of the embossing, and any other features that are noticed in the results of the physical experiment.

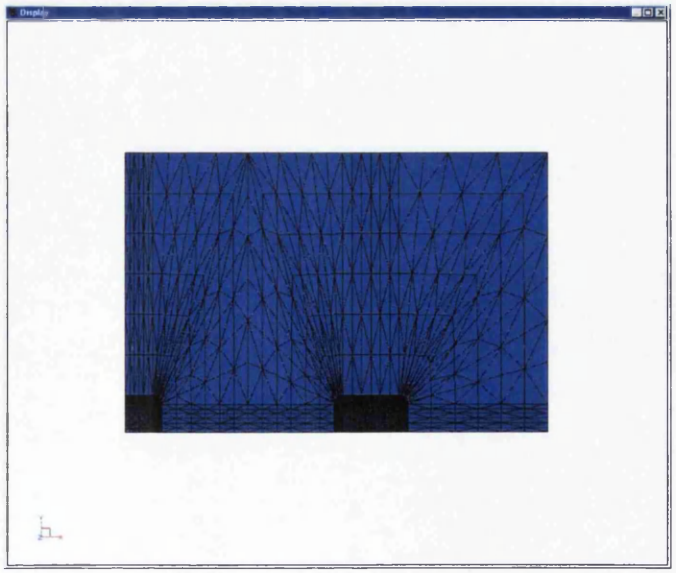

Figure 113: Plan view of flat strip embossing mesh with quarter symmetry

D L Davies dave.davies@orange.net

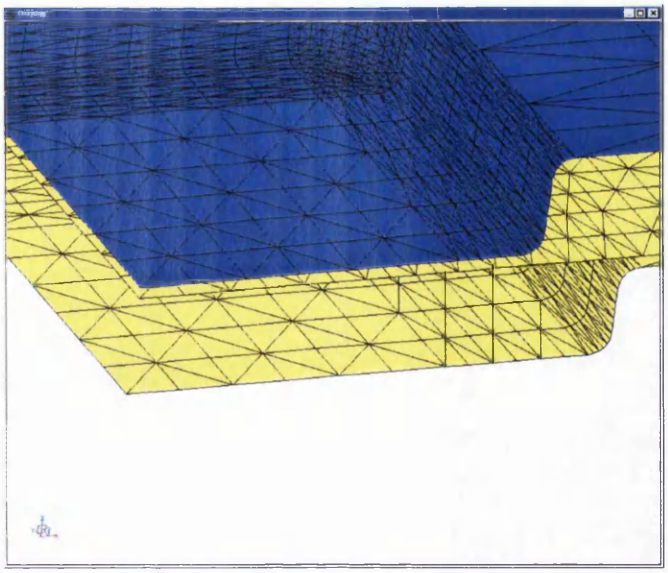

Figure 114: Angled profile of flat strip embossing mesh displaying edge radii of tools

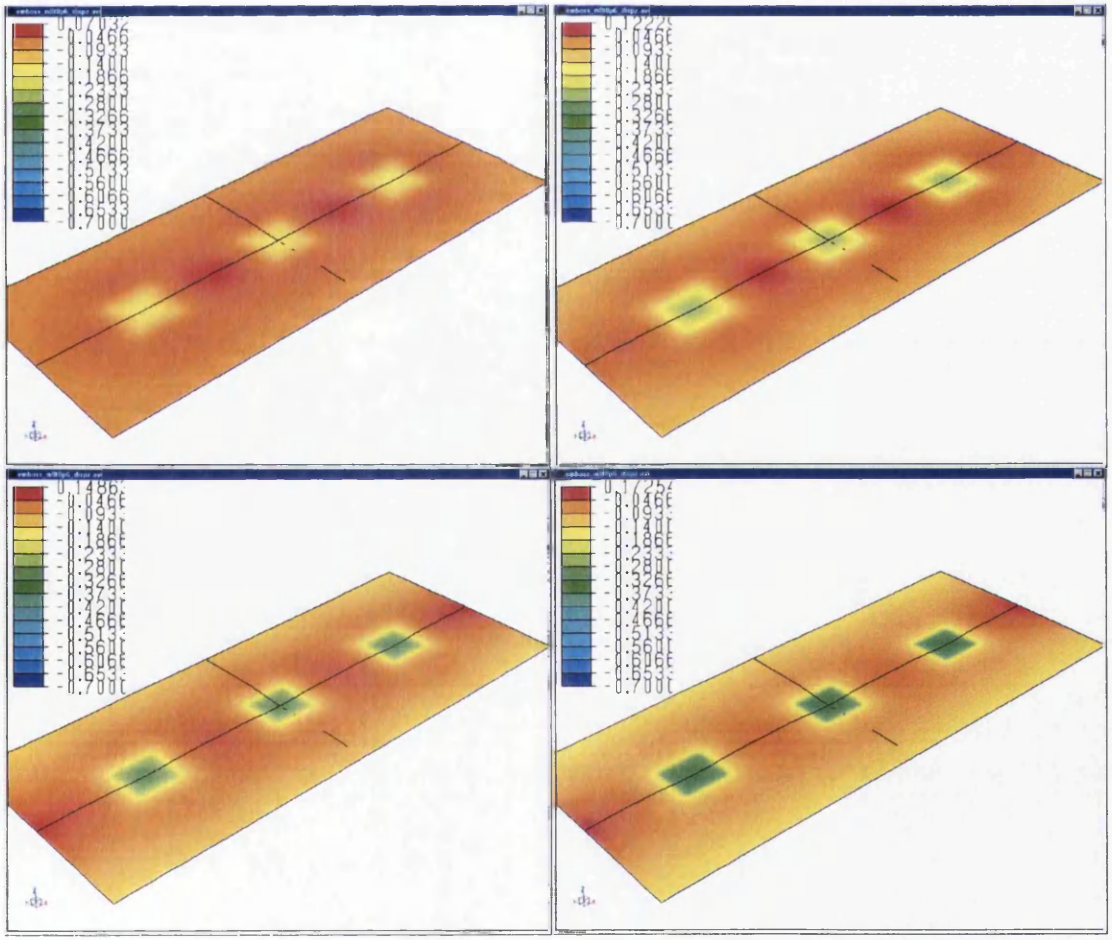

Figure 115: Male 8mm, female 9.6mm, z displacement plots; time 0.3 – 1.2

D L Davies dave.davies@orange.net

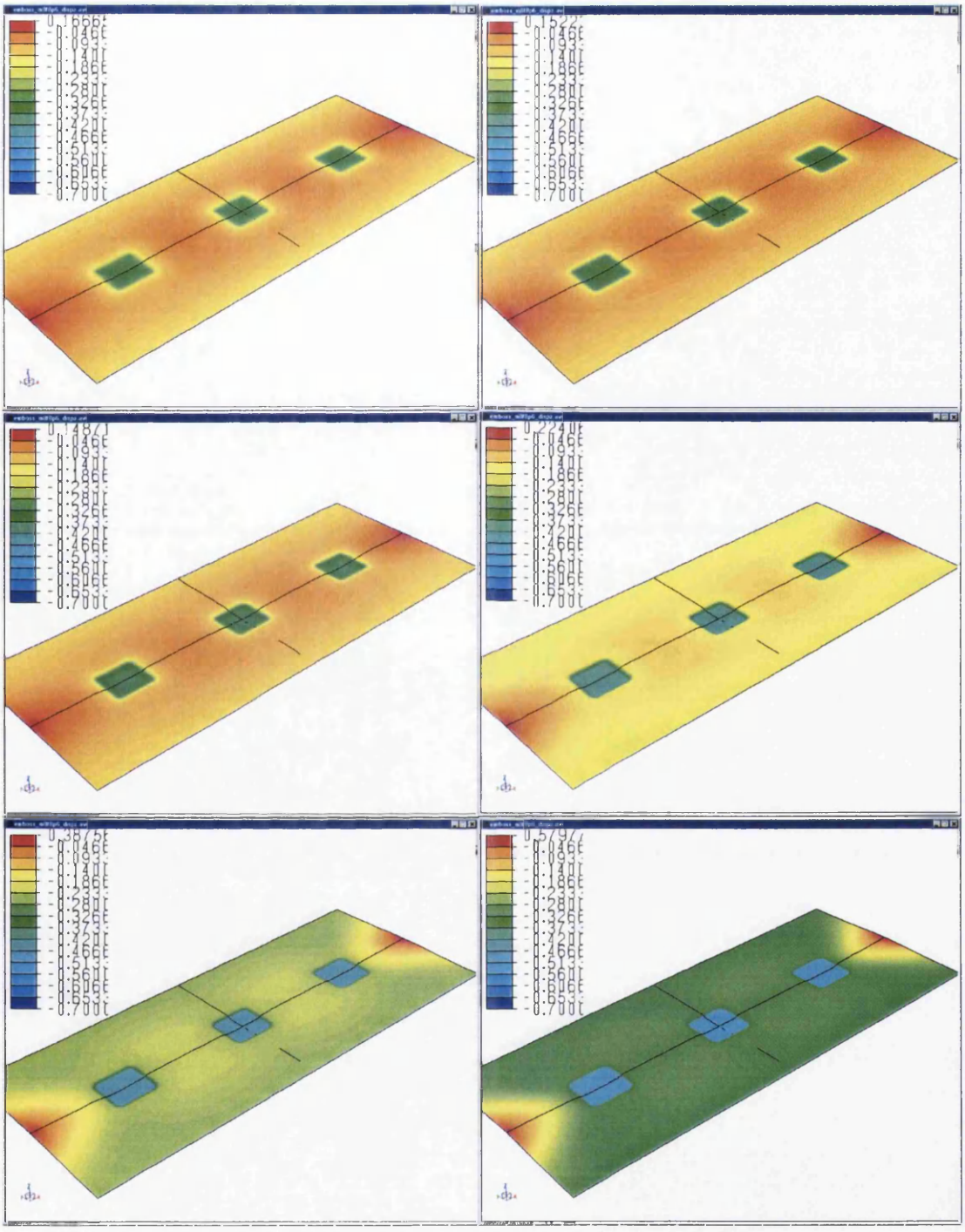

Figure 116: Male 8mm, female 9.6mm, z displacement plots; time 1.5 – 3

D L Davies dave.davies@orange.net

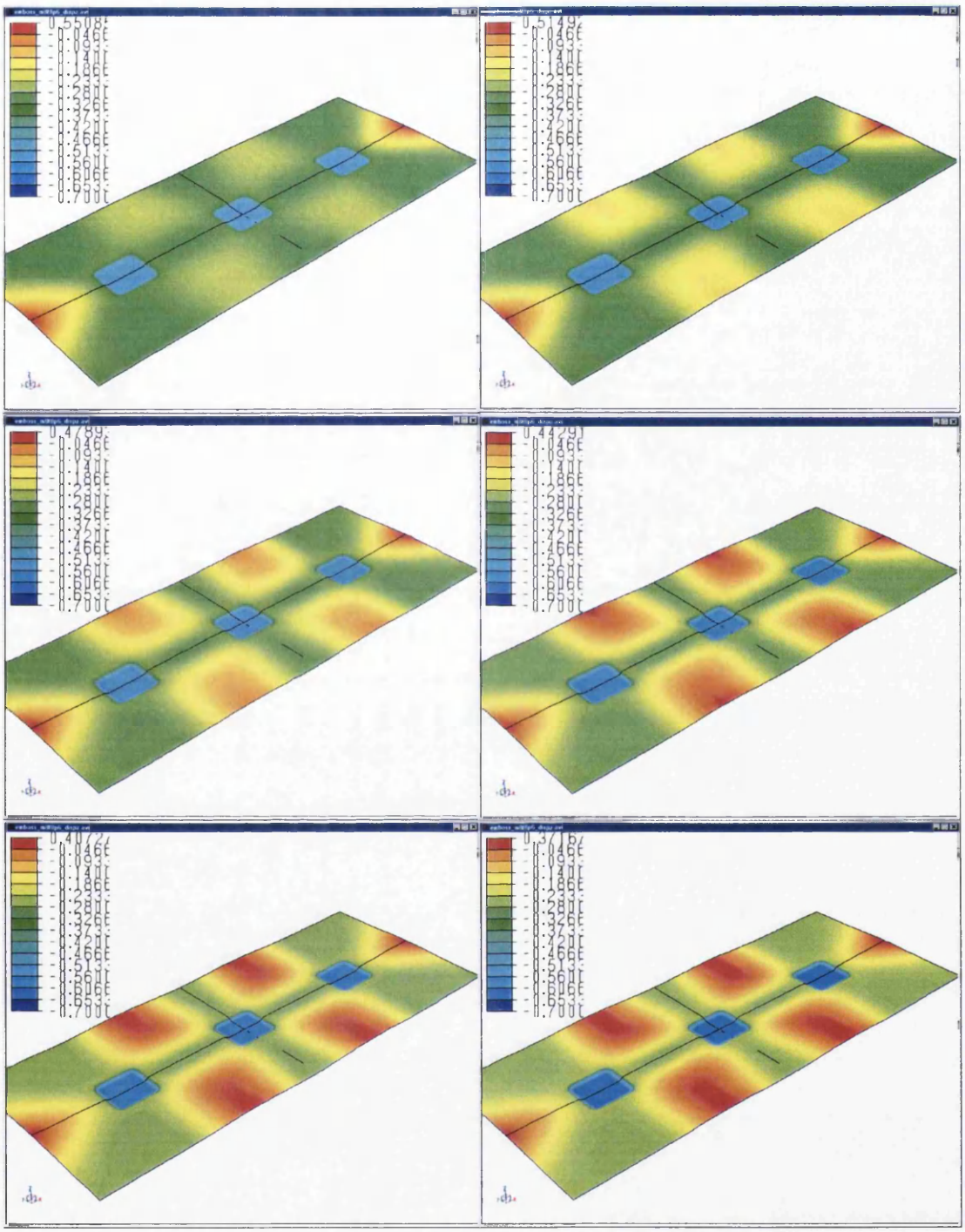

Figure 117: Male 8mm, female 9.6mm, z displacement plots; time 3.3 – 4.5

D L Davies dave.davies@orange.net

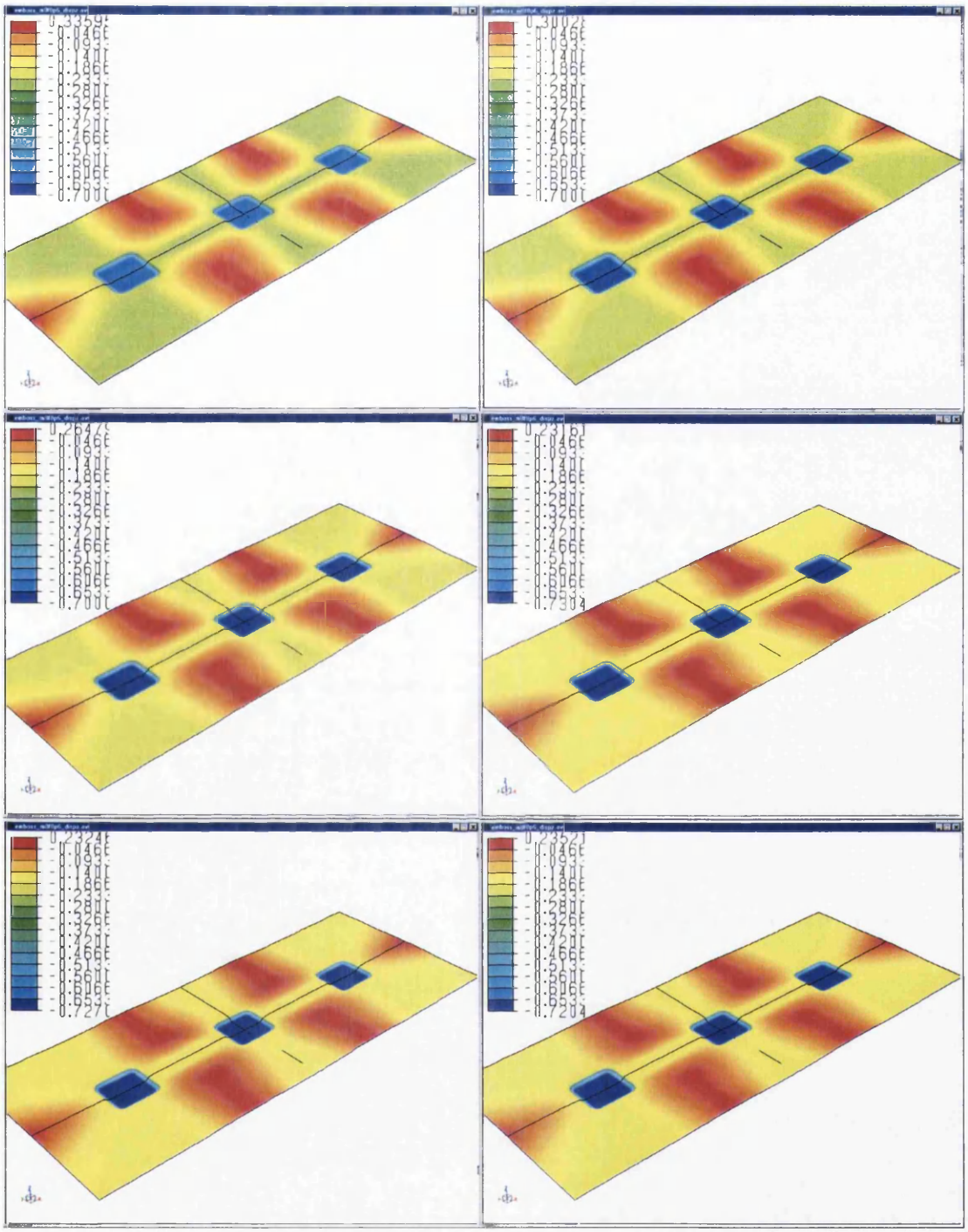

Figure 118: Male 8mm, female 9.6mm, z displacement plots; time 4.8 – 11.6

D L Davies dave.davies@orange.net

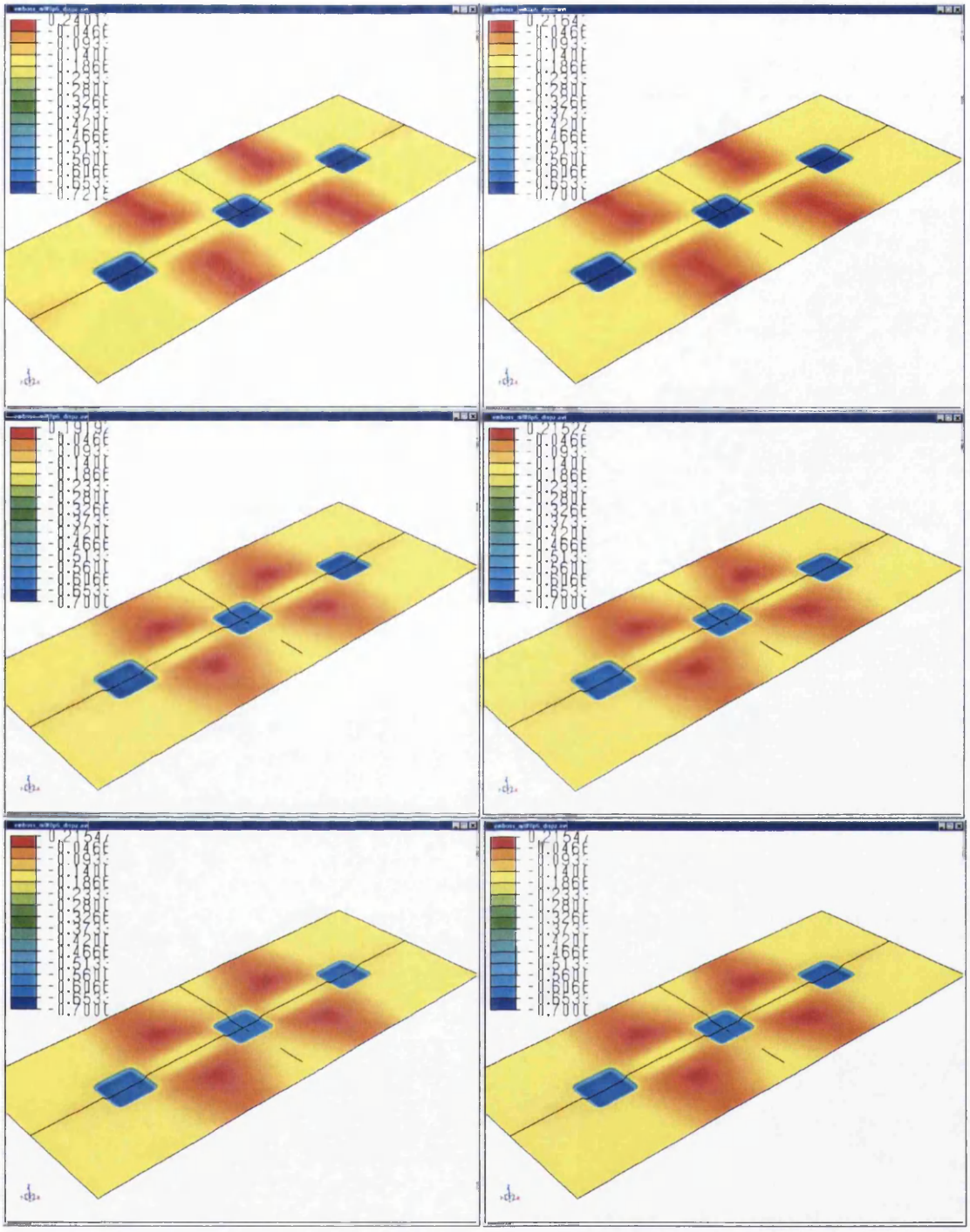

Figure 119: Male 8mm, female 9.6mm, z displacement plots; time 16.6 – 41.6

D L Davies dave.davies@orange.net

5.4.5. Comparison and Validation

There are two different sets of comparisons to be made; the simulations against the physical experiments of tool combinations 1-7, and the simulations against the theory of the plasticity estimates. Comparisons are made for each combination, which include geometric likeness, features, and the peak plastic strain in the corner of the centre square.

5.4.5.1.Geometric comparison

Combination 1 - Male 5mm, Female 5.8mm

All of the samples made with this tooling combination resulted in partial failure. The spacing, 0.4mm, was small enough to tear the material in localised areas. On holding the samples up to the light it could be seen that there were small gaps in the material where the male die edge had been. As such, the sample was not measured with the SVET, and no geometric comparisons made with the simulation, but instead just noted as unformable.

The simulation of this set-up follows in that it could not be formed all the way through to the desired and designed embossing depth. The analysis ran as far as 90% of its embossing depth, i.e. 0.65mm. This could be interpreted that if the experiment were only run to 0.65mm then the formed sample would not have any rips in the material. The fact that the model fails to form when in reality it also doesn't properly is a good sign.

D L Davies dave.davies@orange.net

Combination 2 - Male 5mm, Female 7.8mm

The simulated geometry is shown in Figure 120 that is mirrored into the full strip utilising the facility in the post processor

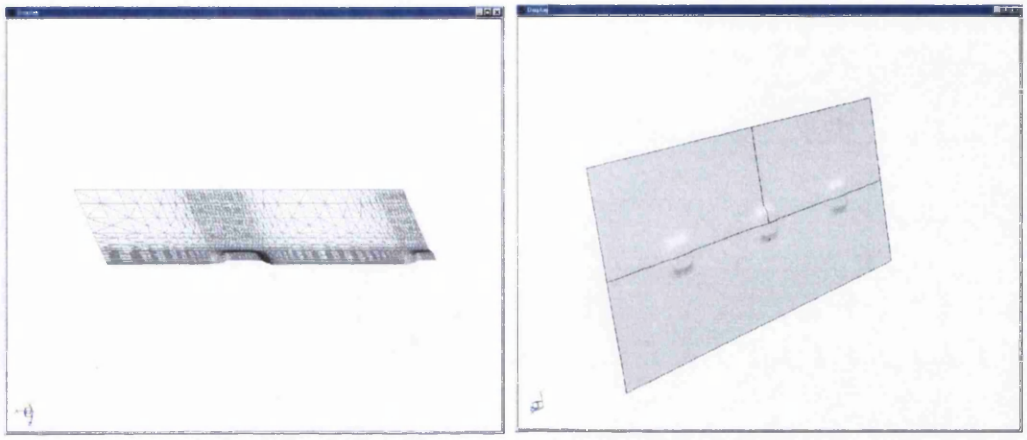

Figure 120: Simulated strip, male 5mm, female 7.8mm

Figure 121 is the surface map of the middle square and the surrounding area. The detail on the right is a 3D plot of the area outlined by the black box. This result shows there is only little spiking present as the maximum height difference between centre of square to edge is 10 microns.

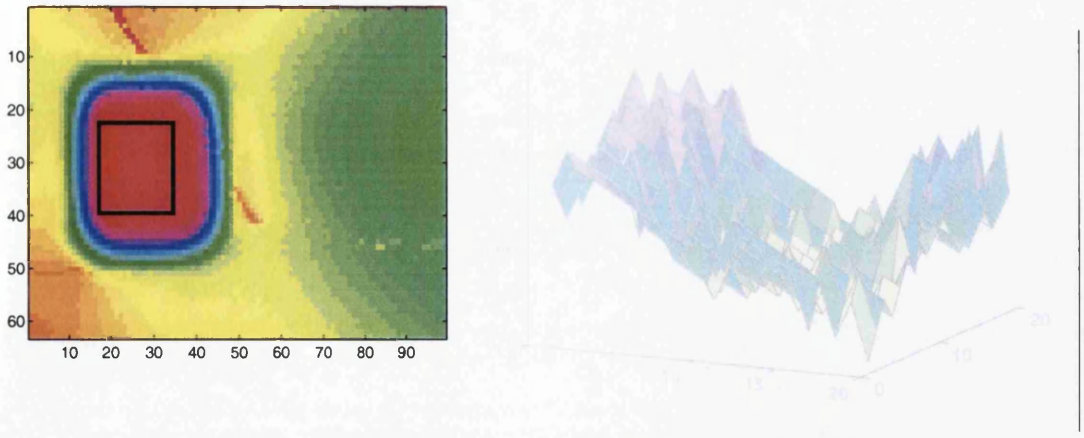

Figure 121: Surface map of male 5mm female 7.8mm strip, with detail of square

Figure 122 is a plan view of the simulated strip zoomed in on the centre square with the scale being displacement in z. This compares well with measurements, as the

D L Davies dave.davies@orange.net

general shape is similar, the scale is very close, and the z-distance between the centre and corner is 10 microns.

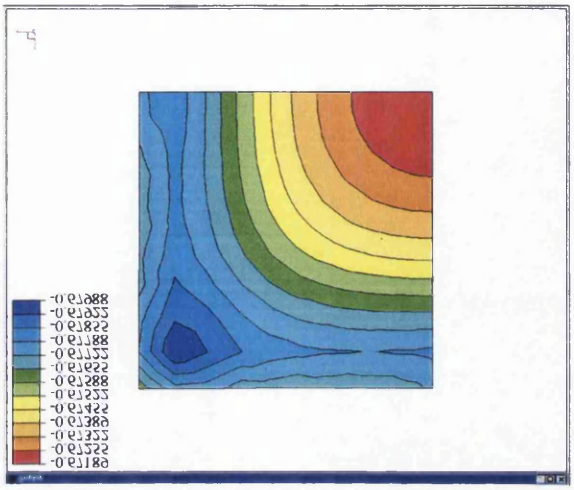

Figure 122: Close up of FE square, male 5mm female 7.8mm; scale z-displacement

Combination 3 - Male 5mm, Female 9.6mm

Figure 123 shows the simulated strip for the male 5mm female 9.6mm after being mirrored about its two lines of symmetry.

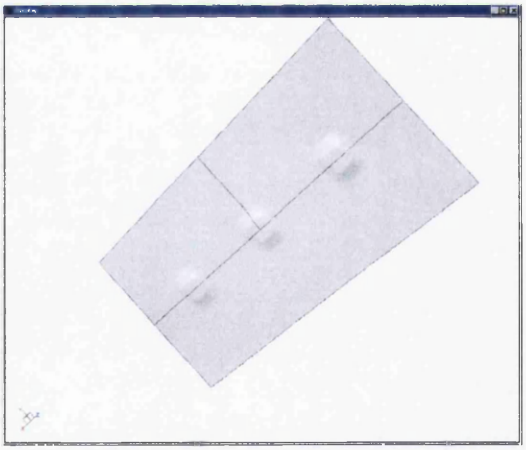

Figure 123: Simulated strip, male 5mm, female 9.6mm

As with the male 5 female 7.8, Figure 124 and Figure 125 show good similarity in terms of general shape, scale, and again approximately 10 micron z-displacement.

D L Davies dave.davies@orange.net

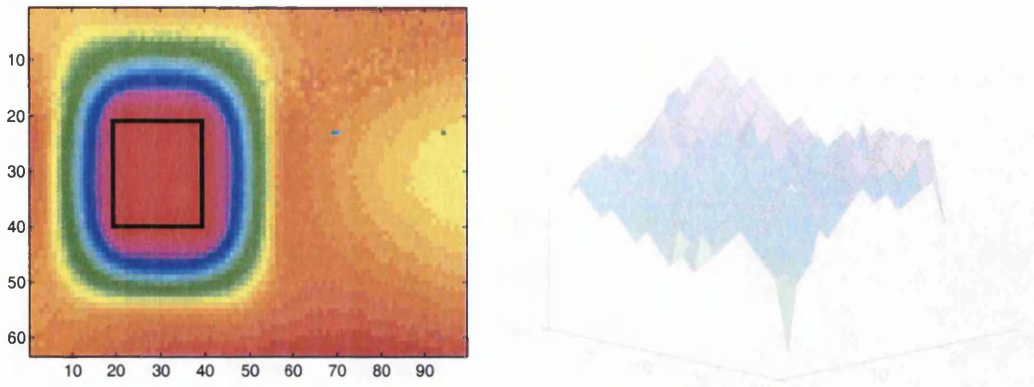

Figure 124: Surface map of male 5mm female 9.6mm strip, with detail of square

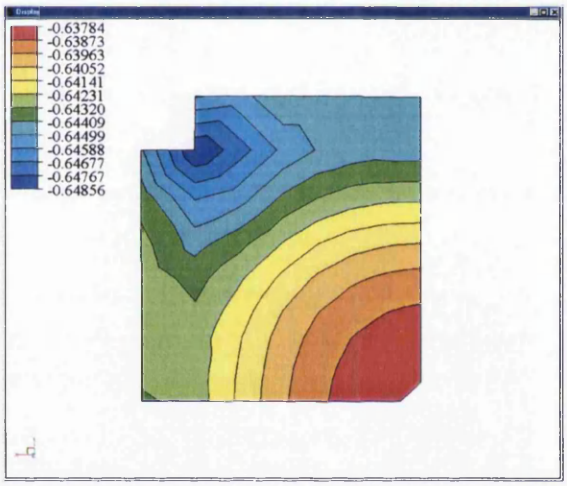

Figure 125: Close up of FE square, male 5mm female 9.6mm; scale z-displacement

Combination 4 - Male 7mm, female 7.8mm

Similar to combination 1 – material fails to form without tearing slightly, and likewise the FE simulation cannot complete the analysis.

Combination 5 - Male 7mm, female 9.6mm

The simulated geometry is shown in Figure 126 along with the same geometry only with the displacements magnified by a factor of 10. The purpose of this is to help visualise the formation of "saddles" between the embossed squares, as they are only small with this tooling combination, although much more evident than combinations 2 & 3 where they essentially cease to exist in both the simulation and reality

D L Davies dave.davies@orange.net

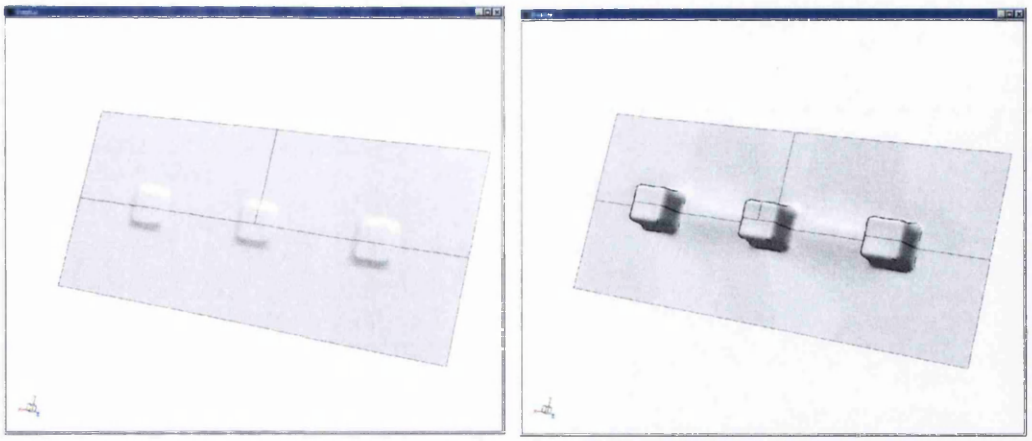

Figure 126: Simulated strip, male 7mm, female 9.6mm, with exaggerated 10 times displacement (right)

Figure 127 contains the surface map of part of the sample male 7mm, female 9.6mm, with a close up 3-D section of the square and a contour plot of the "saddle" area. It shows there is a 30 micron difference in height between the centre of the square and the corner edge, and there is a 100 micron range over the saddle area taking a vertical slice through the centre of the saddle.

D L Davies dave.davies@orange.net

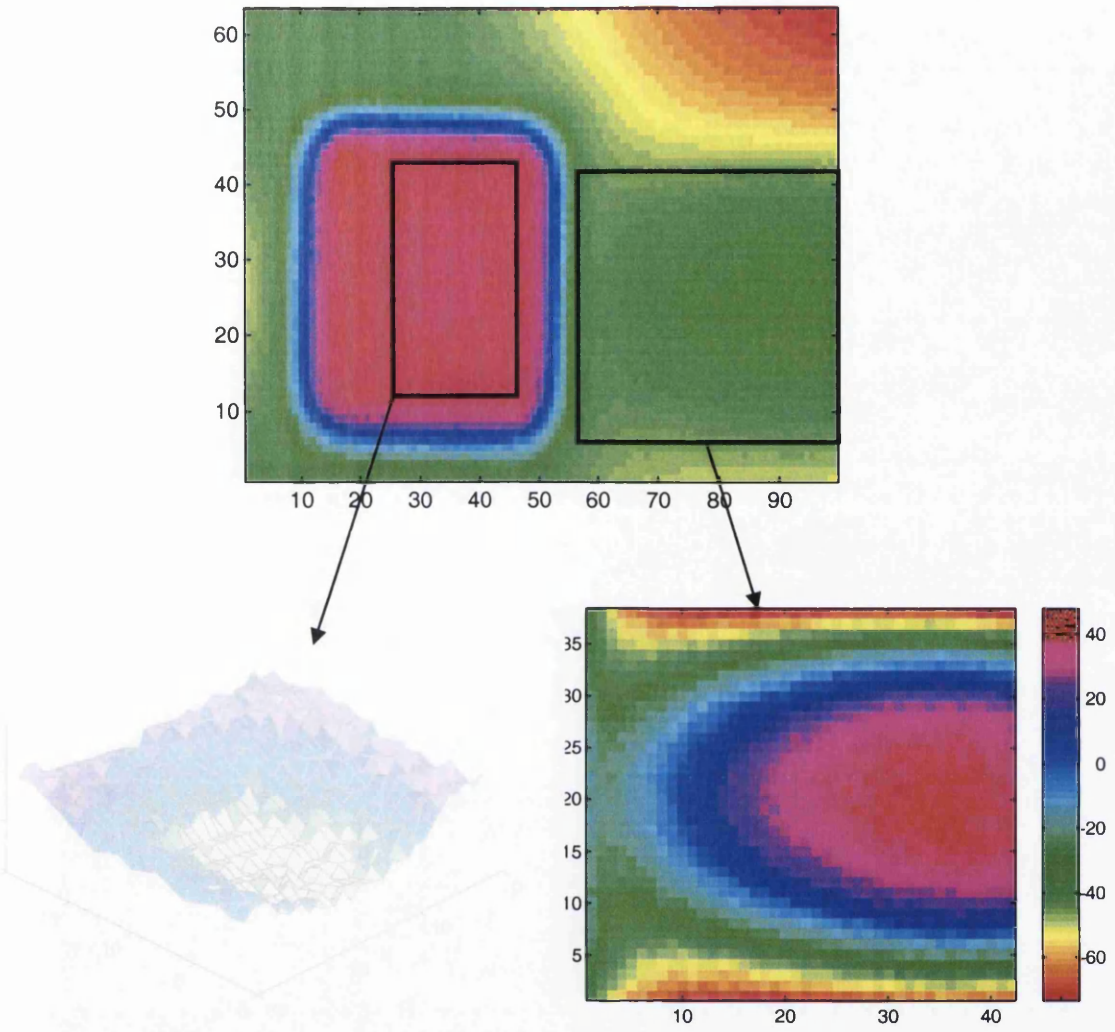

Figure 127: Surface map of male 7mm female 9.6mm strip, with detail of square and saddle

Figure 128 shows the analysis results for the male 7mm, female 9.6mm combination, with a close up of the centre square and the breadth of the strip between two squares. The results are in good accordance with the physical measurements as they show the same 30 micron difference in height over the square, and a 93 micron range over the saddle.

D L Davies dave.davies@orange.net

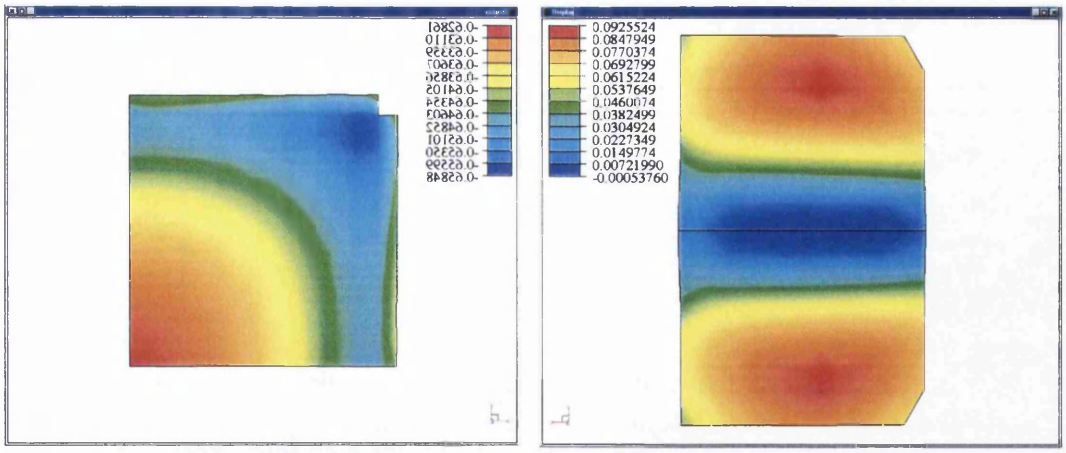

Figure 128: Close up of FE square male 7mm, female 9.6mm, and area between squares containing saddle

Combination 6 - Male 8mm, female 9.6mm

As with combination 5 Figure 129 shows the simulated male 8mm, female 9.6mm alongside its corresponding 10 times displacement mapping. Although the difference here is that the saddle can be seen in the unexaggerated (left) plot, as the saddle in this case is 265 microns tall as can be seen clearly in Figure 131.

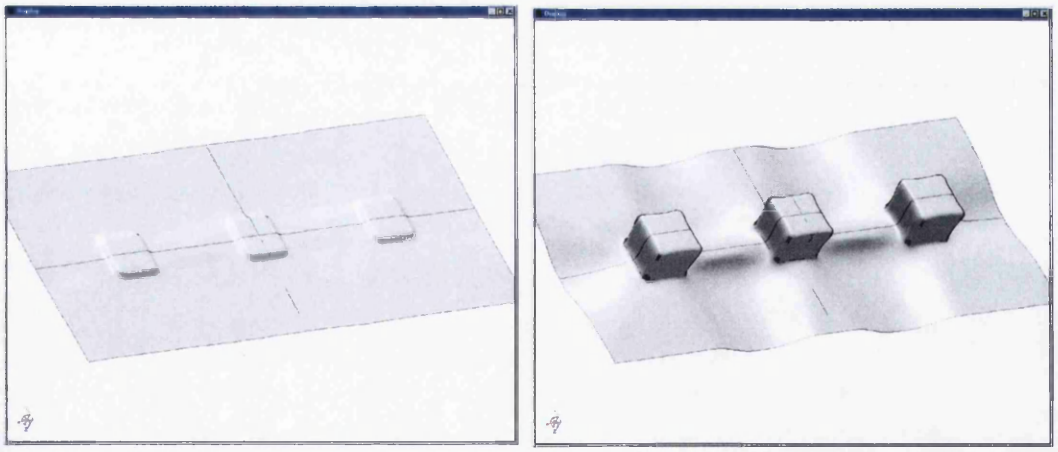

Figure 129: Simulated strip, male 8mm, female 9.6mm, with exaggerated 10 times displacement (right)

Once again, Figure 130 shows the surface map of the male 8mm, female 9.6mm, with a 3-D close up of the square, and a 3-D contour of the saddle area. There is a clear difference in height over the square; the centre is nearly 30 microns lower than the

corner edge. The saddle measured is approximately 250 microns, although may be higher if compared with an area nearer the strip edge.

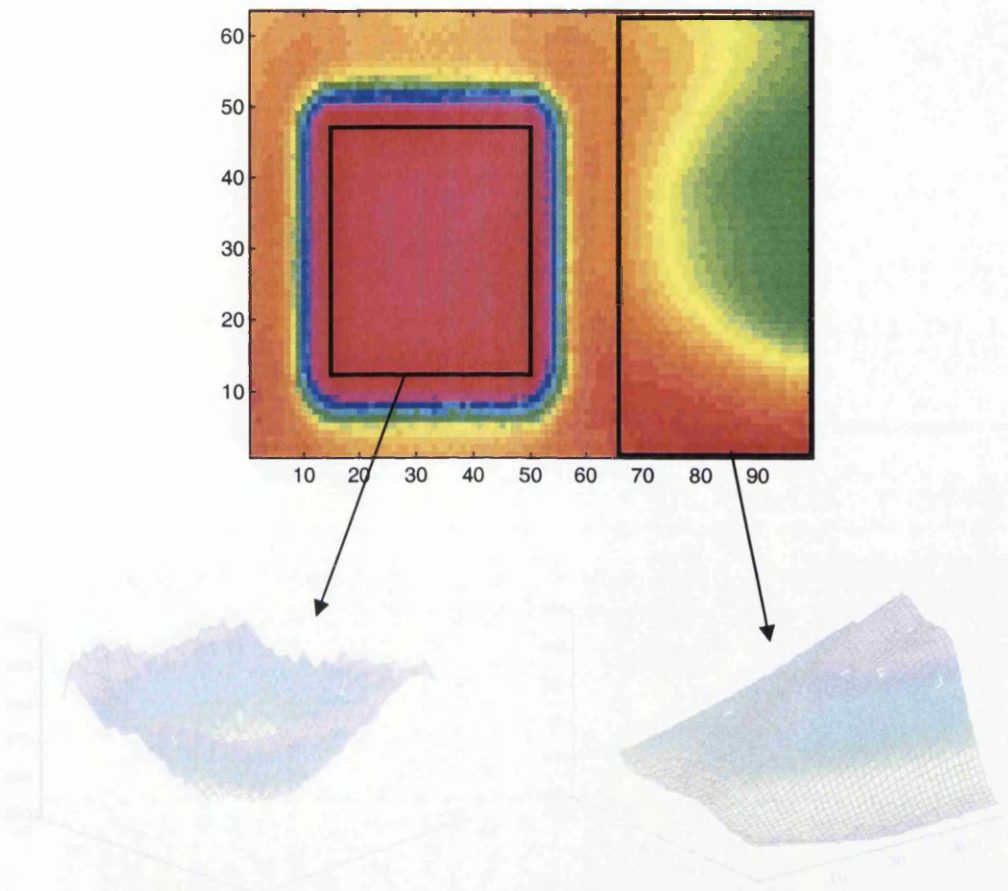

Figure 130: Surface map of male 8mm female 9.6mm strip, with detail of square and saddle

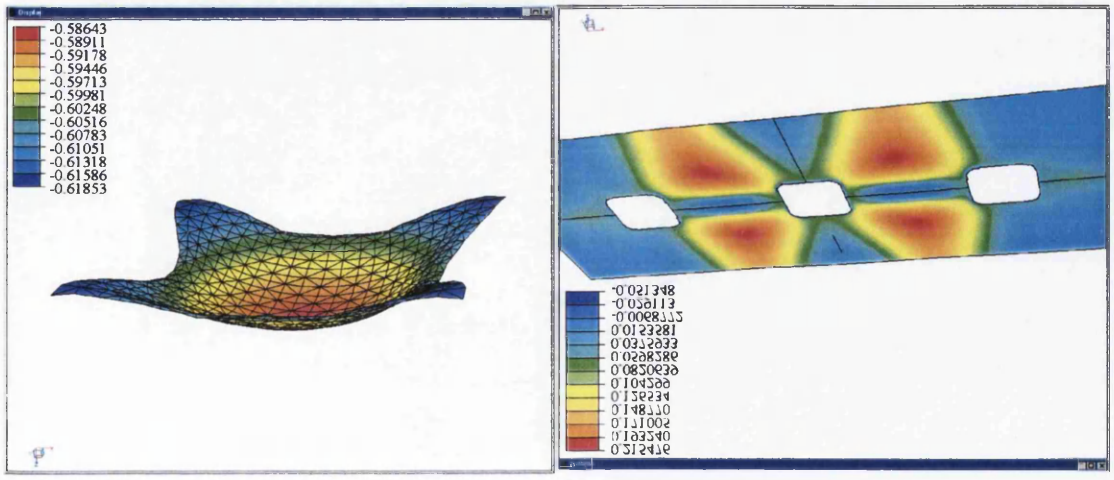

Figure 131: Close up of FE square male 8mm, female 9.6mm, and area between squares containing saddle

D L Davies dave.davies@orange.net

Figure 131 shows the simulated male 8mm female 9.6mm results. The left picture shows the displacement of the centre square, but with the displacements exaggerated 100 times to make the difference more clear to the eye. The height differential of the centre square to the corner edge is 32 microns, and the saddle can be seen to be about 265 microns by subtracting the highest value on the scale by the lowest.

Combination 7 - Male 8.8mm, female 9.6mm

Similar to combination 1 – material fails to form without tearing slightly, and likewise the FE simulation cannot complete the analysis.

D L Davies dave.davies@orange.net

5.4.5.2.Springback

As described in section 5.4.3 the springback is the cause for the spike feature. This can be seen by looking closely at the embossed square edges at two stages; when the male die is fully pressed onto female (Figure 132), and after the release of the male die (Figure 133).

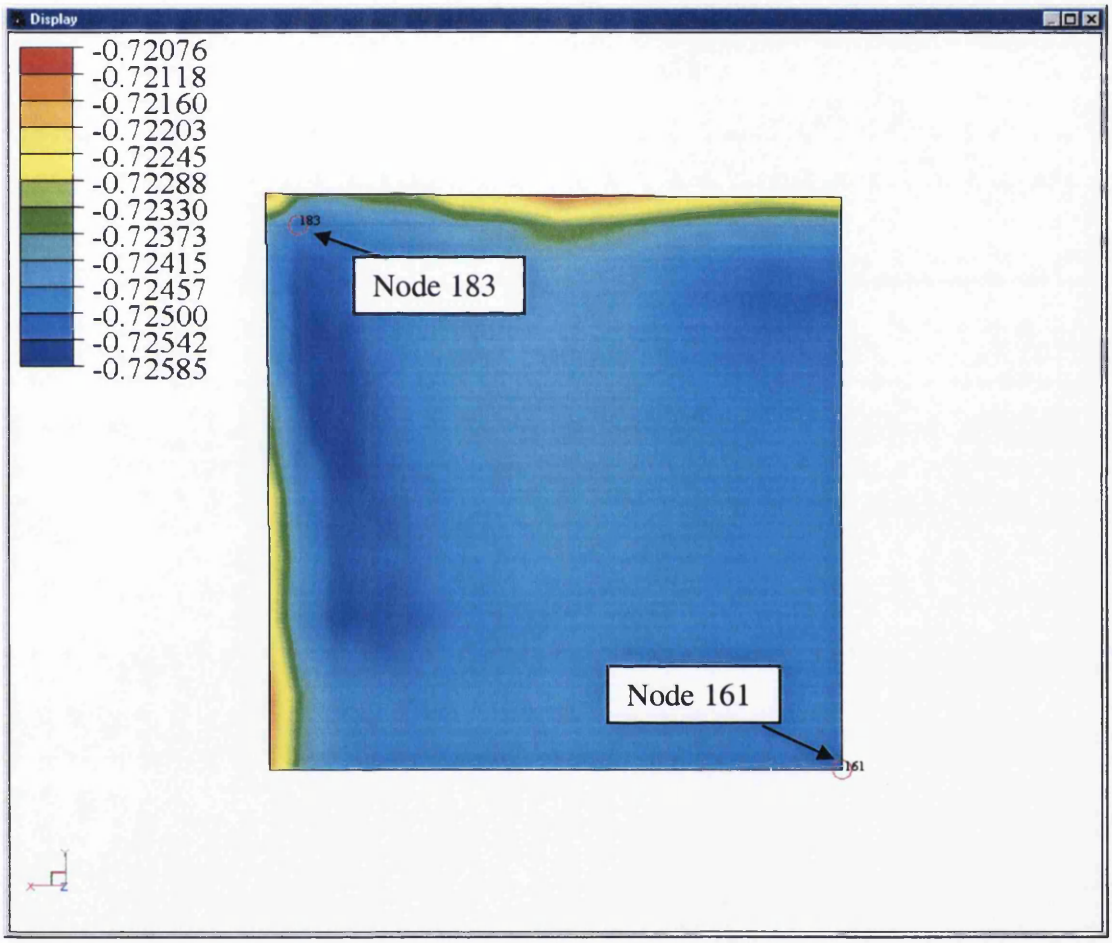

Figure 132: Height displacement of embossed square when male 8mm, and female 9.6mm dies are closed

D L Davies dave.davies@orange.net

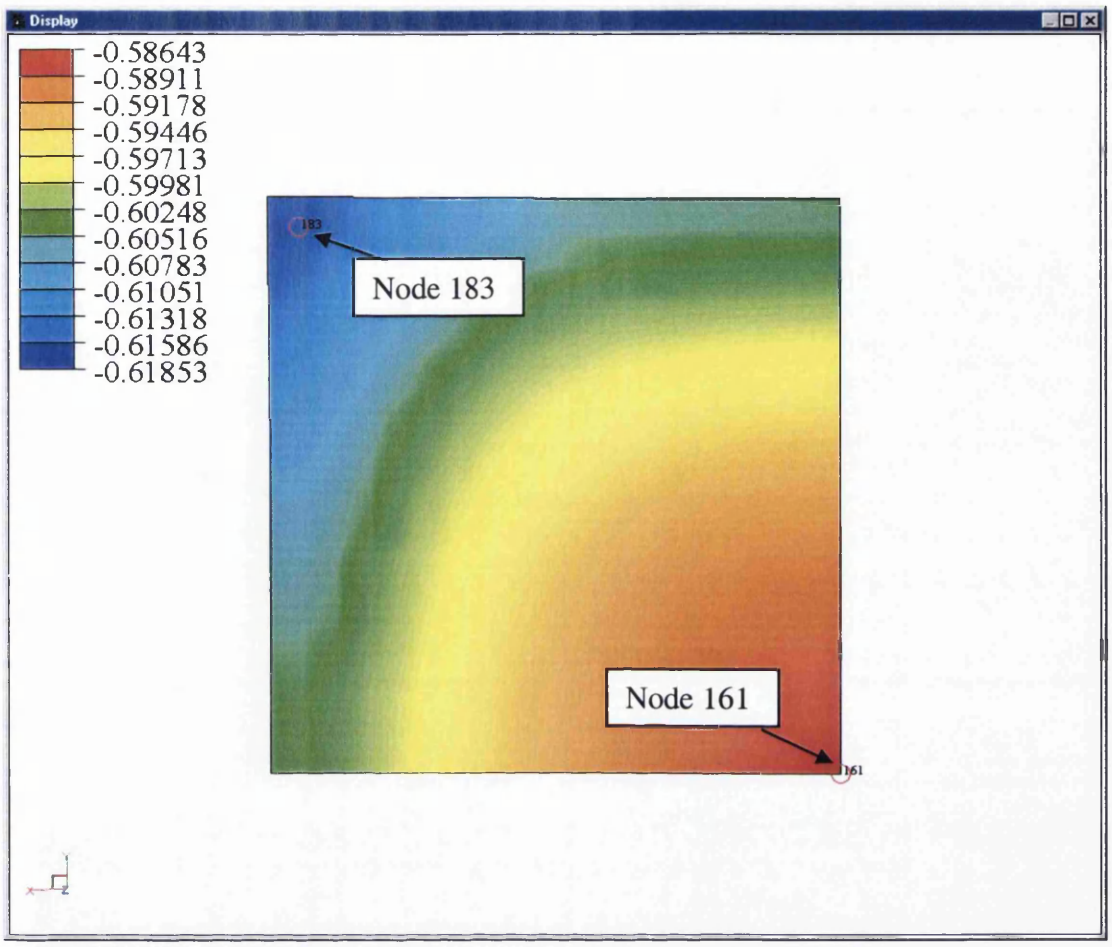

Figure 133: Height displacement of embossed square when male 8mm, and female 9.6mm dies are released

Looking at the scales, it can be seen that there is a reversal in the lowest point of the square during the release of the tooling that results in the centre of the square being approximately 32 microns higher than the corner of the square. As can be seen above (Figure 130, Figure 131), this ties in well with the physical experiment.

Another way to see this springback effect is to look at the history plot height displacement for nodes 161, 183 and 186 (Figure 135). These nodes are the centre of the square, centre of the male die corner radius and a point just outside the female corner radius (Figure 134).

D L Davies dave.davies@orange.net

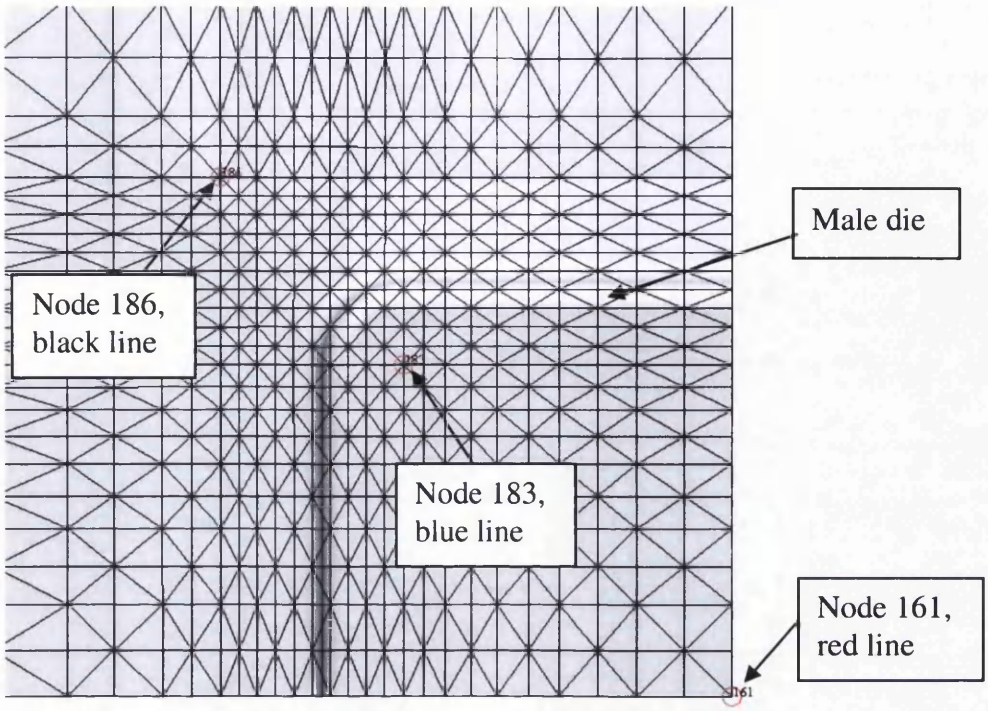

Figure 134: Identification of nodes 161, 183, 186 for run male 8mm, female 9,6mm

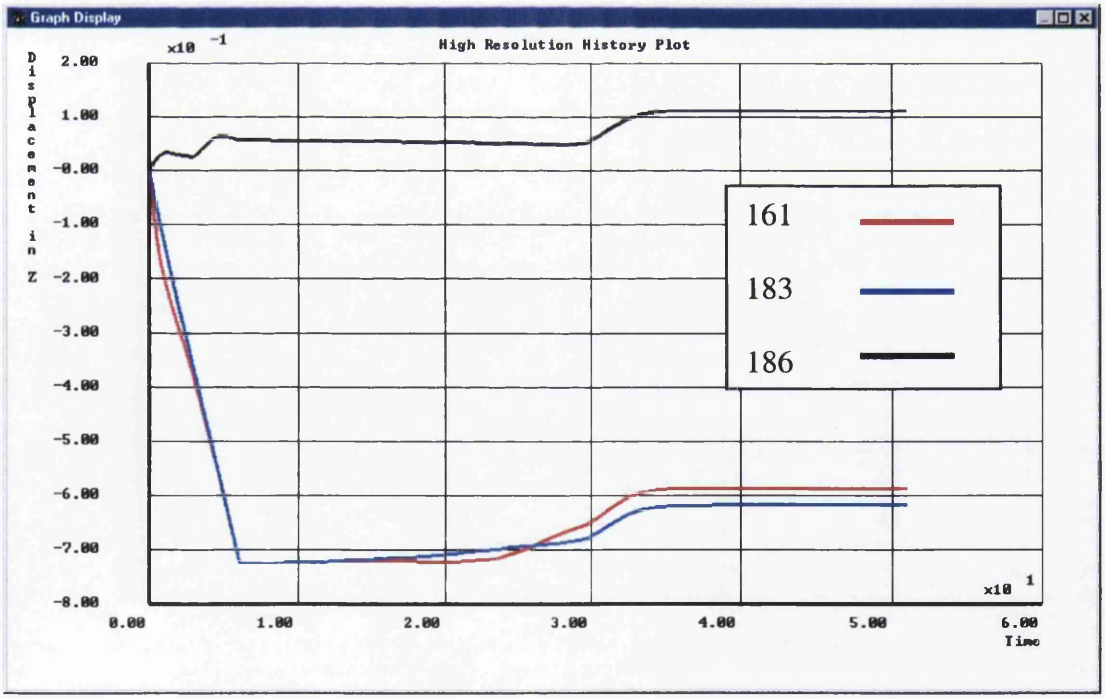

Figure 135: Height displacement for nodes 161, 183, 186 for male 8mm, female 9.6mm

5.4.5.3.Plastic strain comparison

Table 17 lists the theoretical plasticity estimates and spike values for all the tooling die combinations defined above. The three combinations that didn't form properly (1, 4, 7) correspond to the highest plasticity estimates. This suggests that there exists a plasticity estimate limit above which forming cannot take place. Similarly, these three exhibit the highest levels of plastic strains predicted with the FE model.

Combination	Proj	Convex plasticity estimate	Concave plasticity estimate	Spike
1	0.11	23.7	0.5	47.5
2	0.40	6.1	0.2	31.2
3	0.60	4.2	0.12	34.1
4	0.11	33.2	0.36	93
5	0.38	9.1	0.15	60.5
6	0.26	15.7	0.2	78.9
7	0.11	41.7	0.28	147

Table 17: Plasticity estimate and spike values for all tool combinations

The remaining four can be compared to the model by looking at the plastic strain of the inner and outer layers of the strip corresponding to the corner edge of the male die.

Combination	γ	ω	Plastic strain	
			Bottom	Top
2	6.1	0.2	0.24	0.08
3	4.2	0.12	0.12	0.04
5	9.1	0.15	0.23	0.08
6	15.7	0.2	0.38	0.14

Table 18: Plastic strain comparison with theory

D L Davies dave.davies@orange.net

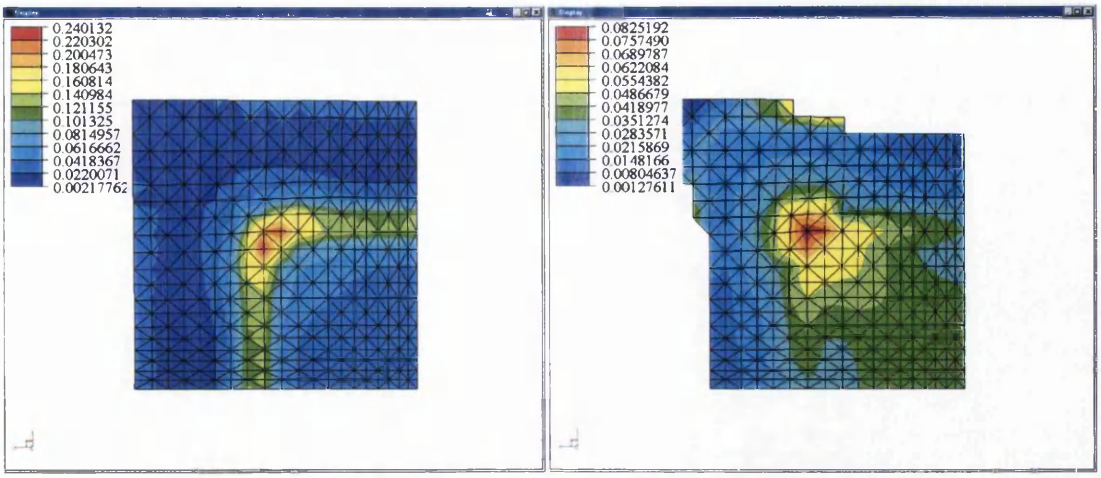

Figure 136: Plastic strain for combination 2; bottom (left), top (right)

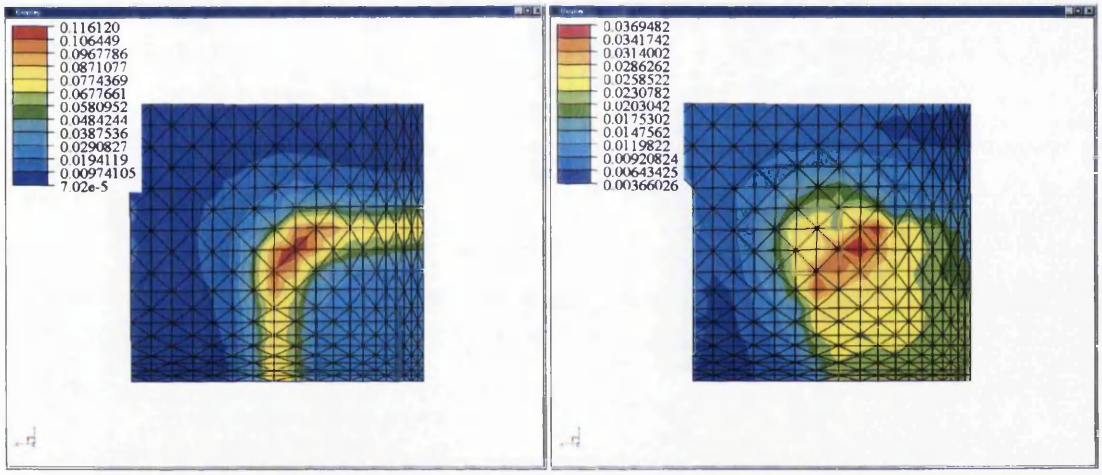

Figure 137: Plastic strain for combination 2; bottom (left), top (right)

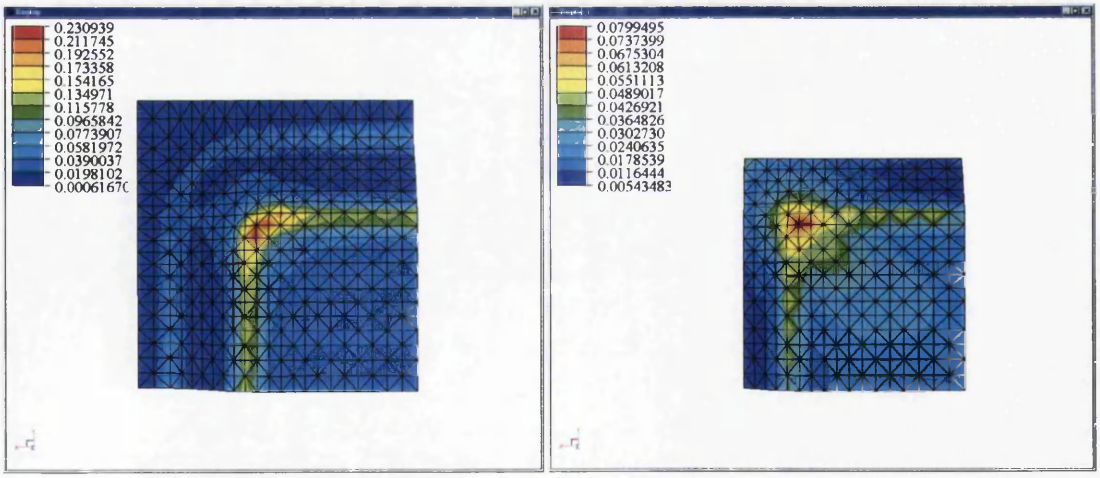

Figure 138: Plastic strain for combination 5; bottom (left), top (right)

D L Davies dave.davies@orange.net

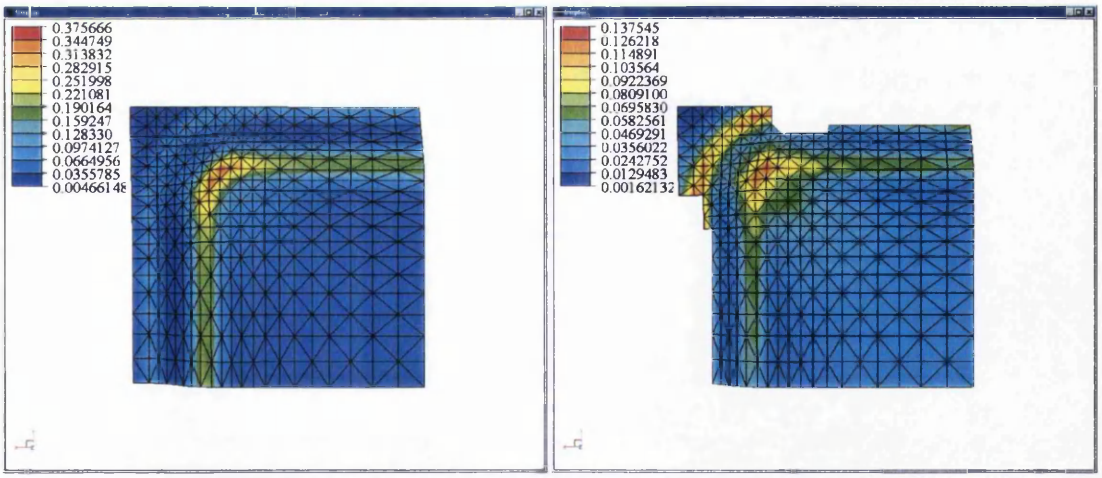

Figure 139: Plastic strain for combination 6; bottom (left), top (right)

5.4.5.4.Spike value assessment

Making the observation that the spike phenomenon occurs more noticeably when there is a large difference between the centre of the embossed square and its corner edge, then the assumption that the spike value is proportional to this height difference can be made. With this assumption it's straight forward to assess how the spike value (calculated by Eq 7) compares to the physical tests and measurements, and the simulation results (Table 19).

Combination	Spike value	Height between centre and corner, mm	
		Experiment	Simulation
Male 5mm, female 7.8mm	31.2	10	10
Male 5mm, female 9.6mm	34.1	12	10
Male 7mm, female 9.6mm	60.5	30	30
Male 8mm, female 9.6mm	78.9	37	32

Table 19: Spike value assessment

D L Davies dave.davies@orange.net

6. CONCLUSIONS

6.1. DWI

- The process can be modelled accurately, predicting features such as final gauge to within 5% and also average cup height (3.5.1)
- The simulated force trace captures all the key features that exist in an actual force trace produced from the production the can (3.5.2)
- The comparison of the DWI and doming model shows that the results of the reversal pressure are different. The doming model predicts a reversal pressure 8.2% higher than the DWI with a 7% standard deviation.
- To assess the integrity of different dome profiles, the doming model may be used to compare their relative strengths. But in order to obtain a true prediction of the reversal pressure the DWI model must be run, alternatively the 8.2% over-prediction may be used if the value is not deemed critical.
- The parametric set-up may be utilised to perform a sensitivity study on any tooling parameter(s).
- The model can be easily adapted to model similar processes, such as DRD or a stepped punch

6.2. Factorial Analysis

- The principles of factorial analysis have been used to create a factorial analysis package that makes a non-linear interpolation model for generic parametric data
- Interrogation programs incorporated within the factorial analysis package have been made that can be used to answer engineering questions such as "what

happens if the system is set-up like .... ?", or "how does the system have to be set-up in order to achieve ...?"

- The factorial analysis package can be applied to the DWI process to ascertain the friction coefficients in all contact areas
- The factorial analysis package may be used in conjunction with the DWI model for sensitivity study or optimality analysis

6.3. Embossing

- The flat strip embossing model simulates the experiment with very good agreement
- The model correctly predicts the general geometry of the formed part
- The model correctly predicts the occurrence of the spike feature when it exists and its magnitude
- The model correctly predicts the occurrence of the saddle feature when it exists and its magnitude
- The failure of the embossing with certain tool set-ups can be predicted with the model. Only the tooling set-ups that result in perforated material or worse cannot be modelled to completion
- Theoretical plasticity estimates show good agreement with the simulation (Table 18)
- Theoretical spike value correlates well with both experimental and simulation results (Table 19)
- Due to the flat strip model capturing the occurrence of small features, then a high confidence can be transferred to all other embossing models that haven't been validated directly

D L Davies dave.davies@orange.net

- The embossing image creator software created can be used in conjunction with the embossing model to simulate the embossing of arbitrary designs to check their feasibility

D L Davies dave.davies@orange.net

APPENDIX A MODEL DETAILS

All the background detail and information about the finite element models used in this project is contained in this section. Each model is summarised by a number of tables and additional information where required. The tables contain all the token (variable) values, the multistage control, constraints and load curve information. Where special features of a model exist they are described individually for each model and feature.

A.I DWI

Group	Long Name	Base Name	Value / Formula
Background		c1x	pr1 + dr1
Background		c1y	punch - l1
Background		c2x	c2x
Background		c2y	c1y - dr1 + dr2
Background		c3x	c2x+dr2*sin(t1)+l2*cos(t1)+dr3*sin(t1)
Background		c3y	c2y-dr2*cos(t1)+l2*sin(t1)-dr3*cos(t1)
Background		c4x	c3x-dr3*sin(t2)+l3*cos(t2)-dr4*sin(t2)
Background		c4y	c3y+dr3*cos(t2)+l3*sin(t2)+dr4*cos(t2)
Background		c5x	c4x+(dr4+ch1+dr5)*sin(t4)
Background		c5y	c4y-(dr4+ch1+dr5)*cos(t4)
Background		c6x	0
Background		c6y	dome - dr6
Background		c7x	c6x+(dr6-dr7)*sin(t5)
Background		c7y	c6y+(dr6-dr7)*cos(t5)
Background		e	210000
Background		ei	620000
Background		hc	-ro
Background		punch_offset	1
Background		r1x	rp1 - r1
Background		r1y	bt+r1
Background		rc	rd1 + ro
Background		re2rr1x	re2red1 + re2r2
Background		re2rr1y	-re2r2
Background		to	0.8
Can_Blank	Canplate_thkness	bt	0.235
Can_Blank	Canplate_width	bw	68
Dome	Dome_reference_y	dome	re2redis+ring
Dome	Dome_Forming_Radius	dr6	50
Dome	Dome_Forming_Corner_Radius	dr7	2.5

D L Davies dave.davies@orange.net

Dome	Dome_Forming_Dome_Wall_Length	l9	10
Dome	Dome_Forming_Taper_Angle_5	t5	arcsin((dextr-dr7)/(dr6-dr7))
Dome_Ring	Dome_Forming_Can_Thickness	ch1	0.2
Dome_Ring	Dome_Forming_Ring_Fillet_Radius	dr5	1.52
Dome_Ring	Ring_line_radius	drr	33.75
Dome_Ring	Dome_Forming_Taper_Length_4	l7	9.52
Dome_Ring	Ring_Line_Length	l8	1
Dome_Ring	Dome_ring_reference_y	ring	-356
Dome_Ring	Dome_Forming_Taper_Angle_4	t4	40
Draw_Blankholder	Blankholder_height	bh	40
Draw_Blankholder	Blankholder_internal_radius	bl1	46.35
Draw_Blankholder	Blankholder_width	blw	21.575
Draw_Die	Die_height	h1	41.3
Draw_Die	Internal_die_radius	rd1	45.65
Draw_Die	External_die_radius	rd2	67.97
Draw_Die	Die_edge_radius	ro	2.4
Draw_Die	Die_Recess_X	xrecess	0.76
Draw_Die	Die_Recess_Y	yrecess	2.7625
Draw_Punch	Punch_height	p1	52.4
Draw_Punch	Punch_edge_radius	r1	3
Draw_Punch	Punch_radius	rp1	45.32
Friction_Levels	Blankholder-strip	bhf	0.07
Friction_Levels	Drawdie-strip	df	0.07
Friction_Levels	Dome_post-strip	dpf	0.1
Friction_Levels	Dome_ring-strip	drf	0.1
Friction_Levels	Ironing_die_1-strip	i1f	0.05
Friction_Levels	Ironing_die_2-strip	i2f	0.045
Friction_Levels	Ironing_die_3-strip	i3f	0.04
Friction_Levels	Ironing_die_4-strip	i4f	0.035
Friction_Levels	Drawpunch-strip	pf	0.16
Friction_Levels	Redraw_sleeve-strip	rbhf	0.05
Friction_Levels	Redrawdie-strip	rdf	0.05
Friction_Levels	Redrawpunch-strip	rpf	0.05
Friction_Levels	punchnose	rpnf	0.4
Friction_Levels	punchshoulder	rpsf	0.2
Iron1	iron_width	ir_w	5.9
Iron1	bottom_taper_angle	ir1_bta	10
Iron1	bottom_taper_length	ir1_btl	7.5
Iron1	iron_entry_radius	ir1_er	0.5
Iron1	iron_face_length	ir1_il	0.5
Iron1	iron_inner_radius	ir1_ir	33.0505
Iron1	top_taper_angle	ir1_tta	8
Iron1	top_taper_length	ir1_ttl	5
Iron1	iron_y_reference	ir1_y	re2redis - 52 + 5
Iron2	bottom_taper_angle	ir2_bta	10
Iron2	bottom_taper_length	ir2_btl	7.5
Iron2	iron_entry_radius	ir2_er	0.5
Iron2	iron_face_length	ir2_il	0.5
Iron2	iron_inner_radius	ir2_ir	32.999
Iron2	top_taper_angle	ir2_tta	8
Iron2	top_taper_length	ir2_ttl	5
Iron2	iron_y_reference	ir2_y	re2redis-52-70+5
Iron3	bottom_taper_angle	ir3_bta	10
Iron3	bottom_taper_length	ir3_btl	7.5
Iron3	iron_entry_radius	ir3_er	3.5
Iron3	iron_face_length	ir3_il	0.5

Iron3	iron_inner_radius	ir3_ir	32.948
Iron3	top_taper_angle	ir3_tta	8
Iron3	top_taper_length	ir3_ttl	5
Iron3	iron_y_reference	ir3_y	re2redis-52-70-85+5
Iron4	bottom_taper_angle	ir4_bta	10
Iron4	bottom_taper_length	ir4_btl	7.5
Iron4	iron_entry_radius	ir4_er	3.5
Iron4	iron_face_length	ir4_il	0.5
Iron4	iron_inner_radius	ir4_ir	32.9375
Iron4	top_taper_angle	ir4_tta	8
Iron4	top_taper_length	ir4_ttl	5
Iron4	iron_y_reference	ir4_y	re2redis-52-70-85-34+5
Redraw_Die	Die_Edge_Radius	re2r2	1.524
Redraw_Die	Internal_Die_Radius	re2red1	33.115
Redraw_Die	External_Die_Radius	re2red2	46.0375
Redraw_Die	Redraw_Reference_Y_Coord	re2redis	-51
Redraw_Die	Die_Height	re2reh1	7.9375
Redraw_Die	Die_Recess_Y	yrecess2	2.159
Redraw_Punch	Punch_Radius_1	dr1	1.27
Redraw_Punch	Punch_Radius_2	dr2	1.02
Redraw_Punch	Punch_Radius_3	dr3	2.96
Redraw_Punch	Punch_Radius_4	dr4	5.08
Redraw_Punch	Punch_Inner_Line_Length	l1	10.9728
Redraw_Punch	Punch_Taper_Length_1	l2	((0.79-dr2)+(dr3+dr2)*cos(t1))/sin(t1)
Redraw_Punch	Punch_Taper_Length_2	l3	((9.75-0.79)-(dr3+dr4)*cos(t2))/sin(t2)
Redraw_Punch	Punch_Taper_Length_3	l4	(rp2-c4x-dr4*sin(t3))/cos(t3)
Redraw_Punch	Punch_Outer_Line_Length	l5a	87.27
Redraw_Punch	Punch_Recess_Y	l5b	10
Redraw_Punch	Punch_Inner_Radius	pr1	22.91
Redraw_Punch	Refernece_Punch_Y	punch	re2redis+bt+dr1+l1
Redraw_Punch	Punch_Upper_Line_Length	retext	72.48
Redraw_Punch	Punch_Recess_X	retrec	0.065
Redraw_Punch	Punch_Taper_Angle_1	t1	70
Redraw_Punch	Punch_Taper_Angle_2	t2	32
Redraw_Punch	Punch_Taper_Angle_3	t3	88
Redraw_Sleeve	Redraw_Blankholder_Height	re2bh	40.899
Redraw_Sleeve	Redraw_Blankholder_Internal_Radius	re2bl1	34.25
Redraw_Sleeve	Redraw_Blankholder_External_Radius	re2bl2	45.025
Redraw_Sleeve	Redraw_Blankholder_Edge_Radius	re2r1	1.4

Table 20: DWI token definitions

D L Davies dave.davies@orange.net

Description of Stage	Stage #	Multistage Name	Control	Stage Time	Geometry	Loading	Constraints	Contact
Blankholder pressurisation	1	Draw bh activation	Draw bh activation	4	Can, draw blankholder, drawdie, drawpunch	Draw blankholder pressure, drawpunch movement	Can, draw general	draw
Cupping whilst strip is under blankholder	2	Draw w bh	Draw w bh	~66	Can, draw blankholder, drawdie, drawpunch	Vacuum force, draw blankholder pressure, drawpunch movement	Can, draw general	draw
Blankholder release	3	Bh release	Bh release	0.1	Can, draw blankholder, drawdie, drawpunch	Vacuum force, draw bh pressure release, drawpunchmovement	Can, draw general	draw
Remainder of cupping	4	Draw wo bh	Draw wo bh	20	Can, draw blankholder, drawdie, drawpunch	Vacuum force, drawpunch movement	Can, draw blankholder restrain, draw general	draw
Cupping tool removal	5	Draw tool removal	Draw punch remove	10	Can, draw blankholder, drawdie, drawpunch	Drawpunch movement	Can, can_tool remove, draw general	draw
Redraw tool location	6	Redraw positioning 1	Redraw tool positioning	0.5	Can, domeforming punch, redraw die, redraw sleeve	Redraw punch movement, redraw tool positioning	Can, redraw general	
	7	Redraw positioning 2	Redraw tool positioning	0.5	Can, domeforming punch, redraw die, redraw sleeve	Redraw punch movement, redraw tool positioning	Can, redraw general	Redraw, redraw punch can
Blankholder pressurisation	8	Redraw blankholder pressure	Redraw blankholder pressure	3	Can, domeforming punch, redraw die, redraw sleeve	Redraw blankholderpressure, redraw punch movement	Can, redraw general	Redraw, redraw punch can
Redrawing	9	Redraw punch movement	Redraw punch movement	32	Can, iron1, domeforming punch, redraw die, redraw sleeve	Redraw blankholder pressure, redraw punch movement	Ironing, can, redraw general	iron1, redraw, redraw punch can

	10	Redrawbh release	Redrawbh release	0.1	Can, iron1, domeforming punch, redraw die, redraw sleeve	Redraw bh pressure release, redraw punch movement	Ironing, can, redraw general	iron1, redraw, redraw punch can
	11	Redraw blankholder restrain	Redraw blankholder restrain	14	Can, iron1, domeforming punch, redraw die, redraw sleeve	Redraw punch movement	Redraw blankhoder restrain, ironing, can, redraw general	iron1, redraw, redraw punch can
Ironing	12	Redraw punch ironing	Redraw punch ironing	15	Can, iron1, domeforming punch, redraw die, redraw sleeve	Redraw punch movement	Redraw blankhoder restrain, ironing, can, redraw general	iron1, iron2, iron3_4, redraw, redraw punch can
	13	iron1 restrain	Redraw punch ironing	10	Can, iron1, iron2, iron3, iron4, domeforming punch, redraw die, redraw sleeve	Redraw punch movement	Redraw blankhoder restrain, ironing, exit ironing ring, can, redraw general	iron2, iron3_4, redraw, redraw punch can
	14	Redraw punch ironing2	Redraw punch ironing	30	Can, iron1, iron2, iron3, iron4, domeforming punch, redraw die, redraw sleeve	Redraw punch movement	Redraw blankhoder restrain, ironing, can, redraw general	iron2, iron3_4, redraw, redraw punch can
	15	iron2 restrain	Redraw punch ironing	10	Can, iron1, iron2, iron3, iron4, domeforming punch, redraw die, redraw sleeve	Redraw punch movement	Redraw blankhoder restrain, ironing, exit ironing ring, can, redraw general	iron3_4, redraw, redraw punch can
	16	Redraw punch ironing3	Redraw punch ironing	85	Can, iron1, iron2, iron3, iron4, domeforming punch, redraw die, redraw sleeve	Redraw punch movement	Redraw blankhoder restrain, ironing, can, redraw general	iron3_4, redraw, redraw punch can

D L Davies dave.davies@orange.net

Doming	17	Dome locate	Dome locate	1	Can, domeblock, domeforming punch, domepost, domering	Dome locate, domepost movement, domering pressure, redraw punch movement	Can, can tool remove, dome locate, doming general	doming
	18	Dome creation	Dome post movement	7	Can, domeblock, domeforming punch, domepost, domering	Dome locate, domepost movement, domering pressure, redraw punch movement	can doming general	doming
	19	Dome release	Dome deactivation	2	Can, domeblock, domeforming punch domepost, domering	Dome locate, domepost movement, domering pressure, redraw punch movement	Can, can tool remove, doming general	doming
	20	reverse	reversal	~	can	Reverse pressure	Can, can tool remove	

Table 21: DWI multistage control

D L Davies dave.davies@orange.net

Group Name	Associated Stage(s)	Associated Load Curve	Load Curve Data		Token
			Time	Value	
Draw blankholder pressure	1 - 2	Draw blankholder pressure	0	0	
			1	0.00216	
			3	1.167	
Draw bh pressure release	3	Bh pressure release*	0	1.167	
			0.1	0	
Draw punch movement	1 - 5	Draw punch movement	0	0	
			4	-1.0001	
			10	-2	
			90	-51	
			91	-50	
			100	4	
vacuum force	2 - 4	vacuum force	0	0	
			4	0	
			17	0.85	
			89.9	0.85	
			90	0	
Redraw punch movement	6 - 19	Redraw punch movement	100	3	
			104	0	
			150	-100	
			300	-319.103	- re2redis + ir4_y + ir4_btl - l5a - l5b/3
Redraw tool positioning	6, 7	Redraw tool positioning	100	0	
			100.5	5	
			101	0	
Redraw blankholder pressure	8, 9	Redraw blankholder pressure	101	0	
			102	1	
			104	2.05	
Redraw bh pressure release	10	Redrawbh pressure release*	0	2.05	
			0.1	0	
Dome ring pressure	17 - 19	Dome ring pressure	300	0	
			301	0	
			302	5	
Dome post movement	17 - 19	Dome post movement	300	0	
			303	36.89666	ir4_y + ir4_btl - l5a - l5b/3 - dome
			308	48.19666	ir4_y + ir4_btl - l5a - l5b/3 – dome + 11.3
			309	0	
Dome locate	17 - 19	Locate	300	0	

			301	-113.714	-ir4_y + c5y + dr5 + ring - 0.01
			302	-113.714	-ir4_y + c5y + dr5 + ring - 0.01
			303	0	
			308.1	-73.1183	c4y - re2redis + ir4_btl - l5a - l5b/3
			309.9	-83.1033	ir4_btl - l5a - l5b/3
			310	-113.704	-ir4_y + c5y + dr5 + ring

Table 22: DWI load curve definitions

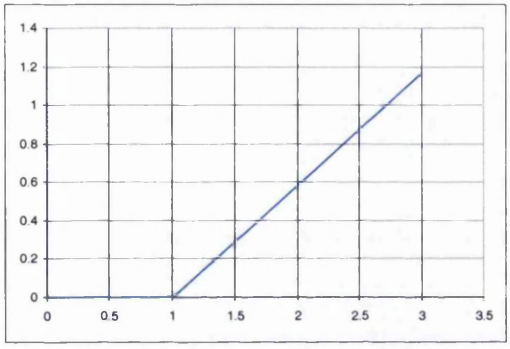

Figure 140: DWI draw blankholder pressure load curve

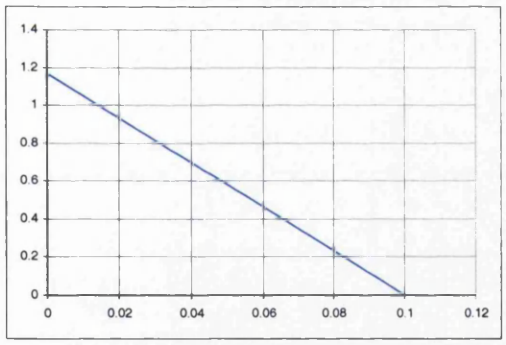

Figure 141: DWI draw blankholder pressure release load curve

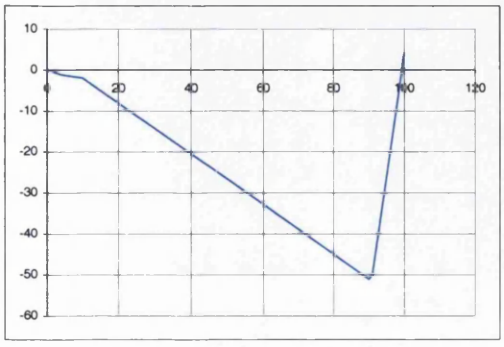

Figure 142: DWI draw punch load curve

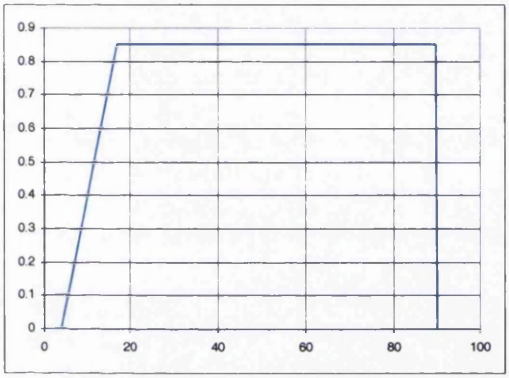

Figure 143: DWI Vacuum force load curve

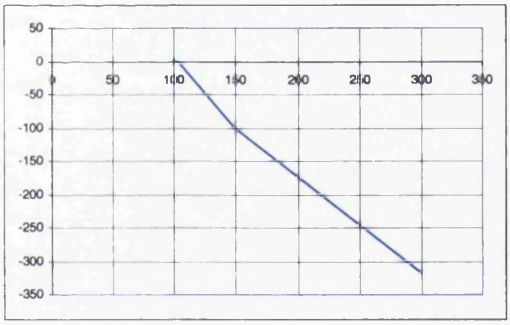

Figure 144: DWI redraw punch load curve

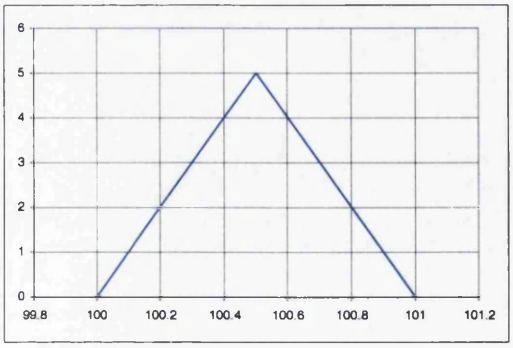

Figure 145: DWI redraw tool positioning load curve

D L Davies dave.davies@orange.net

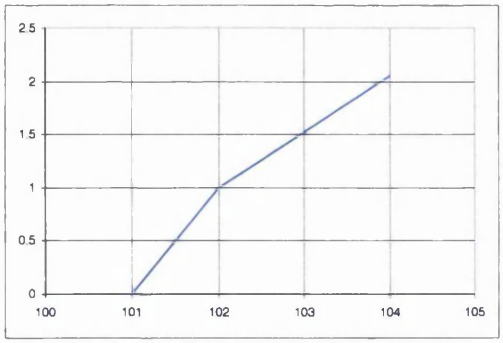

Figure 146: DWI redraw sleeve pressure load curve

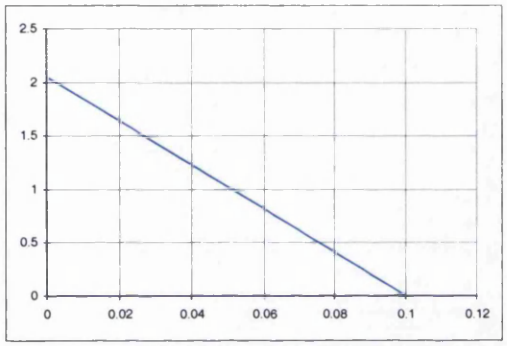

Figure 147: DWI redraw sleeve pressure release

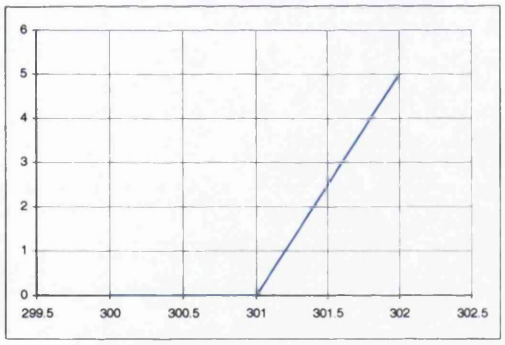

Figure 148: DWI dome ring pressure

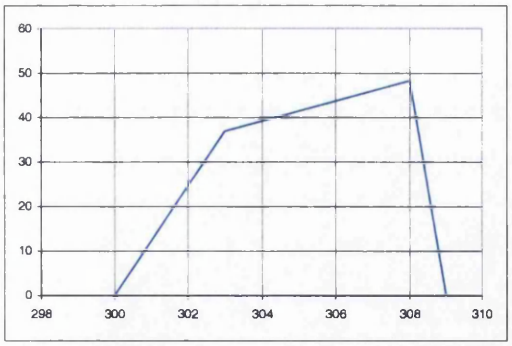

Figure 149: DWI dome post movement load curve

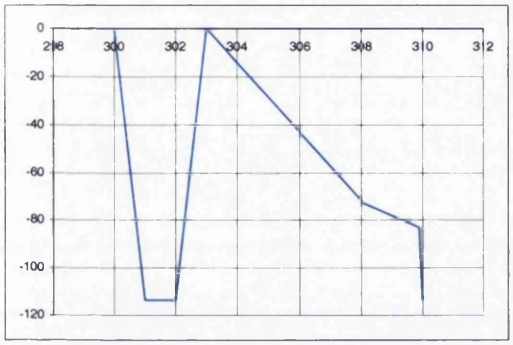

Figure 150: DWI dome locate load curve

Group Name	Associated Stage(s)	Description of constraint
can	1 - 20	x-constraint to utulise symmetry
can_tool_remove	5, 17, 19, 20	y-constraint to top edge to help stability when positioning tooling
draw_general	1 - 5	x-constraint on punch
		X fixity on right-edge vertical lines, xy fixity on bottom-egde horizontal lines
draw_blankholder_restrain	4	y-constraint on blankholder on removal of strip
redraw_general	6 - 16	x-constraint on redraw punch
		x fixity on right-edge vertical lines, xy fixity on bottom-egde horizontal lines
ironing	9 - 16	x fixity on right-edge vertical lines, xy fixity on top and bottom-egde horizontal lines
exit_ironing_ring	13, 15	x-constraint on top edge of can when ironing ring contact switched off
redraw_blankholder_restrain	11 - 16	y-constraint on redraw sleeve after strip leaves it
dome_locate	17	xy fixity on bottom-edge horizontal lines of domering
doming_general	17 - 19	x-constraint on domepost, ring and block

Table 23: DWI constraints summary

Automated Stage Termination

A number of stages in this model are terminated automatically by tracking pre-defined points or nodes and when they pass through a corresponding pre-defined plane the stage terminates and continues to the next control. This is used for two purposes within this project; for releasing blankholder pressures and strip exiting ironing rings.

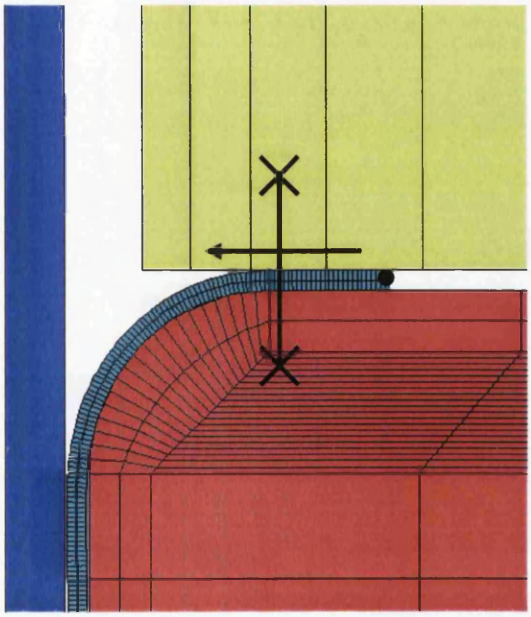

Figure 151: Automatic stage termination to initiate blankholder pressure release

D L Davies dave.davies@orange.net

With reference to Figure 151, when the point passes through the plane defined by the line and to crosses, the stage terminates and the next control stage starts, which is the blankholder pressure release stage. In conjunction with this is the use of a relative time curve to deactivate blankholder pressure just prior to the strip leaving the blankholder. This is needed due to the fact that it is not known exactly what time this occurs and differs with any slight alteration to DWI set-up.

E.g. Stage 2 has blankholder force on – stage starts at time = 4, ends when point at the end of the strip passes through a vertical plane near the exit area for the blankholder (time approximately 55). Stage 3 uses the relative time curve to release the blankholder pressure – stage terminates when the same end point passes through another vertical plane just outside the exit area. Stage 4 has no blankholder force (not needed after strip has passed through), and terminates when global time = 90.

The same principle is used when the strip exits an ironing ring, only instead of a blankholder pressure release an extra constraint is imposed on the strip end for stability in between ironing rings. This extra constraint is then removed when the punch shoulder passes through a plane perpendicular to the ironing ring entrance.

D L Davies dave.davies@orange.net

A.II DOMING

Group	Long Name	Base Name	Value / Formula
Background		a1	90
Background		a2	t1
Background		a3	t2-t1
Background		a4	t3-t2
Background		ac1	arctan((c4y-c2y)/(c4x-c2x))-arcsin((r4-r2)/sqrt(c42))
Background		c1x	pr1+r1
Background		c1y	punch-l1
Background		c2x	pr1+r1
Background		c2y	c1y-r1+r2
Background		c3x	c2x+(r2+r3)*sin(t1)+l2*cos(t1)
Background		c3y	c1y-r1+0.79
Background		c42	(c4x-c2x)^2+(c4y-c2y)^2
Background		c4x	c3x-r3*sin(t2)+l3*cos(t2)-r4*sin(t2)
Background		c4y	c3y+9.75-0.79
Background		c5x	c8x+(r8+r5)*sin(t4)
Background		c5y	c8y-(r8+r5)*cos(t4)
Background		c6x	0
Background		c6y	dome-r6
Background		c7x	dompr-r7
Background		c7y	c6y+(r6-r7)*cos(dbla)
Background		c8x	c4x
Background		c8y	c4y-drydiff
Background		c9x	c3x
Background		c9y	c8y-(r8+r9)*cos(t2)-l5*sin(t2)
Background		cchm	tan(t2)
Background		cchx	(c3x-r3*cos(90-t1+a3))
Background		cchy	(c3y+r3*sin(90-t1+a3))
Background		cpm	tan(ac1)
Background		cpx	(c2x+(r2+ch3)*sin(ac1))
Background		cpy	(c2y-(r2+ch3)*cos(ac1))
Background		drchdiff	cchy+cchm*(drx-cchx)-dry
Background		drx	c9x-r9*sin(ac1)
Background		dry	cpy+cpm*(drx-cpx)
Background		drydiff	-dry+c4y-(r8+r9)*cos(t2)-l5*sin(t2)+r9*cos(ac1)
Background		ph	0.5
Can	Y Reference	can	0
Can	Top Thickness	ch1	ctk*exp(-1.15)
Can	Top Chime Thickness	ch2	ctk*exp(-0.01)
Can	Bottom Chime Thickness	ch3	ctk*exp(-0.005)
Can	Original Thickness	ctk	0.235
Dome post	Dome Blend Angle	dbla	arcsin((dompr-r7)/(r6-r7))
Dome post	Travel	dload	10
Dome post	Y Reference	dome	punch-l1-r1-ctk
Dome post	Dome Height	domph	9.12
Dome post	External Radius	dompr	22.63
Dome post	Outer Line Length	l9	11.4
Dome post	Radius 6	r6	50
Dome post	Radius 7	r7	2.5
Dome Ring	Dome Ring Height	drht	13.21
Dome Ring	Dome Inner Radius	drir	25.5

D L Davies dave.davies@orange.net

Dome Ring	Dome Outer Radius	dror	33.75
Dome Ring	Taper Angle	dta	6
Dome Ring	Line Length	l5	l3+(r8+r9-r3-r4)*tan(t2)
Dome Ring	Radius 5	r5	1.52
Dome Ring	Radius 8	r8	r4+0.2
Dome Ring	Radius 9	r9	r3-0.2
Dome Ring	Y Reference	ring	c5y+r5
Dome Ring	Blend Angle 4	t4	40
Punch	Inner Line Length	l1	6.35
Punch	Punch Straight 1	l2	(c3y-c2y+(r2+r3)*cos(t1))/sin(t1)
Punch	Punch Straight 2	l3	(c4y-c3y-(r3+r4)*cos(t2))/sin(t2)
Punch	Outer Taper Length	l4	(rp2-c4x-r4*sin(t3))/cos(t3)
Punch	Punch Shoulder Height	pht	9.75+tan(t3)*(65.72-64.6)/2
Punch	Punch Load Distance	pload	drchdiff-1/4*(3*ch3+ch2)/cos(t2)
Punch	Inner Radius	pr1	22.91
Punch	Y Reference	punch	l1+r1+ctk
Punch	Radius 1	r1	1.27
Punch	Radius 2	r2	1.02
Punch	Radius 3	r3	2.96
Punch	Radius 4	r4	5.08
Punch	Outer Radius	rp2	32.86
Punch	Blend Angle 1	t1	70
Punch	Blend Angle 2	t2	32
Punch	Blend Angle 3	t3	88

Table 24: Doming token definitions

D L Davies dave.davies@orange.net

Description of Stage	Stage #	Multistage Name	Control	Stage Time	Geometry	Loading	Constraints	Contact
Doming	1	dome	dome	20	can dome_post dome_ring dome_block punch	dome moveblock ring_pressure	can dome_post dome_ring punch	doming
Tooling release	2	release	Dome release	30	can dome_post dome_ring dome_block punch	dome moveblock ring_pressure	can dome_post dome_ring punch	doming
Reversal pressure test	3	reverse	Reverse pressure		can	Reverse pressure	can cantop	

Table 25: Doming multistage control

D L Davies dave.davies@orange.net

Group Name	Associated Stage(s)	Associated Load Curve	Load Curve Data		Token
			Time	Value	
dome	1, 2	doming	0	0	
			2	0	
			20	10	dload
			22	0	
moveblock	1, 2	block_movement	0	0	
			1	0	
			2	5	
			22	5	
			30	0	
ring_pressure	1, 2	ring_pressure	0	0	
			1	5	
reverse_pressure	3	rev	0	0	
			200	0	

Table 26: Doming load curve definitions

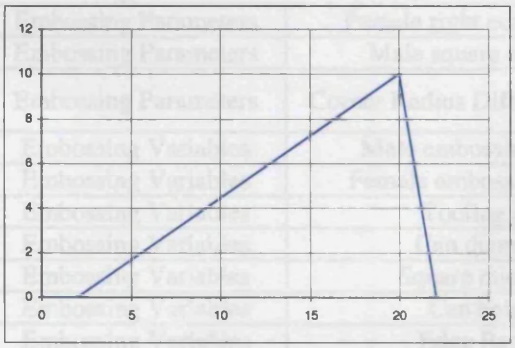

Figure 152: Doming load curve

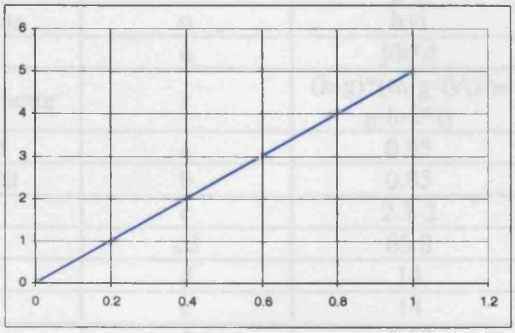

Figure 154: Doming ring pressure load curve

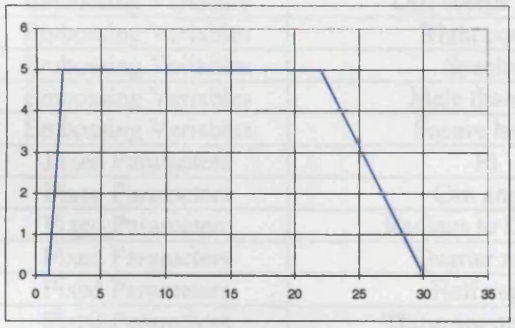

Figure 153: Doming block movement load curve

Group Name	Associated Stage(s)	Description of constraint
can	1 - 3	x-constraint to utulise symmetry
dome_post	1, 2	x-constraint supporting rigid body movement in y direction
dome_ring	1, 2	x-constraint on domering and block supporting y-face pressure to ring and y-rigid movement on block
punch	1, 2	x,y fixity
cantop	2	y-fixity for boundary condition on top of can

Table 27: Doming constraints summary

D L Davies dave.davies@orange.net

A.III EMBHALF

Group	Long Name	Base Name	Value / Formula
Background		p	i+sh/2
Embossing Parameters	Male embossing height	a	0.95
Embossing Parameters	Female embossing height	b	0.85
Embossing Parameters	Tooling gap	c	2.3-2
Embossing Parameters	Square midpoint	d	14
Embossing Parameters	Can height	e	14
Embossing Parameters	Edge Radius	f	0.15
Embossing Parameters	Male left corner radius	g	0.5
Embossing Parameters	Male right corner radius	h	0.75
Embossing Parameters	Spacing	i	0.4
Embossing Parameters	Male die radius	j	md/2
Embossing Parameters	Female die radius	k	fd/2
Embossing Parameters	Can radius	l	cd/2
Embossing Parameters	Square height	m	sh/2
Embossing Parameters	Female left corner radius	n	g+i
Embossing Parameters	Female right corner radius	o	h+i
Embossing Parameters	Male square midpoint	q	j/k*d
Embossing Parameters	Corner Radius Difference Factor	r	(h-g)*(m-g-f)/(sh-g-h-2*f)
Embossing Variables	Male embossing height	a	0.95
Embossing Variables	Female embossing height	b	0.85
Embossing Variables	Tooling gap	c	2.3-2
Embossing Variables	Can diameter	cd	65.8
Embossing Variables	Square midpoint	d	14
Embossing Variables	Can height	e	14
Embossing Variables	Edge Radius	f	0.15
Embossing Variables	Female diameter	fd	64.8
Embossing Variables	Left corner radius	g	0.5
Embossing Variables	Right corner	h	0.75
Embossing Variables	Spacing	i	0.4
Embossing Variables	Male diameter	md	63.65
Embossing Variables	Square height	sh	10
Fixed Parameters	Pi	pi	3.141592654
Fixed Parameters	Can angle	v	w*d*2/k
Fixed Parameters	Radians to Degress	w	180/pi
Fixed Parameters	Quarter angle	x	22.5
Fixed Parameters	Half angle	y	45
Fixed Parameters	Three quarter angle	z	67.5

Table 28: Embhalf token definitions

D L Davies dave.davies@orange.net

Description of Stage	Stage #	Multistage Name	Control	Stage Time	Geometry	Loading	Constraints	Contact
Male die retracting	1	retract	retract	1	strip, all slidelines	pull	strip tools	
Male Die Closing	2	engage	engage	2	strip, all slidelines	pull	strip tools	emboss
Embossing	3	emboss	emboss	102	strip, all slidelines	rotate xtranslation ytranslation	strip tools	emboss

Table 29: Embhalf multistage control

D L Davies dave.davies@orange.net

Group Name	Associated Stage(s)	Associated Load Curve	Load Curve Data		Token
			Time	Value	
pull	1 - 2	pull	0	0	
			1	-2	
			1.9	0	
			2	0	
rotate	3	rotation	0	0	
			2	0	
			102	49.514871	v
xtranslation	3	loadtestx	0	0	
			2	0	
			2.01	2.409E-07	
			2.02	9.638E-07	
			-	-	Y = (j+c+k)(1 - cos(d(X-2)/50k))
			101.99	22.62786	
			102	22.632101	
ytranslation	3	loadtesty	0	0	
			2	0	
			2.01	0.0055762	
			2.02	0.0111525	
			-	-	Y = (j+c+k)sin(d(X-2)/50k)
			101.99	49.072449	
			102	49.07607	

Table 30: Embhalf load curve defintions

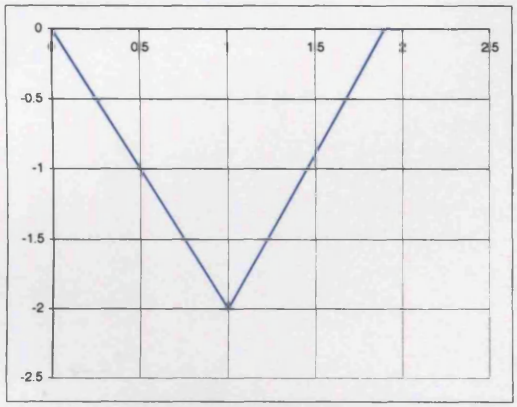

Figure 155: Embhalf male die engagement load curve

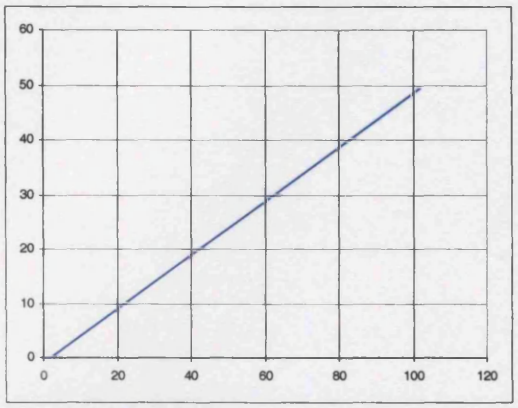

Figure 156: Embhalf male die rotation load curve

D L Davies dave.davies@orange.net

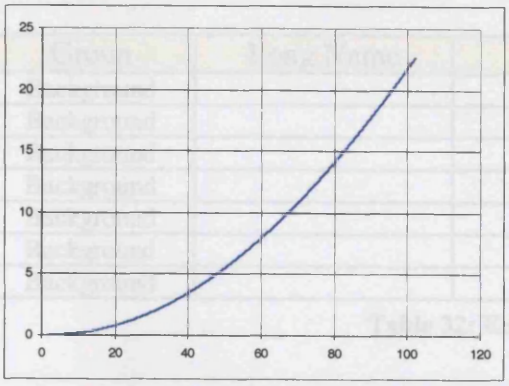

Figure 157: Embhalf male die x movement load curve

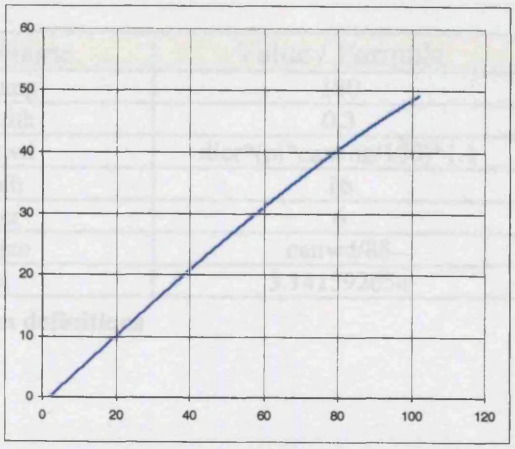

Figure 158: Embhalf male die y movement load curve

Group Name	Associated Stage(s)	Description of constraint
strip	1 - 3	xyz-fixity on both ends of strips
		centre line symmetry, z-fixty xy rotation along curved edge of strip
tools	1 - 3	centre line symmetry
		xy-fixity on female surfaces

Table 31: Embhalf constraints summary

D L Davies dave.davies@orange.net

A.IV EMB3

Group	Long Name	Base Name	Value / Formula
Background		canang	180
Background		canthk	0.3
Background		canwd	dier*(pi*canang/180)*1.1
Background		dieh	16
Background		dier	6
Background		elsize	canwd/88
Background		pi	3.141592654

Table 32: Emb3 token definitions

D L Davies dave.davies@orange.net

Description of Stage	Stage #	Multistage Name	Control	Stage Time	Geometry	Loading	Constraints	Contact
Embossing	1	emboss	emboss		strip and all slidelines	pull rotate	damp tools	emboss

Table 33: Emb3 multistage control

D L Davies dave.davies@orange.net

Group Name	Associated Stage(s)	Associated Load Curve	Load Curve Data		Token
			Time	Value	
pull	1	pull	0	0	
			0.00001	18.849556	dier*(pi*canang/180)
rotate	1	rotate	0	0	
			0.00001	180	canang

Table 34: Emb3 load curve definitons

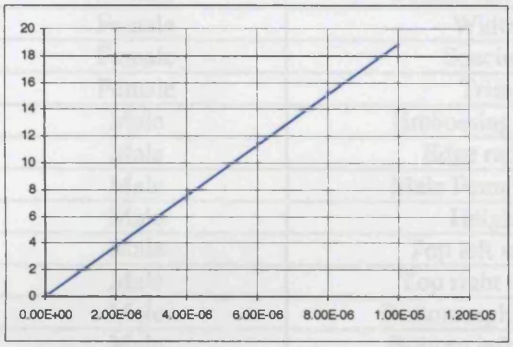

Figure 159: Emb3 strip pull through load curve

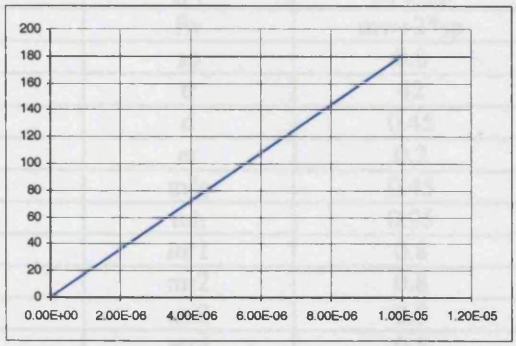

Figure 160: Emb 3 tool die rotation load curve

Group Name	Associated Stage(s)	Description of constraint
damp	1	global damping, 0.5%
tools	1	xyz-fixity on both ends of strip
		z-fixity xy-rotation on curverd edge of dies

Table 35: Emb3 constraints summary

D L Davies dave.davies@orange.net

A.V FLAT STRIP EMBOSSING

Group	Long Name	Base Name	Value / Formula
Female	Male Female Gap Edge Radius	fer	0.1
Female	Height	fh	0.85
Female	Top left radius	fr1	mr1+sp
Female	Top right radius	fr2	mr2+sp
Female	Bottom right radius	fr3	mr3+sp
Female	Bottom left radius	fr4	mr4+sp
Female	Width	fw	mw+2*sp
Female	Soacing	sp	0.8
Female	Trim	tr	42
Male	Embossing depth	d	0.45
Male	Edge radius	er	0.2
Male	Male Female Gap	mfg	0.45
Male	Height	mh	0.95
Male	Top left radius	mr1	0.8
Male	Top right radius	mr2	0.8
Male	Bottom right radius	mr3	0.8
Male	Bottom left radius	mr4	0.8
Male	Width	mw	8
Male	Square to side distance	s2e	20
Male	Square to square distance	s2s	28
Male	Tool Edge	te	63.25
Male	Tool Side	ts	96
Strip	Length	l	ts-0.5
Strip	Gauge	t	0.22
Strip	Width	w	tr-0.5

Table 36: Flat strip embossing token definitions

D L Davies

dave.davies@orange.net

Description of Stage	Stage #	Multistage Name	Control	Stage Time	Geometry	Loading	Constraints	Contact
Embossing	1	s1	emboss	6	strip and all slidelines	contact emboss	symmetry tooling	Dies
Tools release	2	S2	release	51	strip and all slidelines	contact	symmetry tooling	Dies

Table 37: Flat strip embossing multistage control

D L Davies dave.davies@orange.net

Group Name	Associated Stage(s)	Associated Load Curve	Load Curve Data		Token
			Time	Value	
contact	1	contact	0	0	
			0.01	0.007	
emboss	1	emboss	0	0	
			6	0.72	mh-mfg+t

Table 38: Flat strip embossing load curve definitions

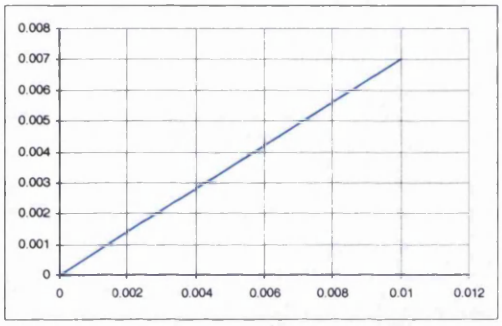

Figure 161: Flat strip embossing contact initialisation load curve

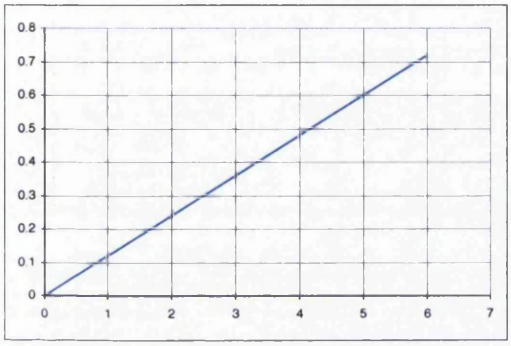

Figure 162: Flat strip embossing emboss load curve

Group Name	Associated Stage(s)	Description of constraint
symmetry	1	utilising 2 centre lines of symmetry on all objects; x-fixity yz-rotation, y-fixity xz-rotation
tooling	1	xy-fixity z-rotation on male die surfaces
		z-fixity on female die surfaces

Table 39: Flat strip embossing constraints summary

Slideline deactivation load curve

As with most cases that involve the release of tooling, there is often a problem of stability and/or lack of convergence problems for implicit solvers due to the elastic nature of the material being simulated. A useful way to deal with this problem is to use slideline deactivation load curves. It works by instead of unloading the forming tool via an applied displacement load curve, the tool stays where it is but the penalty number that simulates contact pressure is ramped down to zero.

D L Davies dave.davies@orange.net

APPENDIX B MATLAB® PROGRAMS

Throughout the project computer programs were needed for various reasons and applications and the code I used to write them was MATLAB® - a "c" based code with file extension *.m, which can be run without being compiled using the MATLAB® software. The main applications it was used for were factorial analysis programs, and the image to emboss tool co-ordinates interface. A few additional programs were also written, but the only one to note is the one that measures the error for DWI profile plots.

B.I FACTORIAL ANALYSIS PROGRAMS

Fact.m

```
data=input('To enter data, copy selection, type [ ctrl^v ] then hit "enter"  ');      %input data
M=0;                                                                                  %size # of factors by level
m=[];

dimdata=size(data);
factors=dimdata(2)-1;

%level=dimdata(1)^(1/factors);

interpolationstep=0.1;

level=1;
list=data(1,1);
for j=1:factors;                                    %checking level

        for i=1:dimdata(1);

                diffcheck=data(i,j)-list;
                if min(abs(diffcheck))~0;

                        list=[list data(i,j)];      %make sure levels are evenly split
                                                    %only tested for 3 level
                end

        end
        level=max(level,length(list));

end

ave=mean(data(:,dimdata(2)));                       %average response

list=sort(list);
```

```
x=list(1):interpolationstep:list(length(list));
yi=[];

for j=1:factors                                          %main effects

        for lev=1:level

                levcheck=data(:,j)-list(lev);
                levcheck=abs(levcheck);
                [levcheck ind]=sort(levcheck);
                count=0;
                while levcheck(count+1)==0;

                        count=count+1;

                end
                if count>0

                        M(j,lev)=mean(data(ind(1:count),dimdata(2)))-ave;

                end

        end
        yi(j,:)=interp1(list,M(j,:),x,'cubic')';
        m=[m;['factor ' num2str(j)]];

end

combinations=[];
for i=1:level;                                           %1st order interaction effects

        for j=1:level

                combinations=[combinations;list(j) list(i)];

        end

end

count=0;
zi=[];
I1=[];
for loop=1:factors-1

        for j=1:factors-loop

                count=count+1;
                for k=1:level^2

                        Itemp=[];
                        for i=1:dimdata(1);

                                levcheck=[data(i,loop) data(i,j+loop)]-combinations(k,:);
                                if sum(abs(levcheck))==0

                                        Itemp=[Itemp data(i,dimdata(2))];

                                end
```

```
                    end

                    nulltest=isnan(mean(Itemp));

                    if nulltest==1

                            I(k)=ave;

                    else

                            I(k)=mean(Itemp);
                            I(k)=I(k)-value(list,yi(loop,:),combinations(k,1));
                            I(k)=I(k)-value(list,yi(loop+j,:),combinations(k,2));

                    end

            end
            for i=1:level

                    I1(i,:)=I((i-1)*level+1:i*level);

            end

            I1=I1-ave;
            I1collective(:,level*(count-1)+1:level*count)=I1;

% I1collective - standard order form for 1st order interaction surface
%
% level x level*factors*(factors-1)/2

            zi=[zi interp2(list,list,I1,x',x,'bicubic')];

    end

end

factplot
```

D L Davies dave.davies@orange.net

value.m

```
function [v] = value(list,yi,facta)

l=length(list);
y=length(yi);

if list(1)<=facta & list(l)>=facta

        rescalex =  y*(facta-list(1))/(list(l)-list(1)) + (facta-list(l))/(list(1)-list(l));

        rescalex = round(rescalex);

        v = yi(rescalex);

else

        v = 'Extrapolating - out of range';

end
```

Ivalue.m

```
function [Iv] = Ivalue(list,zi,facta,factb)      %facta, left to right
                                                 %factb, top to bottom w.r.t. matrix I1
l=length(list);
z=length(zi);

if list(1)<=facta & list(1)<=factb & list(l)>=facta & list(l)>=factb

        rescalex = z*(facta-list(1))/(list(l)-list(1)) + (facta-list(l))/(list(1)-list(l));
        rescaley = z*(factb-list(1))/(list(l)-list(1)) + (factb-list(l))/(list(1)-list(l));

        rescalex = round(rescalex);
        rescaley = round(rescaley);

        Iv = zi(rescaley,rescalex);

else

        Iv = 'Extrapolating - out of range';

end
```

D L Davies dave.davies@orange.net

Mvalue.m

```
function [response, contributions] = mvalue(ave,yi,zi,factlevs,list);

                                        %dimension check
level=length(list);                 %level of factorial analysis
f=length(factlevs);                     %number of factors
y=length(yi);
z=length(zi)/(f*(f-1)/2);
nc=f+f*(f-1)/2;                         %number of contributions

contributions=[];

if y==z

        response=ave;
        for i=1:f

                contrib=value(list,yi(i,:),factlevs(i));
                response=response+contrib;
                contributions=[contributions  contrib];
        end
        count=0;
        for f1=1:f-1

                for f2=1:f-f1

                        count=count+1;
                        contrib=Ivalue(list,zi(:,(count-1)*y+1:count*y),factlevs(f1),factlevs(f1+f2));
                        response=response+contrib;
                        contributions=[contributions contrib];

                end

        end

else

        response='dimension mismatch';

end
```

Fmodel.m

```
factlevs=[];
factors=min(size(yi));

for i=1:factors

        factlevs(i)=input(['Enter factor ' num2str(i) ' test value?     ']);

end
```

```
%response=mvalue(ave,yi,zi,factlevs,list)                    % choice whether want to see
                                                                    % individual contributions
[response, contributions]=mvalue(ave,yi,zi,factlevs,list)
```

Max3fact.m

```
factors=min(size(yi));

%density=100;          %number of elements in i unit,
step=0.01;             %i.e. if density=100, length=1/100

testvalue=list(1)*ones(factors);
response=mvalue(ave,yi,zi,testvalue,list);
maxfact=testvalue;
l=length(list);

for f1=list(1):step:list(l)

        for f2=list(1):step:list(l)

                for f3=list(1):step:list(l)

                        testvalue=[f1 f2 f3];
                        tresponse=mvalue(ave,yi,zi,testvalue,list);

                        if tresponse>response

                                response=tresponse;
                                maxfact=testvalue;

                        end

                end

        end

end
response
maxfact
```

tmodel.m

```
maxjump=0.2;           %twice the max amount any test factor can change in one iterate
probaccept=1;          %probability of switching to a lower response value if found
factors=size(yi,1);
lev=length(list);
fact23_tolerance=0.1;  %logical constraint - blank holder and die frictions will be close

target=input('What is your desired response?');

searchlength=input('How long to search for optimum (loop time)?');

for i=1:factors
```

```
        testvalue(i)=rand*(list(lev)-list(1))+list(1);

end

%testvalue(3)=testvalue(2)+fact23_tolerance*2*(rand-0.5);    %using logical contstraint

response=mvalue(ave,yi,zi,testvalue,list);          %initial guess
reserr=abs(target-response);                              %initial error
optf=testvalue;
factseries=[testvalue';reserr];

initial_guess=response
initial_input=testvalue

iterate=1;
while iterate<=searchlength

        for i=1:factors

                tempvalue(i)=testvalue(i)+maxjump*(rand-0.5);
                if tempvalue(i)<list(1)

                        tempvalue(i)=list(1);

                elseif tempvalue(i)>list(lev)

                        tempvalue(i)=list(lev);

                end

        end

%       tempvalue(3)=tempvalue(2)+fact23_tolerance*2*(rand-0.5);
%       if tempvalue(3)<list(1)
%
%               tempvalue(3)=list(1);
%
%       elseif tempvalue(3)>list(lev)
%
%               tempvalue(3)=list(lev);
%
%       end

        tresponse=mvalue(ave,yi,zi,tempvalue,list);  %test response value
        treserr=abs(target-tresponse);                        %test response error

        if treserr<reserr                           %optimal test

                response=tresponse;
                reserr=treserr;
                testvalue=tempvalue;
                optf=testvalue;                               %new optimum

        elseif rand>probaccept

                response=tresponse;
                reserr=treserr;
                optf=testvalue;                               %new optimum
```

```
        end

        T=[testvalue';reserr];
        factseries=[factseries, T];
        iterate=iterate+1;

end
response
reserr
optf

m=[];

for i=1:factors

        m=[m;['factor ' num2str(i)]];

end
sf=size(factseries,2);
if sf>1

        fignumber=figure;

        h=get(fignumber,'Position');
        figw=h(3);                              %default figure width

        set(fignumber,'Position',[h(1)-h(3)/2 h(2) 2*h(3) h(4)]) %doubling width

        subplot(211)
        plot(1:sf,factseries(1:factors,:))
        legend(m)

        hc=get(fignumber,'Children');
        sp1=get(hc(1),'Position');          %default top plot position
        lp=get(hc(2),'Position');           %default legend position
        tl=get(hc(1),'TickLength');         %tick length

        lpos=[sp1(1)+sp1(3)-tl(1)-lp(3) (sp1(4)-lp(4))/2+sp1(2) lp(3) lp(4)];    %new legend position
        set(hc(2),'Position',lpos)

        subplot(212)
        plot(1:sf,factseries(factors+1,:))
        xlabel('Iterations')
        ylabel('Error')

else
        'not improved on initial guess'
end
```

multiopt.m

```
maxjump=2;              %twice the max amount any test factor can change in one iterate

probaccept=1;           %probability of switching to a lower response value if found

load base
lev=size(list,2);
```

```
factors=size(yi,1);
basethk=0.23;
fact23_tolerance=0.1;      %logical constraint - blank holder and die frictions will be close

%density=100;              %number of elements in i unit,
step=0.1;                  %i.e. if density=100, length=1/100

def=input('Use default targets (y/n)','s');

searchlength=input('How long to search for optimum (loop time)?');

if def=='n'

        target(1)=input(['Enter target for base?    ']);
        target(2)=input(['Enter target for lowwall?    ']);
        target(3)=input(['Enter target for topwall?    ']);

else

        target=[basethk basethk 1.17*basethk];          %Default target gauges

end

for i=1:factors                                         %initial factor input

        testvalue(i)=rand*(list(lev)-list(1))+list(1);

end

testvalue(3)=testvalue(2)+fact23_tolerance*2*(rand-0.5);    %using logical contstraint

opterr=0;                                       %test error - to be measured by least squares

load base
response=mvalue(ave,yi,zi,testvalue,list);
opterr=opterr+(target(1)-response)^2;

load lowwall
response=mvalue(ave,yi,zi,testvalue,list);
opterr=opterr+(target(2)-response)^2;

load topwall
response=mvalue(ave,yi,zi,testvalue,list);
opterr=opterr+(target(3)-response)^2;

opterr=sqrt(opterr);
optfact=testvalue;

l=length(list);

factseries=[optfact';opterr];

initial_guess_error=opterr
initial_input=optfact

iterate=1;
while iterate<=searchlength
```

```
        for i=1:factors

                testvalue(i)=testvalue(i)+maxjump*(rand-0.5);
                if testvalue(i)<list(1)

                        testvalue(i)=list(1);

                elseif testvalue(i)>list(lev)

                        testvalue(i)=list(lev);

                end

        end

        testvalue(3)=testvalue(2)+fact23_tolerance*2*(rand-0.5);
        if testvalue(3)<list(1)

                testvalue(3)=list(1);

        elseif testvalue(3)>list(lev)

                testvalue(3)=list(lev);

        end

        err=0;

        load base
        response=mvalue(ave,yi,zi,testvalue,list);
        err=err+(target(1)-response)^2;

        load lowwall
        response=mvalue(ave,yi,zi,testvalue,list);
        err=err+(target(2)-response)^2;

        load topwall
        response=mvalue(ave,yi,zi,testvalue,list);
        err=err+(target(3)-response)^2;
        err=sqrt(err);

        if err<opterr                   %optimum error test

                optfact=testvalue;%new optimums
                opterr=err;             %
                'improvement';

        end

        T=[optfact';opterr];
        factseries=[factseries, T];
        iterate=iterate+1;

end


least_error=opterr
best_inputs=optfact
```

D L Davies dave.davies@orange.net

```
m=[];

for i=1:factors

        m=[m;['factor ' num2str(i)]];

end

sf=size(factseries,2);

if sf>1

        fignumber=figure;

        h=get(fignumber,'Position');
        figw=h(3);                              %default figure width

        set(fignumber,'Position',[h(1)-h(3)/2 h(2) 2*h(3) h(4)]) %doubling width

        subplot(211)
        plot(1:sf,factseries(1:factors,:))
        legend(m)

        hc=get(fignumber,'Children');
        sp1=get(hc(1),'Position');          %default top plot position
        lp=get(hc(2),'Position');           %default legend position
        tl=get(hc(1),'TickLength');         %tick length

        lpos=[sp1(1)+sp1(3)-tl(1)-lp(3) (sp1(4)-lp(4))/2+sp1(2) lp(3) lp(4)];     %new legend position
        set(hc(2),'Position',lpos)

        subplot(212)
        plot(1:sf,factseries(factors+1,:))
        xlabel('Iterations')
        ylabel('Error')

else
        'not improved on initial guess'
end

load base

basevalue=mvalue(ave,yi,zi,optfact,list);

load lowwall

lowwallvalue=mvalue(ave,yi,zi,optfact,list);

load topwall

highwallvalue=mvalue(ave,yi,zi,optfact,list);

[target;basevalue lowwallvalue highwallvalue]
```

D L Davies dave.davies@orange.net

B.II EMBOSS IMAGE CREATOR PROGRAMS

nodco.m

```
clear

rad=10;
gap=0.34;
%disp=rad+gap;                  % disp must be >= rad+gap

canang=30;
diewmes=12*4;
diehmes=20;
diewmes=2*ceil(diewmes/2);
diehmes=2*ceil(diehmes/2);
canht=10;
res=canht/diehmes               %emb3 or embtest
angres=pi*(canang)/(diewmes*180);
rad*angres

%res=5*pi/12;          %emboss
%canht=20*res;
%rad=25;
%angres=pi/60;

maxembht=0.5;
translation=2*rad+gap;

%%%%%%%%%%%%%%%%%%
%
%
%       Open test file


%fid=fopen('emboss.neu');
%fid=fopen('embtest.neu');
%fid=fopen('emb2.neu');
%fid=fopen('emb3.neu');
%fid=fopen('imbost.dat');
fid=fopen('emboss.dat');

%%%%%%%%%%%%%%%%%%
%
%
%       Locate start of coordinates within file

str=fgetl(fid);
strfnd=0;

while ~strfnd

        if size(str,2)>=13

                if str(1:13)==' Coordinates'

                        strfnd=1;
                        break
```

```
                end

        end

        str=fgetl(fid);

end

%%%%%%%%%%%%%%%%%%%%%%%%
%
%
%       Create new file of just coordinates

s=str(36);      %       where number of lines is located on line

for i=1:10

        s=str(36+i);
        if strcmp(s,' ')

                break

        end

end

n=str(37:37+i-2);
n=str2num(n);

fid2=fopen('D:\David\mfiles\emboss.txt','wt');

for i=1:n

        str=fgetl(fid);
        fprintf(fid2,'%s\n',str);

end

fclose(fid);
fclose(fid2);

%%%%%%%%%%%%%%%%%%%%%%%%
%
%
%       Obtain coordinates


load D:\David\mfiles\emboss.txt

A=emboss;

%%%%%%%%%%%%%%%%%%%%%%%%
%
%
%       Splitting up male/female die and strip coordinates

mind=find(A(:,1)<rad+gap/2);                                    %#
restind=find(A(:,1)>=rad+gap/2);                        %#
```

```
Bmale=[A(mind,:) mind];
Brest=[A(restind,:) restind];                                                    %#

Brest(:,1)=Brest(:,1)-translation;
[th,r,z]=cart2pol(Brest(:,1),Brest(:,2),Brest(:,3));
Brest(:,1)=th;
Brest(:,2)=r;
Brest(:,3)=z;

ms=size(Bmale,1);
rs=size(Brest,1);

[Bordered,ind]=sort(Brest(:,2));

Bfemale=Brest(ind(1:ms),:);
Bstrip=Brest(ind(ms+1:rs),:);

[Bstrip(:,1),Bstrip(:,2),Bstrip(:,3)]=pol2cart(Bstrip(:,1),Bstrip(:,2),Bstrip(:,3));
Bstrip(:,1)=Bstrip(:,1)+translation;

%%%%%%%%%%%%%%%%%%%%%%%
%
%
%       Convert die coordinates into cylindrical coordinates

[th,r,z]=cart2pol(Bmale(:,1),Bmale(:,2),Bmale(:,3));
Bmale(:,1:3)=[th r z];

%%%%%%%%%%%%%%%%%%%%%%%
%
%
%       Set up initial plot with 1-1 aspect

%temp canht
%canht=7;

figNumber=figure(...
                'Name','Male Embossing Die', ...
                'NumberTitle','Off');
figpos=get(figNumber,'Position');

enlargefactor=2;                                        % figure width enlargement

figpos(1)=figpos(1)-(1/2*(enlargefactor-1))*figpos(3);
figpos(3)=figpos(3)*enlargefactor;
set(figNumber,'Position',figpos)

plot(Bmale(:,1)*rad,Bmale(:,3),'y.');
canht=max(Bmale(:,3));
canwd=max(Bmale(:,1))*rad;
axis([0 canwd 0 canht])

axpos=get(gca,'Position');
axpos(4)=2/3*axpos(4);          %want space for buttons at bottom

htaspect=figpos(4)*axpos(4)/canht;
wdaspect=figpos(3)*axpos(3)/canwd;
```

```
if htaspect>wdaspect

        axpos(4)=wdaspect/htaspect*axpos(4);
        axpos(2)=0.9-axpos(4);

        axpos(1)=1/2*(1-axpos(3));

else

        axpos(3)=htaspect/wdaspect*axpos(3);
        axpos(1)=1/2*(1-axpos(3));

        axpos(2)=0.9-axpos(4);

end

set(gca,'Position',axpos)
axis([0 canwd 0 canht])
axpos=axis;
hold on

field=[Bmale(:,1)*rad Bmale(:,3)];


%%%%%%%%%%%%%%%%%%%%%%%%%%%%%%%%%%%%
%
%
%       Set up figure window

labelcolor=[0.8 0.8 0.8];
btnwid=0.1;
btnht=0.1;

%%%%%%%%%%%%%%%%%%%%%%%%%%
%
%
%       Create make image button

mibtn=uicontrol(...
        'Style','push', ...
        'Units','normalized', ...
        'Position',[0.32 0.02 btnwid btnht], ...
        'String','Make Image', ...
        'Callback','legalpt=3;');

%%%%%%%%%%%%%%%%%%%%%%%%%%
%
%
%       Create insert image button

iibtn=uicontrol(...
        'Style','push', ...
        'Units','normalized', ...
        'Position',[0.43 0.02 btnwid btnht], ...
        'String','Insert Image', ...
        'Enable','Off', ...
        'Callback','legalpt=3;');

%
```

```
%       close button
%

cbtn=uicontrol(...
        'Style','push', ...
        'Units','normalized', ...
        'Position', [0.87 0.05 btnwid btnht], ...
        'String','Finish', ...
        'Callback','legalpt=2;currPt=[-1 -1];done=1;');

zoomfactor=2;

%
%       zoom out button
%

callbackstr=[...
        'wd=axpos(2)-axpos(1);', ...
        'ht=axpos(4)-axpos(3);', ...
        'axpos(1:2)=[axpos(1)-1/2*(zoomfactor-1)*wd axpos(2)+1/2*(zoomfactor-1)*wd];', ...
        'axpos(3:4)=[axpos(3)-1/2*(zoomfactor-1)*ht axpos(4)+1/2*(zoomfactor-1)*ht];', ...
        'axis(axpos);', ...
        'legalpt=2;'];
zoutbtn=uicontrol(...
        'Style','push', ...
        'Units','normalized', ...
        'Position', [0.2 0.02 btnwid btnht], ...
        'String','Zoom Out', ...
        'Callback',callbackstr);

%
%       zoom in button
%

callbackstr=[...
        'wd=axpos(2)-axpos(1);', ...
        'ht=axpos(4)-axpos(3);', ...
        'axpos(1:2)=[axpos(1)+1/2*(1-1/zoomfactor)*wd axpos(2)-1/2*(1-1/zoomfactor)*wd];', ...
        'axpos(3:4)=[axpos(3)+1/2*(1-1/zoomfactor)*ht axpos(4)-1/2*(1-1/zoomfactor)*ht];', ...
        'axis(axpos);', ...
        'legalpt=2;'];
zinbtn=uicontrol(...
        'Style','push', ...
        'Units','normalized', ...
        'Position', [0.2 0.14 btnwid btnht], ...
        'String','Zoom In', ...
        'Callback',callbackstr);



vertmov=0.3;
horizmov=0.3;


%
%       Down
%

callbackstr=[...
```

```
        'ht=axpos(4)-axpos(3);', ...
        'mment=vertmov*ht;', ...
        'axpos(3:4)=[axpos(3)-mment axpos(4)-mment];', ...
        'axis(axpos);', ...
        'legalpt=2;'];
dbtn=uicontrol(...
        'Style','push', ...
        'Units','normalized', ...
        'Position', [0.05 0.02 0.5*btnwid btnht], ...
        'String','Down', ...
        'Callback',callbackstr);

%
%       Left
%

callbackstr=[...
        'wd=axpos(2)-axpos(1);', ...
        'mment=horizmov*wd;', ...
        'axpos(1:2)=[axpos(1)-mment axpos(2)-mment];', ...
        'axis(axpos);', ...
        'legalpt=2;'];
lbtn=uicontrol(...
        'Style','push', ...
        'Units','normalized', ...
        'Position', [0.02 0.13 0.5*btnwid btnht], ...
        'String','Left', ...
        'Callback',callbackstr);


%
%       Right
%

callbackstr=[...
        'wd=axpos(2)-axpos(1);', ...
        'mment=vertmov*wd;', ...
        'axpos(1:2)=[axpos(1)+mment axpos(2)+mment];', ...
        'axis(axpos);', ...
        'legalpt=2;'];
rbtn=uicontrol(...
        'Style','push', ...
        'Units','normalized', ...
        'Position', [0.08 0.13 0.5*btnwid btnht], ...
        'String','Right', ...
        'Callback',callbackstr);


%
%       Up
%

callbackstr=[...
        'ht=axpos(4)-axpos(3);', ...
        'mment=vertmov*ht;', ...
        'axpos(3:4)=[axpos(3)+mment axpos(4)+mment];', ...
        'axis(axpos);', ...
        'legalpt=2;'];
ubtn=uicontrol(...
```

```
        'Style','push', ...
        'Units','normalized', ...
        'Position', [0.05 0.24 0.5*btnwid btnht], ...
        'String','Up', ...
        'Callback',callbackstr);

%
%       Text Box
%

txthndl=uicontrol(...
        'Style','text', ...
        'Units','normalized', ...
        'Max',10', ...
        'Position', [0.32 0.12 0.38 0.15], ...
        'String','Click on point you want to edit', ...
        'Callback','');

%
%       "Continue" (Carry on) button - after happy with radial adjustment
%

extbtn=uicontrol(...
        'Style','push', ...
        'Units','normalized', ...
        'Position', [0.71 0.02 0.1 0.13], ...
        'String','Continue', ...
        'Visible','Off', ...
        'CallBack','carryon=1;');

%
%       Slider control
%

callbackstr=[...
        'v=get(radsl,"Value")*maxembht;', ...
        'set(radtxt,"String",v);'];
radsl=uicontrol(...
        'Style','slider', ...
        'Units','normalized', ...
        'Position', [0.82 0.02 0.03 0.25], ...
        'Visible','Off', ...
        'CallBack',callbackstr);

%
%       Output Box
%

radtxt=uicontrol(...
        'Style','text', ...
        'Units','normalized', ...
        'Position', [0.71 0.16 0.1 0.09], ...
        'Visible','Off');

done=0;

%%%%%%%%%%%%%%%%%%%%%%%%%%%%%%%%%%%%
%
%
```

```
%

ptlist=[];
changedptsind=[];

while done==0

        legalpt=0;      % point must be chosen within given axis, or a ui-button

        while legalpt==0

                waitforbuttonpress;

                if done==0

                        currPt=get(gca,'CurrentPoint');
                        currPt=currPt(1,1:2);

                end

                if currPt(1) > axpos(1)  &  currPt(1) < axpos(2)  &  currPt(2) > axpos(3)  &  currPt(2)
< axpos(4)

                        legalpt=1;

                elseif legalpt==0

                        set(txthndl,'String',' Please click inside the axis square');

                end;

        end;

        if legalpt==1

%
%       Check to see if point previously selected
%


                set(radsl,'Visible','On')
                set(radtxt,'Visible','On')

                nearestpoint=(field(:,1)-currPt(1,1)).^2+(field(:,2)-currPt(1,2)).^2;
                [nearestpoint fieldi]=min(nearestpoint);
                ptselected=field(fieldi,:);


                if size(ptlist,1)==0

                        firstpt=plot(ptselected(1),ptselected(2),'ro');

                else

                        xcheck=find(rad*Bmale(changedptsind(:,1),1)==ptselected(1));

                        if size(xcheck,1)>1

                                ycheck=find(Bmale(changedptsind(xcheck,1),3)==ptselected(2));
```

```
                        if size(ycheck,1)>0

                                plhndl=xcheck(ycheck(size(ycheck,1)));
                                ext=changedptsind(plhndl,2);
                                set(radsl,'Value',ext/maxembht)
                                set(radtxt,'String',ext)

                                set(cptshndl(plhndl),'Color',[1 0 0])

                        end
                end

                set(firstpt,'Xdata',ptselected(1), ...
                        'Ydata',ptselected(2))

        end

        i1=find(Bmale(:,1)*rad==ptselected(1));
        i2=find(Bmale(i1,3)==ptselected(2));
        node=Bmale(i1(i2),4);

%%
%%      Make appropriate handles and switches for figure
%%

        s=str2mat(...
                'Use slider to change radial extension', ...
                ' ', ...
                'Click "Continue" button when ready');
        set(txthndl,'String',s);
        set(extbtn,'Visible','On')

        carryon=0;

        while carryon==0%wait until extend has been hit

                waitforbuttonpress

        end

        data=get(radsl,'Value')*maxembht;

        set(txthndl,'String','Select another point')

        set(extbtn,'Visible','Off')

        set(radsl,'Value',0)
        set(radsl,'Visible','Off')

        set(radtxt,'String','')
        set(radtxt,'Visible','Off')

        ptlist=[ptlist;node data];

%
%       Make radial adjustments
%
```

```
            l=size(ptlist,1);

            ind=find(Bmale(:,4)==node);
            changedptsind=[changedptsind;ind data];

            femind1=find(abs(pi-Bfemale(:,1)-Bmale(ind,1))<=0.001);
            femind2=find(Bfemale(femind1,3)==Bmale(ind,3));

            Bmale(ind,2)=rad+data;

            for i=1:size(femind2,1)

                  Bfemale(femind1(femind2(i)),2)=rad-data;

            end

            xdat=Bmale(changedptsind(l,1),1)*rad;
            ydat=Bmale(changedptsind(l,1),3);

            cptshndl(l)=plot(xdat,ydat,'wo');

            cont=data/maxembht;
            set(cptshndl(l),'Color',[cont cont cont])


%
%     Making and inserting binary image
%

      elseif legalpt==3

            if strcmp(get(gco,'String'),'Make Image')

                  imtxt
                  set(imfig,'Position',[360 124 560 420])

                  set(iibtn,'Enable','On')
                  plonce=0;

            elseif strcmp(get(gco,'String'),'Insert Image')

                  set(txthndl,'String','Select upper left point')

                  legalpt=0;        % point must be chosen within given axis

                  while legalpt~=1

                        waitforbuttonpress;

                        currPt=get(gca,'CurrentPoint');
                        currPt=currPt(1,1:2);

                        if currPt(1) > axpos(1)  &  currPt(1) < axpos(2)  &  currPt(2) >
axpos(3)  &  currPt(2) < axpos(4)

                              legalpt=1;

                        else
```

```
                    set(txthndl,'String',' Please click inside the axis square');

                end

            end

            nearestpoint=(field(:,1)-currPt(1,1)).^2+(field(:,2)-currPt(1,2)).^2;
            [nearestpoint fieldi]=min(nearestpoint);
            startpt=field(fieldi,:);

            for i=1:ydim

                ptselected(2)=startpt(2)-(i-1)*res;

                for j=1:xdim

                    ptselected(1)=startpt(1)+(j-1)*angres*rad;

                    nearestpoint=(field(:,1)-ptselected(1)).^2+(field(:,2)-
ptselected(2)).^2;
                    [nearestpoint fieldi]=min(nearestpoint);
                    ptselected=field(fieldi,:);

                    i1=find(abs(Bmale(:,1)*rad-ptselected(1))<0.0001);
                    i2=find(abs(Bmale(i1,3)-ptselected(2))<0.0001);
                    node=Bmale(i1(i2),4);

                    data=txt(i,j);
                    ptlist=[ptlist;node data];

%
%       Make radial adjustments
%

                    l=size(ptlist,1);

                    ind=find(Bmale(:,4)==node);
                    changedptsind=[changedptsind;ind data];

                    femind1=find(abs(pi-Bfemale(:,1)-
Bmale(ind,1))<=0.001);
                    femind2=find(Bfemale(femind1,3)==Bmale(ind,3));

                    Bmale(ind,2)=rad+data;
                    Bfemale(femind1(femind2),2)=rad-data;

                    xdat=Bmale(changedptsind(l,1),1)*rad;
                    ydat=Bmale(changedptsind(l,1),3);

                    cptshndl(l)=plot(xdat,ydat,'wo');

                    cont=data/maxembht;
                    set(cptshndl(l),'Color',[cont cont cont])
%waitforbuttonpress
                end

            end

            if plonce==0
```

```
                    close(imfig)

                end

                plonce=1;

            end

        end

end

close('Male Embossing Die')

%%%%%%%%%%%%%%%%%%%%
%
%
%       Convert back to node ordered cartesian coordinates

[Bmale(:,1) Bmale(:,2) Bmale(:,3)]=pol2cart(Bmale(:,1),Bmale(:,2),Bmale(:,3));
[Bfemale(:,1) Bfemale(:,2) Bfemale(:,3)]=pol2cart(Bfemale(:,1),Bfemale(:,2),Bfemale(:,3));

Bfemale(:,1)=Bfemale(:,1)+translation;

C=[Bmale;Bstrip;Bfemale];
[n ind]=sort(C(:,4));
C=C(ind,1:3);

%%%%%%%%%%%%%%%%%%%%%%%%
%
%
%       Create new file of new coordinates


fid=fopen('D:\David\mfiles\coords.txt','wt');

fprintf(fid,'%13.7g %12.7g %12.7g\n',C');

fclose(fid);
```

imtxt.m

```
embht=0.1;
increment=0.1;

%%%%%%%%%%
%
%
%       Image Area Setup

xdim=5;
ydim=5;

txt=zeros(ydim,xdim);

if ~exist('imfig')
```

```
        imfig=figure(...
                'Name','Binary Image Template', ...
                'NumberTitle','Off');

else

        figure(imfig)

end

colormap(gray)
imagesc(txt)
set(gca,'Ytick',1:ydim)
set(gca,'Xtick',1:xdim)
grid

t1=text(0,0,'Embossing Height');
t2=text(0,0,'Increment');

set(t1,'Units','normalized')
set(t1,'Position',[0.02 -0.1])

set(t2,'Units','normalized')
set(t2,'Position',[0.6 -0.1])


embhtbtn=uicontrol(...
                'Style','Text', ...
                'Units','Normalized', ...
                'Position',[0.43 0.01 0.05 0.05], ...
                'String',embht, ...
                'Callback','');

incbtn=uicontrol(...
                'Style','Push', ...
                'Units','Normalized', ...
                'Position',[0.48 0.01 0.04 0.05], ...
                'String','+', ...
                'Callback','embht=min(embht+increment,maxembht);set(embhtbtn,"String",embht)');

decbtn=uicontrol(...
                'Style','Push', ...
                'Units','Normalized', ...
                'Position',[0.39 0.01 0.04 0.05], ...
                'String','-', ...
                'Callback','embht=max(0,embht-increment);set(embhtbtn,"String",embht)');

embincbtn=uicontrol(...
                'Style','Text', ...
                'Units','Normalized', ...
                'Position',[0.76 0.01 0.05 0.05], ...
                'String',increment, ...
                'Callback','');

incincbtn=uicontrol(...
                'Style','Push', ...
                'Units','Normalized', ...
                'Position',[0.81 0.01 0.04 0.05], ...
```

```
                'String','+', ...
                'Callback','increment=increment+0.01;set(embincbtn,"String",increment)');

decincbtn=uicontrol(...
                'Style','Push', ...
                'Units','Normalized', ...
                'Position',[0.72 0.01 0.04 0.05], ...
                'String','-', ...
                'Callback','increment=increment-0.01;set(embincbtn,"String",increment)');

%%%%%%%%%%
%
%
%       Done Button

donbtn=uicontrol(...
                'Style','Push', ...
                'Units','Normalized', ...
                'Position',[0.02 0.02 0.1 0.05], ...
                'String','Done', ...
                'Callback','done2=1;return;');



done2=0;

while done2==0

        waitforbuttonpress;
        cp=get(gca,'CurrentPoint');
        cp=round(cp(1,1:2));
        i=cp(2);
        j=cp(1);

        if i>0 & i<=ydim & j>0 & j<=xdim

                txt(i,j)=embht-txt(i,j);
                imagesc(txt)
                set(gca,'Ytick',1:ydim)
                set(gca,'Xtick',1:xdim)
                grid

                t1=text(0,0,'Embossing Height');
                t2=text(0,0,'Increment');

                set(t1,'Units','normalized')
                set(t1,'Position',[0.02 -0.1])

                set(t2,'Units','normalized')
                set(t2,'Position',[0.6 -0.1])

        end

end

%close(imfig)
```

D L Davies dave.davies@orange.net

B.III MISCELLANEOUS PROGRAMS

Level.m

Program used to realign measurement data from the SVET scan of the embossed tinplate samples, such that the data is symmetric as realistically possible. Essentially involves rotating the co-ordinates a certain amount until certain conditions are met.

```
%
%       set A to be sample
%

%A=sample;

s=size(A);

xmd=0.195;                      %x mesh density
ymd=0.195;                      %y mesh density

'       Centre coordinates'
cpx=input('x(j) coordinate?');
cpy=input('y(i) coordinate?');

mss=input('Male square size used?');

nsqx=floor(mss/2*0.8/xmd);      %number of squares to move away from centre point in x dir
nsqy=floor(mss/2*0.8/ymd);      %number of squares to move away from centre point in y dir

'height matrix'

a=A(cpy-nsqy,cpx-nsqx);
b=A(cpy-nsqy,cpx+nsqx);
c=A(cpy+nsqy,cpx-nsqx);
d=A(cpy+nsqy,cpx+nsqx);
[a b cpy-nsqy cpx-nsqx;c d cpy+nsqy cpx+nsqx]

count=1;
xgrad=10;
ygrad=10;
newA=A;
Xgrad=-0.0;
Ygrad=-0.0;
convfx=1;
convfy=1.5;

check=-1;

while check==-1

        A=newA;

        dline=[];
        dline2=[];
        for i=1:min(cpx-1,s(2)-cpx)
```

```
            dline(i)=A(cpy,cpx+i)-A(cpy,cpx-i);
            dline2(i)=dline(i)/(2*i);
        end

        xgrad=mean(dline2(1:nsqx))*convfx;
        abs(xgrad-Xgrad)

        dline=[];
        dline2=[];
        for i=1:min(cpy-1,s(1)-cpy)
            dline(i)=A(cpy+i,cpx)-A(cpy-1,cpx);
            dline2(i)=dline(i)/(2*i);
        end

        ygrad=mean(dline2(1:nsqy))*convfy;
        abs(ygrad-Ygrad)

        newA=[];
        for i=1:s(1)
            for j=1:s(2)
                newA(i,j)=A(i,j)-(xgrad-Xgrad)*(j-1)-(ygrad-Ygrad)*(i-1);
            end
        end

        count=count+1

        figure(2);imagesc(newA);colorbar;drawnow

        if abs(xgrad-Xgrad)>0.00001
        else
            if abs(ygrad-Ygrad)>0.00001
            else
                check=1;
            end
        end

end
```

intdiff.m

This program evaluates the difference of two definite integrals over a given domain, and thus essentially measures how close one curve is to another over the specified range. It is used to calculate the error in the validation profile plots for DWI (Figure 42 - Figure 47)

```
pdat=input('Enter physical data results? ')

mdat=input('Enter model data results? ')

a=min(pdat(:,1)); % interval
b=max(pdat(:,1));% range
```

D L Davies dave.davies@orange.net

```
n=18;                   % order of polynomial

Pc=polyfit(pdat(:,1),pdat(:,2),n);
Mc=polyfit(mdat(:,1),mdat(:,2),n);
Dc=Pc-Mc;
z=sort(roots(Dc));
ztemp=[];

for i=1:n

        if isreal(z(i))                 % checking root is real

                if z(i)>=a & z(i)<= b   % checking if root is in range

                        ztemp=[ztemp,z(i)];

                end

        end

end

interv=[a,ztemp,b]
sz=length(interv);

x=a:0.1:b;
I=[];

for i=1:sz-1

        aa=interv(i);                   % intervals designed so Pc is either
        bb=interv(i+1);                 % always smaller or always larger
        Ip=int(aa,bb,Pc,n);             % over interval [aa bb], such that
        Im=int(aa,bb,Mc,n);             % Ip-Im doesn't lose information

        I(i)=Ip-Im;
%       perc_error=100*abs(I(i))/Ip

end

Ip=int(a,b,Pc,n);
I
sum(abs(I))
perc_error=100*sum(abs(I))/Ip

figure(1)

yp=polyval(Pc,x);
ym=polyval(Mc,x);
plot(x,yp,x,ym)
hold on
plot(pdat(:,1),pdat(:,2),'ro',mdat(:,1),mdat(:,2),'bo')
hold off
```

int

D L Davies dave.davies@orange.net

A function that is called on with intdiff – calculates the area under the curve with the limits, coefficients and the order of polynomial specified in the argument of the function.

```
function [I] = int(a,b,c,n)

l=0;
h=0;

for i=1:n+1

        x=b;                    % eqn of curve is c(n+1)x^(0) + c(n)x^(1) + ... + c(1)x^(n)
        h=h+c(n+2-i)/i*x^i;     % ie, i=1:n+1, c(n+2-i)x^(i-1)
        x=a;                    % area = integral of this c(n+2-i)x^(i)/i
        l=l+c(n+2-i)/i*x^i;     % evaluated at a and b

end

I=h-l;
```

APPENDIX C INDEX OF FIGURES AND TABLES

References

1. Tufecki, S. S., Ahmetoglu, M. A., Kinzel, G. L., and Altan, T., "Process Simulation for Can Manufacturing by Deep Drawing and Ironing", SAE Paper No. 950696, International Congress and Exposition, Detroit, Michigan, February 27-March 2 (1995)
2. Schünemann, M., Ahmetoglu, M. A., Altan, T., "Prediction of Process Conditions in Drawing and Ironing of Cans". *Journal of Materials Processing Technology*, 59, (1-2), May, 1-9, 1996
3. Merchant, H.D., Hodgson, D. S., O'Reilly, I., and Embury, J. D., "Structure and Property Evolution During Drawing and Wall Ironing of AA 3004", *Materials Characterisation*, vol. 25, pp. 251-261 (1990)

4. Baudelet, B., and Grange, B., "Damage in Deep Drawn and Ironed Can Bodies in an Aluminium Alloy", *Scripta Metallurgia*, vol 26, no.3 pp. 375-379 (1992)
5. Huang, Y. M., 1991, Lu, Y. H., and Chan, J. W., "An Elasto-Plastic Finite Element and Experimental Study of the Ironing Process", *Journal of Materials Processing Technology*, 26, pp. 53-80, 1991
6. Jianjun, W., 1994, "The Calculation of Ironing Ring Force", *Journal of Materials Processing Technology*, 41, pp. 461-467, 1994
7. Sachs, G., and Espey, G., "Effect of Spacing Between Dies in the Tandem Drawing of Tubular Parts", *Trans. Of the ASME*, February (1947)
8. Pankinin, W., "Grundlagen des Tiefziehens zur Herstellung Zweiteiliger Dosen", *Werkstatt und Betrieb*, vol 110, no. 5, pp. 313-319 (1977) – referenced from [2]
9. Shawki, G. S. A., 1970, "Optimum Design of Ironing Dies", *Sheet Metal Industries*, pp. 855-863, Septmeber 1970
10. Knowles, W. S., and Swift, H. W., "Ironing of Metal Cups: Effects of Die Angle and Wall Thickness", *The Motor Industry Research Association*, Report No. 1946/R/3, (1946), 23 pages. – referenced from [9]
11. Bunten. R., Kopp, R., "Simulation of Microscopic Surface Changes During Metal Forming Operations by Finite-Element-Method. Friction and Roughening Phenomenons in Metallic Contact", *19th IDDRG Biennial Congress*, p315-324, June, 1996
12. Rajagopal, S., and Misra, S., "Measurements of Differential Friction Coefficients in Ironing", Proceedings of 18th NAMRC, pp. 89-95 (1990)
13. Stribeck Curve, http://www.tribologie.nl/goto/stribeck_e.htm (last accessed 2002)